

# **FINAL REPORT**

**U.S. Department of Energy**

**Managing Tight Binding Receptors for New Separations Technologies**

Daryle H. Busch and Richard S. Givens, CoPIs  
University of Kansas Center for Research, Inc.

EMSP #73831

**Grant Number DE-FG07-96ER14708**

Grant Project Officers: Roland Hirsch, Mark Gilbertson, Marshall C. Garr,  
Dallas L. Hoffer

Project Duration: 9/15/96—9/14/04

## TABLE OF CONTENTS

<b>EXECUTIVE SUMMARY</b> .....	5
<b>INTRODUCTION</b> .....	6
<b>RESEARCH OBJECTIVES</b> .....	6
Soil Poultice	
Switch binding	
Switch-release	
<b>METHODS AND RESULTS</b>	
<b>The Soil Poultice</b>	
<b>Introduction</b> .....	7
<b>Results and Discussion</b> .....	8
<i>Selectivity of macrocyclic metal complex formation</i> .....	9
<i>Molecularly imprinted polymer</i> .....	9
<i>MIPs based on hydrogen bonding &amp; electrostatic interaction</i> .....	11
<i>MIPs based on hydrogen bonding &amp; minor ligand bonding</i> .....	12
<i>Stereoselectivity of MIPs based on hydrogen bonding</i> .....	13
<i>Reuse of polymers</i> .....	14
<i>Conclusions</i> .....	14
<b>Switch Binding</b>	
<b>Introduction</b> .....	15
<b>Results</b> .....	17
<i>Equilibrium studies</i> .....	17
<i>Kinetic studies--kinetics of formation of Ni(L<sup>L/C</sup>)<sup>2+</sup></i> .....	18
<i>Fast process (k<sub>obs1</sub>)</i> .....	19
<i>Resolution of Specific Rate Constants</i> .....	20
<i>Slow process (k<sub>obs2</sub>)</i> .....	21
<b>Discussion</b>	
<i>Equilibrium Studies</i> .....	24
<i>Kinetic Studies</i> .....	25
<b>Switch Release</b>	
<b>Introduction</b> .....	26
<b>Results</b> .....	27
<i>Synthesis of tight-binding cryptand</i> .....	27
<i>Capturing of metals by cryptand: <sup>1</sup>H NMR studies</i> .....	29
<i>Photochemistry of the cryptand and the Ca<sup>+2</sup> cryptate: Product studies</i> .....	30
<i>Mechanistic studies of calcium cryptate photolysis</i> .....	31

<i>Quantum efficiencies for Ca(BF<sub>4</sub>)<sub>2</sub> cryptate disappearance</i> .....	31
<i>Quantitative determination of Ca<sup>+2</sup> release using a calcium-specific electrode</i> ...	32
<i><sup>1</sup>H NMR study of calcium cryptand</i> .....	34
<i>Synthesis of the Lariat macrocycle</i> .....	35
<i>Structural features of the cryptand-cryptate system</i> .....	35
<i>Effects of metal on the structure and chemistry</i> .....	36
<i>Photochemistry</i> .....	36
<b>RELEVANCE, IMPACT AND TECHNOLOGY TRANSFER</b> .....	36
<b>The Soil Poultice</b>	
<b>Relationship to Critical DOE EM problems</b> .....	36
<b>How Can These Results Be Used?</b> .....	36
<b>Bridging the Fundamental Science/Applications Gap</b> .....	37
<b>Impact of Work on Individuals, Institutions, Etc.</b> .....	37
<b>Is Scaleup Needed? Applied Impact?</b> .....	37
<b>Improved Capabilities of Scientists</b> .....	38
<b>Advanced Understanding of Area</b> .....	38
<b>What are the Remaining Hurdles?</b> .....	38
<b>Have Others Shown Interest?</b> .....	38
<b>Molecular Switching to Provide Rapid Rates</b> .....	38
<b>Relationship to Critical DOE EM problems</b> .....	38
<b>How Can These Results Be Used?</b> .....	39
<b>Bridging the Fundamental Science/Applications Gap</b> .....	39
<b>Impact of Work on Individuals, Institutions, Etc.</b> .....	39
<b>Is Scaleup Needed? Applied Impact?</b> .....	40
<b>Improved Capabilities of Scientists</b> .....	40
<b>Advanced Understanding of Area</b> .....	40
<b>What are the Remaining Hurdles?</b> .....	40
<b>Have Others Shown Interest?</b> .....	40
<b>PROJECT PRODUCTIVITY</b>	
<b>Soil Poultice</b> .....	40
<b>Molecular Switching to Provide Rapid Rates</b> .....	40
<b>PERSONNEL SUPPORTED</b> .....	41
<b>PUBLICATIONS</b> .....	41
<b>INTERACTIONS</b> .....	41
<b>TRANSITIONS</b> .....	42
<b>PATENTS</b> .....	42

<b>LITERATURE CITED</b> .....	42
<b>FEEDBACK</b> .....	46
<b>APPENDICES</b> .....	47
<b>QUANTITIES/PACKAGING</b> .....	116

## EXECUTIVE SUMMARY

Final Report: Grant Number **DE-FG07-96ER14708**

### **“Managing Tight Binding Receptors for New Separations Technologies”**

CoPIs Daryle H. Busch and Richard S. Givens  
Chemistry Department, University of Kansas, Lawrence, KS 66045

Much of the earth's pollution involves compounds of the metallic elements, including actinides, strontium, cesium, technetium, and RCRA metals. Metal ions bind to molecules called ligands, which are the molecular tools that can manipulate the metal ions under most conditions. This DOE-EMSP sponsored program strives (1) to provide the foundations for using the most powerful ligands in transformational separations technologies and (2) to produce seminal examples of their applications to separations appropriate to the DOE EM mission. These ultra tight-binding ligands can capture metal ions in the most competitive of circumstances (from mineralized sites, lesser ligands, and even extremely dilute solutions), but they react so slowly that they are useless in traditional separations methodologies. Two attacks on this problem are underway. The first accommodates to the challenging molecular lethargy by developing a seminal slow separations methodology termed the *soil poultice*. The second designs ligands that are only tight-binding while wrapped around the targeted metal ion, but can be put in place by *switch-binding* and removed by *switch-release*. We envision a kind of molecular switching process to accelerate the union between metal ion and tight-binding ligand.

Molecular switching processes are suggested for overcoming the slow natural equilibration rate with which ultra tight-binding ligands combine with metal ions. Ligands that bind relatively weakly combine with metal ions rapidly, so the trick is to convert a ligand from a weak, rapidly binding species to a powerful, slow releasing ligand – during the binding of the ligand to the metal ion. Such switch-binding ligands must react with themselves, and the reaction must take place under the influence of the metal ion. For example, our *generation 1* ligands showed that a well-designed linear ligand with ends that readily combine, forms a cyclic molecule when it wraps around a metal ion. Our generation 2 ligands are even more interesting. They convert from rings to structures that wrap around a metal ion to form a cage. These ligands are called cryptands. Switch release is accomplished by photolytic cleavage of a bond to convert a cyclic ligand into a linear ligand or to break similar bonds in a cryptate. Our studies have demonstrated switch binding and switch release with cryptates of calcium. These remarkable cyclic ligands and cage-like ligands are indeed tight-binding and may, in principle, be incorporated in various separations methodologies, including the soil poultice.

The soil poultice mimics the way in which microbes secrete extremely powerful ligands into the soil in order to harvest iron. The cellular membrane of the microbe recognizes the *iron/ligand complex* and admits it into the cell. The soil poultice uses molecularly imprinted polymers (MIPs) to play the role of the cellular membrane. Imprinting involves creation of the polymer in the presence of the metal/ligand complex. In principle, a well design ligand/MIP combination can be highly selective toward almost any targeted metal ion. The principles for that design are the focus of these investigations. An imprinting molecule can interact with the polymer through any, some, or all of the so-called supramolecular modes; e.g., hydrogen bonding, electrostatic charge, minor ligand bonding, Pi-Pi stacking, and hydrophobic and van der Waals interactions. Historically these modes of binding have given MIPs only small re-binding capacities and very limited selectivities. This program has shown that each mode of interaction can be made more powerful than previously suspected and that combinations of different supramolecular interaction modes can produce remarkable synergisms. The results of this systematic study provide a firm foundation for tailoring molecular imprinted polymers for reclamation of specific metal ion, including those important to the DOE EM mission.

## INTRODUCTION

Much of the earth's pollution involves compounds of the metallic elements, including actinides, strontium, cesium, technetium, and RCRA metals. Metal ions bind to molecules called ligands, which are the molecular tools that can manipulate the metal ions under most conditions. This DOE-EMSP sponsored program set out (1) to provide the foundations for using the most powerful ligands in transformational separations technologies and (2) to produce seminal examples of their applications to separations appropriate to the DOE EM mission. These ultra tight-binding ligands can capture metal ions in the most competitive of circumstances (from mineralized sites, lesser ligands, and even extremely dilute solutions), but they react so slowly that they are useless in traditional separations methodologies. Two attacks on this problem were chosen. The first approach worked within the challenging molecular lethargy of tight-binding ligands by developing a seminal slow separations methodology termed the *soil poultice*. The second designed ligands that are extremely tight-binding while wrapped around the targeted metal ion, but can be put in place by *switch binding* and removed by *switch-release*. We envision a kind of molecular switching process to accelerate the union between metal ion and tight-binding ligand.

Molecular switching processes are suggested for overcoming the slow natural equilibration rate with which ultra tight-binding ligands combine with metal ions. Ligands that bind relatively weakly combine with metal ions rapidly, so the trick is to convert a ligand from a weak, rapidly binding species to a powerful, slow releasing ligand – during the binding of the ligand to the metal ion. Such switch binding ligands must react with themselves, and the reaction must take place under the influence of the metal ion. For example, our *generation 1* ligands showed that a well-designed linear ligand with ends that readily combine, forms a cyclic molecule when it wraps around a metal ion. More interesting and of substantial promise are the *generation 2* molecules which were designed to wrap around a metal ion to form a cage, called a cryptate. The opposite process, *switch release*, is accomplished by photolytic cleavage of a bond to convert a cyclic ligand into a linear ligand or to break similar bonds in a cryptate. Our studies have demonstrated both switch binding and switch-release with cryptates of calcium. Finally, both switch binding and switch-release have been built into a single ligand molecule. These remarkable cyclic ligands and cage-like ligands are indeed tight-binding and may, in principle, be incorporated in various separations methodologies, including the soil poultice.

The soil poultice mimics the way in which microbes secrete extremely powerful ligands into the soil in order to harvest iron. The cellular membrane of the microbe recognizes the *iron/ligand complex* and admits it into the cell. The soil poultice uses molecularly imprinted polymers (MIPs) to play the role of the cellular membrane. Imprinting involves creation of the polymer in the presence of the metal/ligand complex. In principle, a well design ligand/MIP combination can be highly selective toward almost any targeted metal ion. The principles for that design were the focus of the investigations summarized here. An imprinting molecule can interact with the polymer through any, some, or all of the known *supramolecular* modes; e.g., hydrogen bonding, electrostatic charge, minor ligand bonding, Pi-Pi stacking, and hydrophobic and van der Waals interactions. Historically these modes of binding have given MIPs only small re-binding capacities and very limited selectivities. This program has shown that each mode of interaction can be made much more powerful than previously suspected and that combinations of different supramolecular interaction modes can produce remarkable synergisms. The results of this systematic study provide a firm basis for tailoring molecular imprinted polymers for reclamation of a specific metal ion, including those important to the DOE EM mission.

## RESEARCH OBJECTIVES

**Soil Poultice.** Building on hints from the literature, disclose the full potential for separations science of the proposed innovative methodology we have named the *soil poultice*.

- Determine the capacities and selectivities that can be achieved by optimal use of each of the supramolecular modes of imprint-polymer interaction, (hydrogen bonding, electrostatic (counter ion) attraction, minor ligand bonding,  $\pi$ - $\pi$  stacking).

- Evaluate the synergism achievable between binary and ternary combinations of the supramolecular modes of imprint-polymer interaction.
- Apply the generalizations and principles revealed by these basic studies to the specific case of separating mercury (II) ion from other common metal ions under a variety of challenging conditions.
- Explore corresponding applications to the separation of cesium, strontium, and other metal ions from their congeners using *generation 3*, cryptand-forming ligands.
- When the chemical structure and reaction parameters are appropriate, adapt the materials produced in the soil poultice program to other methodologies; e.g., chromatography and ion exchange.
- Combine the switch binding and–release with the soil poultice principles.

**Switch binding.** Seek proof of concept and applications of switch binding between ligands and metal ions.

- Focus first on kinetic and equilibrium studies of templated switch binding of first generation macrocycle-forming ligands, using the Schiff base reaction for cyclization.
- Explore the conditions for target-metal ion templated ring closure for generation 2 cryptate ligands. Generation 2 ligands form cryptand ligands by amide formation from a precursor ester.
- Extend the cryptand selectivity to capture other metal ions; e.g., Hg(II), Cs(I), Sr(II).
- Extend generation 2 ligands to both switch binding and switch-release by combining structural feature of molecules previously developed in this program.

**Switch-release.** Build on the literature results by demonstrating metal ion cryptand formation by the previously unstudied cryptate ligand having amide functions in place of the literature reported tertiary amine groups to demonstrate and expand on Switch-release.

- Prepare and demonstrate the reaction of these generation 2 cryptand ligands with selected alkali, alkaline earth, or RECRA metal ions.
- Demonstrate and characterize the switch release of the metal ion from these ligands.
- Design and synthesize a lariat macrocycle/cryptate ligand pair to combine switch binding and switch release for selected ions.
- Demonstrate and characterize the switch binding and switch release of that lariat macrocycle/cryptate ligand pair.
- Design and demonstrate a recycle strategy, in which closure of photo ruptured cryptates are converted back to the cryptand.
- Modify the cryptand and cryptand-forming ligands to amplify their binding to MIPs (macroporous imprinted polymers), in accord with the results of studies on macrocyclic ligands.

## METHODS AND RESULTS

Because this program involved three distinct components, the Soil Poultice, Switch Binding, and Switch Release, this section is presented in sub-sections bearing those titles.

### The Soil Poultice

**Introduction.** Microbes satisfy their need for iron by secreting extremely powerful ligands called siderophores into their surroundings to extract iron from the iron oxides in the soil, after which the microbe's cell membrane selectively brings the iron-siderophore complex into its interior.<sup>1</sup> We see this natural system as a model for a new way of recovering metal ions from various sources, such as soil deposits and surface contaminations. Such a synthetic system requires a strongly binding, highly selective ligand and that requirement is clearly within the capabilities of modern coordination chemistry.<sup>2</sup> However, the system also requires the equivalent of the cell membrane that selectively adsorbs the targeted metal complex. Here we propose that a molecularly imprinted polymer can serve

this latter purpose. For convenience in discussion we will call this synthetic system a “soil poultice”, implying that this substance can be contacted with contaminated soil and, like a medicinal poultice, it will cure the ill represented by metal ion contamination.

Because of the great importance of molecular recognition and selective binding to both fundamental science and its many applications, molecularly imprinted polymers (MIPs, first introduced by Wulff in 1972<sup>3</sup>) have received much attention in the fields of chemistry and analytical sciences,<sup>4</sup> In a molecular templating process, an imprint (or template) molecule is reversibly bound to functional monomers and copolymerized in a proper solvent (porogen) with an excess of cross-linking monomer. Removal of the imprint affords tailored binding cavities, which, ideally, are complementary in size, shape and functional group orientation to the imprint molecule. Thus, the resulting polymer can selectively re-bind the original imprint in competition with its structural analogues or environmental competitors.

In our soil poultice, it is important that the guest, the metal complex, bind easily and smoothly with the imprinted polymer host. Based on the interactions between an imprint and functional monomers, molecularly imprinted systems can be divided into two groups: covalent and non-covalent. The rebinding capacity of covalent systems is high because of the strong covalent interaction, and often over 80% of the theoretical sites can be reoccupied. In comparison, rebinding capacity of non-covalent systems (e.g. the combination of single-point hydrogen bonding and electrostatic interactions) has not previously exceeded about 20%.<sup>4f, 5</sup> However, for many purposes non-covalent MIPs have distinct advantages, including easy and rapid removal of imprint and rapid rebinding. These features make non-covalent MIPs especially attractive for our soil poultice, as indeed it would be for well known separation methodologies, such as chromatography and solvent extraction. Consequently, we applied the principles<sup>2</sup> of modern coordination chemistry and supramolecular chemistry in studies dedicated to optimizing non-covalent binding by MIPs. For reasons stated above, our focus has been on imprinting by and rebinding of complete metal complexes.

Much less attention has been directed at metal-imprinted polymers than those imprinted with organic compounds. About 30 years ago, Nishide *et al.* reported an early study of ionic imprinting in the synthesis of chelating polymers.<sup>6</sup> Recently, Kuchen *et al.*<sup>7</sup> and Lemaire *et al.*<sup>8</sup> developed highly efficient cation imprinted polymers for Cu/Zn and Gd/La separations. Fish *et al.*<sup>9</sup> proposed a sandwich structure for bis{*N*-(4-vinylbenzyl)-1,4,7-triazacyclononane}zinc(II) in a polymer matrix, and Borovik *et al.*<sup>10</sup> have incorporated cobalt(II) dioxygen carriers in imprinted polymers. Typically in most work involving MIPs and metal complexes, the ligand of interest is covalently incorporated in the polymer and any rebinding involves the reaction of the free metal ion with the ligand that is part of the polymer. In our novel metal extraction concept, MIPs rebind the *entire metal complex*, selectively, enhancing any selectivity the ligand may exhibit in binding to the targeted metal ion. This procedure provides two consecutive recognition events, a combination that, in principle, favours effective selectivity even in the presence of competing metal ions.

In this exploratory study we focused on learning the efficacy attainable through the use of different modes of supramolecular interactions and the synergism that may exist between those different kinds of interactions. Attention was given to the binding capacities of the substrate-free imprinted polymers, the selectivity of that re-uptake process, the robustness of the polymers to repeated use, and the relationship of the binding behaviour to the morphology of the polymer samples. The results show that dramatically better results are attainable with noncovalent substrate binding that would be expected on the basis of the literature devoted to the subject.

**Results and Discussion.** In its final, fully functional form, the soil poultice exerts selectivity at two levels: first, in the binding of the metal ion by the ligand and, second, in the binding of the metal complex by the molecularly imprinted polymer. In the best case, the selective binding at each of the

two stages is very strong, and, in addition, the rate at which the binding occurs would be rapid. But as we have seen, the latter is not the case. The studies summarized here have focused on a small number of broad but essential issues. Because covalent interactions tend to involve slow kinetics we restrict attention to those inter-molecular interactions that are non-covalent or, at best, weakly covalent. The immediate issue then becomes “can non-covalent interactions be strong enough to produce the proposed new methodology?” The literature indicates that imprinting using, for example, hydrogen bonding or electrostatic interaction, instead of covalent binding, supports only 10 to 15%, certainly less than 20%, rebinding capacity. An equally compelling issue relates to the compatibility of the combined goals of selective binding during complex formation and selectivity during the binding of the complex to the polymer. Further, are these porous imprinted polymers likely to be durable enough to actually be used in a separations methodology? In considering these issues the binding capacity has been studied at both the complex formation and the polymer/imprint level for the first system of this kind.

Selectivity of macrocyclic metal complex formation. The complexing ability and metal ion selectivity of the macrocyclic ligand **2**, (Chart 1) were investigated by equilibrium methods.

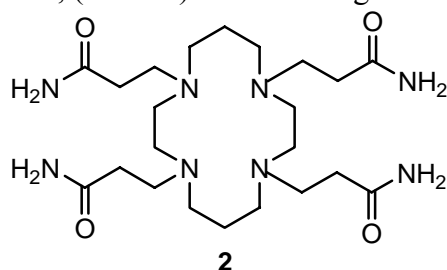


Chart 1

Protonation constants for **2** and formation constants of **2** with Cu(II), Hg(II), Cd(II), Pb(II), Zn(II) and Ni(II) were determined by glass-electrode titration measurements (Table 1 in appended manuscript). Cu(II) and Hg(II) form complexes having the highest stability constants ( $\log\beta_{101}$ ), and the large  $\log\beta_{101}$  difference compared to other metal ions ( $>12$ ), is indicative of very strong chelation to Cu(II) and Hg(II).<sup>11</sup> This result for ligand **2** is especially promising for selectively binding these metal ions and possibly removing them from polluted sites. Equilibration of all metal ion complexes showed no precipitate even at high pH values with the exception of Pb(II) which precipitated at pH  $\sim 7$ .

Because of their kinetic inertness, as also shown in our previous study,<sup>12</sup> the nickel(II) complexes with tetradentate tetraazamacrocyclic ligands are less likely to dissociate during the molecular imprinting process. Therefore they have been employed in all of the MIPs studies reported here.

Molecularly imprinted polymers. MIPs based on multiple and multi-site hydrogen bonding: EGDMA (ethylene glycol dimethacrylate) vs EBA (*N,N'*-ethylenebisacrylamide). In the extensively investigated chiral separation of amino acid derivatives, a molar ratio of 1:4:20 (imprint to functional monomer to crosslinker) was found to be an optimized recipe for preparing non-covalent MIPs, using methacrylic acid as the functional monomer (approximately two- to three-fold molar equivalents of the functional monomer relative to each polar group of the template).<sup>13</sup> The maximum rebinding capacity was 10-15%,<sup>4f,5</sup> as mentioned above.

In an effort to build strength into the non-covalent interactions, amide groups were chosen for our MIPs instead of carboxylic acid groups because they form stronger hydrogen bonds than carboxyl groups in polar solvents, such as acetonitrile.<sup>14</sup> Chart 2 (right) shows the interaction mode between the nickel(II) complex **4** (Chart 3) and the functional monomer acrylamide.

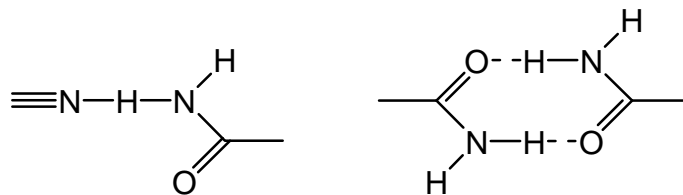


Chart 2

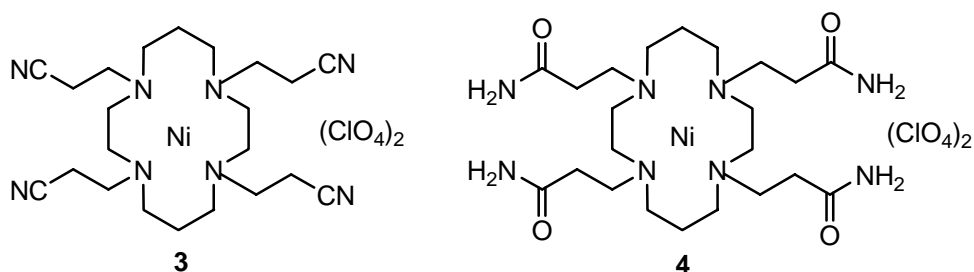


Chart 3

Pairs of amide groups form two-point hydrogen bonding interactions, creating relatively strong 4-center hydrogen bonded linkages. In addition, the four pendant amide groups on the complex provide ample opportunity for hydrogen bonding with corresponding groups in the polymer. Further, both EGDMA and EBA were investigated as cross-linking agents. Whereas EGDMA can only serve as a proton acceptor in a hydrogen bonding network, EBA adds both proton donors and proton acceptors to the hydrogen bonding inventory. Generally, EGDMA polymers have significantly larger surface area and pore volume than EBA polymers. In both cases there was a decrease in surface area and pore volume with the incorporation of the imprint molecule.

In early results, the imprinted polymer **P2**, (Table 2 in appended manuscript) prepared with a molar ratio of 1:4:20 of  $\beta$ -4 to acrylamide to EGDMA, showed a re-uptake of 3.5mg Ni/g polymer, or 26% rebinding of the theoretical sites. This represented a new high for rebinding capacity in a non-covalent MIP. Because high functional monomer concentration favours the formation of adduct between the imprint and the functional monomer,<sup>15</sup> polymers with a 12:20 ratio of acrylamide to EGDMA were prepared (**P4**). Remarkably, the nickel(II) re-uptake of the resulting imprinted polymer **P4** almost tripled the value previously determined for **P2**. From these data we have learned that it is possible to produce high binding and rebinding capacities in MIPs by providing an abundance of amide-based hydrogen binding sites. Capacities have been found that far exceed any previously reported.

Polymer recognition of the metal complex can also be realized with different specific positions and orientations of the hydrogen bonding groups in the polymer; e.g., the functional groups can be located on either the functional monomer or the crosslinker. EBA was introduced for two reasons. On one hand, it was known that, under most conditions, not all of the acrylamide enters into the polymerization and the presence of EBA could replace that loss of functional groups (acrylamide). On the other hand, replacing EGDMA with EBA made it possible to learn the effect of increasing the number of amide groups in the polymers (two amide groups in each EBA molecule). Consequently,

EBA polymers were prepared in the absence of the usual acrylamide “functional monomer”. The expected hydrogen bonding interaction pattern is the same as that of the EGDMA/acrylamide polymers (Chart 2, right). EBA polymers exhibited considerably higher nickel(II) re-uptake than EGDMA polymers, which reflects the large excess of amide groups on the crosslinker. For such an imprinted polymer **P6** with 1:18 of  $\beta$ -4 to EBA, the nickel(II) re-uptake was 38 mg/g, whereas the value for the control polymer was only 22 mg/g. This difference also demonstrates a marked increase in capacity based on the imprinting effect. However, further increases in the relative amount of imprint during the polymerization process resulted in lower rebinding capacity (**P7** and **P8**).

MIPs based on hydrogen bonding & electrostatic interaction: acetonitrile vs water; Scatchard analysis. In studies on enantiomeric selectivity by MIPs it has been shown that the combination of electrostatic binding and hydrogen bonding can be made far more effective than either mode of interaction alone.<sup>4f</sup> We introduced the second mode of interaction, electrostatic attraction, by using the imprint  $\beta$ -5 with a polymerizable counter ion that can also be incorporated into the polymer. The rebinding capacity of the corresponding sample **P9** (1:4:20) amounted to 7.2 mg/g, or 54%, more than three times that of the control polymer **P1** and much higher than those reported in the literature for non-covalently imprinted polymers.

Since the relatively weak non-covalent interactions are favoured by lower temperature, <sup>16</sup> 2,2'-azobis(2,4-dimethylvaleronitrile) (ABDV), a more reactive initiator than AIBN, was used to foster polymerization at 40°C, in place of the previously applied 50°C temperature. Unexpectedly, the corresponding imprinted polymer **P12** exhibited inferior rebinding, but still three times that of the polymer involving hydrogen bonding alone. Even larger imprinting effects can be realized by preparing polymers with extremely high crosslinker to functional monomer ratios, e.g. 120:4 for EGDMA:acrylamide. Those three polymers, **P13** (control), **P14** (hydrogen bonding alone) and **P15** (hydrogen bonding & electrostatic interaction) have surface areas and pore volumes so close in value that reasonable comparisons can be made with little doubt about the close similarities of their important morphologically dependent properties (e.g., availability of accessible sites). The samples whose binding is limited to hydrogen bonding exhibited very poor rebinding, while the nickel(II) re-uptake by the polymer benefiting from two synergistic modes of interaction (hydrogen bonding and electrostatic attraction) **P15** was enhanced by a factor of 18, compared to that of the control polymer. This is an excellent example of imprint-enhanced rebinding capacity.

Corresponding *rebinding* experiments have also been carried out in water, because water is the appropriate solvent for eventual deployment of the soil poultice. In all cases in water, the polymers having hydrogen bonding and electrostatic interactions bound *ca.* twice as much of the nickel(II) complex  $\beta$ -4 as did the control polymers. Good rebinding in water has also been reported in the molecular imprinting of biologically related compounds.<sup>17</sup> According to the literature,<sup>15,18</sup> water is adverse with respect to hydrogen bonding and electrostatic interactions, while it is conducive to hydrophobic interactions which play an important role in non-covalent binding.

Batch binding tests were also performed to examine the concentration dependence of rebinding to the imprinted polymers. It is clear from the binding data that **P9** (hydrogen bonding & electrostatic attractions) possesses a substantially larger number of stronger binding sites. The corresponding Scatchard plots (Figure 1), reveal quite different binding properties for the two polymers. The plot for **P9** is nonlinear with two straight lines fitting the Scatchard equation, indicating that there are two populations of binding sites with different affinities for the imprint molecule. The association constants  $K_a$  for the high- and low-affinity binding sites were calculated to be  $(2.3 \pm 0.48) \times 10^3 \text{ M}^{-1}$  and  $52 \pm 4.5 \text{ M}^{-1}$ , respectively. In contrast, the Scatchard plot for **P2** represents relatively homogeneous binding sites low binding affinity ( $K_a = 13 \pm 6.1 \text{ M}^{-1}$ ). We rationalize these distinctly different binding sites in

terms of the positioning of the co-polymerized counter ions. The strong binding probably arises from sites enjoying both hydrogen bonded linkages and maximum presence of negatively charged sulfonate groups. The weak binding is attributed to sites having one or no counter ions in close proximity to the re-bound cationic metal complex.

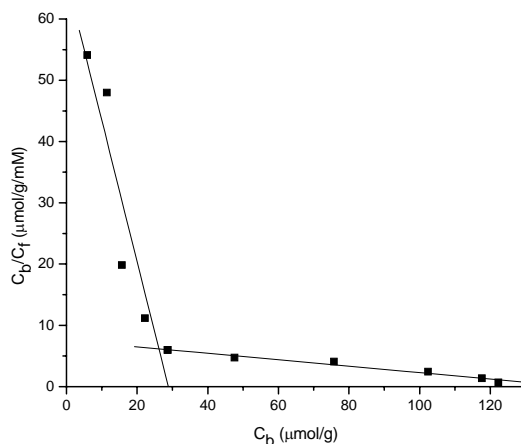


Figure 1. Scatchard plot of **P9** in acetonitrile to determine  $K_a$  values from concentration dependence of binding capacity of MIPs.

MIPs based on hydrogen bonding & minor ligand bonding. As functional monomers, vinyl pyridines provide supplementary ligating groups (1 or 2 of the pyridine nitrogens) to bind nickel(II), in addition to those on the primary ligand. The nickel(II) re-uptake of polymers based solely on such minor ligand interaction show the same effect previously found for the hydrogen bonding (only) polymers. As the excess of 4-vinyl pyridine increased from 2:1 to 6:1, the rebinding capacity of the imprinted polymer increased from 2.5 mg/ g to 14 mg/g, and, at the same time, the imprinting effect became more pronounced.

The position of the vinyl substituent on the pyridine has a great influence on the rebinding capacity. Replacing 4-vinyl pyridine with 2-vinyl pyridine, produced an “imprinted” polymer (P26) with essentially zero binding ability, and 3-vinyl pyridine yielded an intermediate behaviour. This parallels the accessibility of the nitrogen atom for binding to a metal atom.

When 4-vinyl pyridine was added as a second functional monomer (in addition to acrylamide), nickel(II) re-uptake increased by a factor of two. Incrementally increasing the concentration of 4-vinyl pyridine by replacing equivalent molar amount of acrylamide affords continuing improvement of the rebinding capacity (Figure 2), thereby providing our second example of synergistic bimodal binding of the macrocyclic metal complexes to the imprinted polymer.

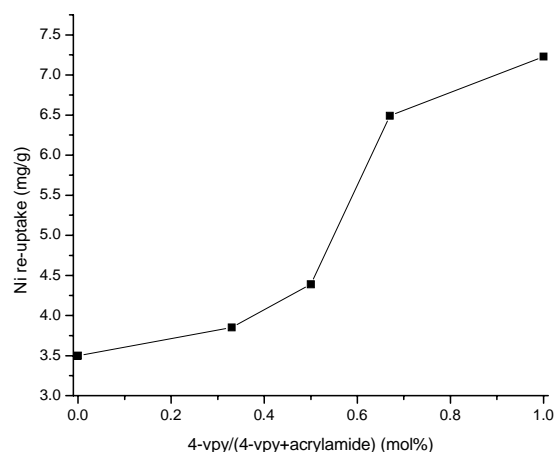


Figure 2 Rebinding capacity of the MIPs (AIBN, 50°C;  $\beta$ -4/ 4-vinyl pyridine+acrylamide/EGDMA=1/4/20).

Stereoselectivity of MIPs based on hydrogen bonding. The stereochemistry of macrocyclic metal complexes allows us to explore the selective recognition of stereo-isomers by molecular imprinting, which to the best of our knowledge, has not previously been studied. Earlier work revealed that the nickel complexes **3** and **4** (Chart 3) exist in two isomeric structures (Chart 4): The symbol  $\beta$  (**I**) is assigned to the thermodynamically favored form and  $\alpha$  (**II**), to the kinetically favored form.<sup>19</sup>

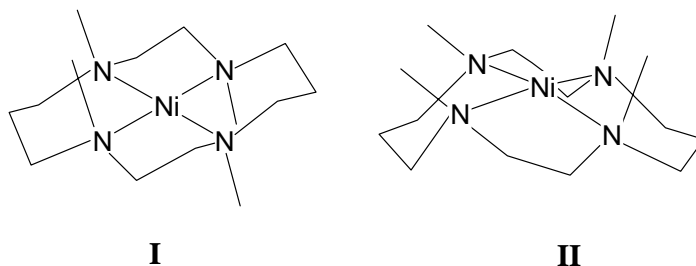


Chart 4

Based on Barefield's procedure,<sup>19</sup> four nickel complexes,  $\alpha$ -**3**,  $\alpha$ -**4**,  $\beta$ -**3** and  $\beta$ -**4** were prepared by the reaction of nickel perchlorate with the corresponding macrocyclic ligands at room and reflux temperatures, respectively. Considering the possibility of the transformation of the  $\alpha$  isomer to the  $\beta$  isomer during the thermally initiated polymerizations, we focused on polymers imprinted by the  $\beta$  isomer in this work. The stereoselectivity is expressed as the ratio of  $\beta$  isomer to  $\alpha$  isomer that was found to rebind to the  $\beta$  imprinted polymers.

To Our surprise, all of the imprinted polymers and control polymers had better rebinding capacities for  $\beta$ -**4** over  $\alpha$ -**4**. It is noteworthy that  $\beta$ -**4** binds to its well studied imprinted polymer **P2** seven times more strongly than does  $\alpha$ -**4**. Further, the stereoselectivity of the control polymer **P1** (not imprinted) for  $\beta$ -**4** is 5.1. We must conclude that, beyond imprinting, the orientation of the pendant amide groups in  $\beta$ -**4** is more favorable for hydrogen bonding. Stated more generally, this shows that the structure of imprints is crucial to the efficiency of imprinting and rebinding processes. Consequently, it was not surprising to find that the  $\beta$ -**4** isomer was superior in binding affinity (0.86 mg/g for  $\beta$ -**4**) even with the

sample **P27** imprinted with  $\beta$ -**3**, the complex having pendant nitrile groups on its ligand, rather than amide functions.

Reuse of polymers. Chemical stability is an important property of MIPs. Very recently Nicholls *et al.* studied the chemical stability of theophylline imprinted polymers which were based on the copolymerization of methacrylic acid and ethylene glycol dimethacrylate.<sup>20</sup> The polymers retained their affinity ( $\geq 95\%$ ) for the imprint on exposure (24 h) to 10 M hydrochloric acid. In this work, we studied the durability of the imprinted polymers by treating them with concentrated hydrochloric acid, and, in separate experiments, with the very strong oxidizing agent, concentrated nitric acid.

For each cycle of reuse, a polymer sample was treated with the imprint  $\beta$ -**4**, then after digestion in acid, it was washed repeatedly with water, methanol and dried in vacuo in order to remove the freshly bound  $\beta$ -**4**, in preparation for the next re-uptake experiment. The imprinted polymers displayed increases in rebinding capacity during the reuse by a factor of 1.5-2 in the course of several rebinding runs when the polymers had been treated with concentrated hydrochloric acid or nitric acid for about 50 h. Clearly, these polymers are quite resistant to strong and oxidizing acids. The mechanism by which acid treatment increases rebinding capacity remains unknown. Solid-state  $^{13}\text{C}$  NMR analyses showed nearly identical spectra for the samples before and after nitric acid digestion,<sup>21</sup> although the ester groups in EGDMA units are subject to hydrolysis under such harsh conditions.<sup>4f</sup> Elemental analyses showed an increase in nitrogen content after nitric acid treatment.<sup>22</sup> Further, the color of the polymers was changed from pure white to light yellow, supporting the possibility of introduction of nitro groups, whose presence could bring about additional hydrogen bonding in the polymers.

Imprint removal with hydrochloric acid followed by soxhlet extraction had no obvious influence on the polymer morphology. To the contrary, nitric acid treatment led to a marked decrease of surface area and pore volume.

Conclusions. These feasibility studies provide strong indications that the *soil poultice* concept may someday be realized through practical applications. Success will depend on maximizing the rebinding capability and selectivity of MIPs designed specifically for the soil poultice. The requirements are very strong binding with great lability and our strategy to impart these properties on a molecularly imprinted polymer has been focused on optimising combinations of the known supramolecular interactions; e.g., hydrogen bonding, electrostatic attraction, and additional monodentate ligand binding. Using macrocyclic nickel complexes having pendant functional groups, we have developed molecularly imprinted polymer systems having non-covalent rebinding capabilities that are much greater than has previously been observed. This clearly shows that the potential of labile, non-covalent binding MIPs has not been fully developed. In view of the limited attention that has been given to systems of this kind, these results are viewed as substantial advances.

A general principle of the soil poultice is the dual selective processes that are built into the system: (1) chelate selectivity--that associated with metal ion binding to the ligands of choice and (2) MIPs selectivity--that associated with selective adduct formation between the complex and the imprinted polymer. For the MIPs studies themselves, low spin square planar, substitution-inert nickel(II) complexes were used in these studies to avoid any possibility of complications, during polymerisation, due to rapid dissociation of the imprinting complex.

The chelate selectivity of ligands employed in the MIPs studies was explored by determining the binding constants for a selection of metal ions. The protonation constants for ligand **2** and the stability constants for the complexes of **2** with the labile metal ions Cu(II), Hg(II), Cd(II), Pb(II) and Zn(II) were determined, leading to important results. Ligand **2** is highly selective toward Cu(II) and Hg(II) compared to the other metal ions. This suggests the possibility of using a MIPs system based on **2** for recovering Cu(II) and/or Hg(II) from spills.

According to the literature, hydrogen bonded MIPs are weak in performance with their rebinding capacities being limited to 10 to 15% of the available polymer sites. In our design, the first and simplest polymers depending on hydrogen bonding alone exceeded these limits substantially (~26%). We showed by careful choice and balance of the components of the polymer very large binding capacities can be achieved through hydrogen bonding alone—but that does not necessarily assure high selectivity.

Proceeding on the basis of leads provided by earlier studies on chiral substrates, we showed that synergism between pairs of supermolecular modes of binding can lead to very strong and selective substrate binding. With the combination of hydrogen bonding and electrostatic attraction, rebinding in excess of 50% is readily available. However, in many cases, the addition of imprints results in deleterious modifications in the polymer morphology. Under proper conditions the morphology can be maintained constant and the impact of binding group changes has been clearly demonstrated. Under such conditions, hydrogen bonding alone gives marginal results, as reported in the literature; however, the synergism between hydrogen bonding and electrostatic attraction produces ~20 times better rebinding. Careful control of composition and functional parameters can move these polymer materials from behaviours properly described as not especially interesting to those recognized to be quite useful. The combination of a monodentate ligand delivered as a functional monomer in the polymer and a hydrogen bonding functional monomer gives results parallel to those found for the duo comprised of hydrogen bonding plus electrostatic attraction.

All of the initial studies were carried out with acetonitrile as porogen. The ideal medium for a soil poultice is water. Remarkably, water is, at least in some cases, about 90% as good as acetonitrile when it comes to rebinding of substrates to the imprinted polymers benefiting from two supramolecular modes of interaction. This is surprising in view of the expectation that water would be a poor solvent for hydrogen bonding and electrostatic interactions.

Some more detailed studies on systems having both electrostatic and hydrogen bonding groups revealed two distinctive kinds of binding sites with affinities for substrates differing by a factor of 40-50x. It is proposed that the strongly binding sites have a maximum positioning of vinyl sulfonate moieties in their near vicinities, as compared to the weaker sites. Further, even the weaker site is some 4x stronger than the binding sites in polymers linking to substrates by hydrogen bonding alone.

Stereoselectivity is evident and reflects the uniqueness of the macrocyclic complex imprinted systems. We have also shown that the rebinding capacity improves with reuse and that the MIPs are robust in the presence of oxidizing agents and strong acids.

## Switch Binding

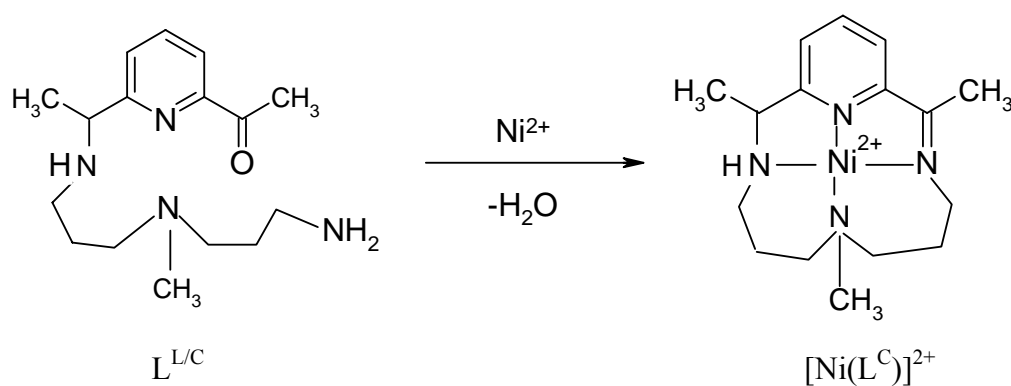
**Introduction.** In principle the most powerful known ligands can capture metal ions in the most competitive of circumstances, for example from mineralized sites, from lesser ligands, and even from extremely dilute solutions; i.e., under circumstances where ordinary ligands, such as those used in well-known separations technologies, are completely ineffective. Clearly there are compelling incentives for finding ways to apply these tight-binding ligands to the management of the metallic elements under many conditions, but there are major hurdles that must be overcome.

The applications of such tight-binding ligands have been limited by the slow rates at which their equilibria are established. It is an experimental fact that the equilibrium constants for the binding of any kind of receptee (e.g., a metal ion) to its complementary receptor (i.e., ligand) commonly vary monotonically with the rates at which the receptee is liberated from the receptee/receptor complex.<sup>23</sup> Consequently, ultra tight-binding ligands, whose equilibrium constants for binding exceed ordinary

values by factors of millions or billions, will release their complement at least that many millions or billions of times slower. Most often, the slowness is even more lethargic since the rate of binding is also retarded and  $K_{\text{equil}} = k_{\text{binding}}/k_{\text{release}}$ . In order to make best use of tight-binding receptors it is, therefore, necessary to either accommodate any specific methodology to these slow kinetic processes or to find means of accelerating the formation and dissociation rates associated with complexation.

Here we present the concept of replacing slow rates of complex formation by a chemical switching process that we will refer to as *switch binding*. The combined chemical processes of ligand binding and release constitute metal ion/ligand equilibration and complete replacement of that natural process with chemical switching requires both switch binding and switch-release. Switch-release is broadly used to generate immediate sizeable infusions of biological substrates, including metal ions, in life science studies.<sup>24</sup> Switch-release is the subject of other work in these laboratories. The concept of switch binding and switch-release is in step with the goals of science to move beyond what nature gives to us spontaneously.

Here switch binding is accomplished by a change in the structure of the ligand in accompaniment to its binding to the metal. The structural change is from a rapidly reacting, more weakly binding ligand structure in the free state to a more slowly reacting, more strongly binding ligand structure in the target metal complex. *Complementarity* and *ligand constraints* determine the stabilities of metal complexes.<sup>25</sup> Complementarity, a necessary but not sufficient condition for maximum affinity, implies a consonance between metal ion and ligand in bond type (often including charge), geometry, and size. Given equal complementarity, the constraints built into the structure of the ligand determine just how strong its complexes will be. For the example presented here, the topological constraint built into the ligand changes from that of a linear tetradentate ligand to that for a macrocycle (Scheme 1). Given equal complementarity, the stabilities of complexes increase dramatically with increasing topological constraint: (simple ligand < chelate < macrocycle < cryptand). Further, as described above, the rates of their binding to and dissociation from metal ions decrease as complex stability increases.



**Scheme 1.** Switch binding process in which a rapidly reacting linear chelate becomes an inert macrocyclic ligand coordinated to a nickel(II) ion.

The switch binding ligand investigated in this work,  $L^{L/C}$ , was designed to have complementary functional groups at its ends, primary amino and ketone groups, which react to close the macrocycle,  $L^C$ , about the metal ion. This Schiff base condensation, produces a macrocyclic ligand that is known to be nicely complementary to the nickel(II) ion. The square planar complex,  $[Ni(L^C)]^{2+}$ , has been prepared by a more traditional route and characterized<sup>26</sup>. Because the expected product of the

complete switch binding process has been characterized, this is a good system to test the switch binding concept. For comparison, a very similar ligand ( $L^L$ , Chart 5) that is not capable of undergoing cyclization was also synthesized, and details of the syntheses are reported (see appended manuscript on this subject). Detailed kinetic and mechanistic information has been obtained for the complexation reactions of both ligands,  $L^{L/C}$  and  $L^L$ , with nickel(II). The work also includes the determination of the protonation and complex formation constants for the two ligands.

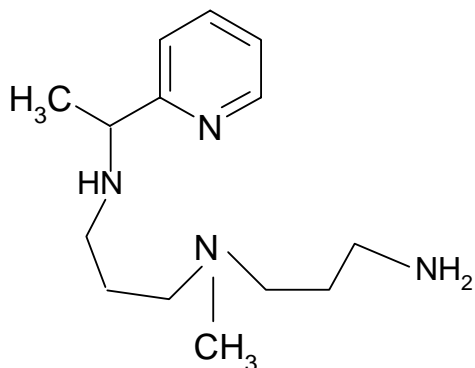


Chart 5

**Results.** Strategies for the synthesis of the switch binding ligand 1-[6-{3-[(3-amino-propyl)-methyl-amino]-propylamino}ethyl]-pyridin-2-yl]ethanone,  $L^{L/C}$ , and 3-(3-[pyridine-2-yl]-ethylamino)-propyl-N-methyl-1-amino)propane,  $L^L$ , as the hydrobromide salts are reported in the appended manuscript.<sup>27-30</sup>

Equilibrium studies. Protonation constants for  $L^L$  and  $L^{L/C}$  for formation of their acid salts and their complex stability constants were calculated by computer fitting of potentiometric data. The initial results of the computations were obtained in the form of overall protonation constants

$$\beta^H_i = [H_iL] / [L][H]^i$$

or overall stability constants

$$\beta_{pqr} = [MpLqHr] / [M]^p[L]^q[H]^r$$

Differences between the various  $\log \beta^H_i$  or the  $\log \beta_{pqr}$  give the stepwise protonation constants or the stepwise formation and protonation constants of the complex reactions

The titration curve for  $L^{L/C}$  was found to be reproducible and reversible despite the expectation that it would quickly form a variety of products in solutions, due to its innate ability to condense inter- or intramolecularly at a variety pH levels. The anticipated variety of products and intermediates was expected to greatly complicate the potentiometric measurements since the identity of the ligand might constantly shift among numerous linear and cyclic structures. The protonation constants for  $L^L$  and  $L^{L/C}$ , together with literature data for related ligands, are summarized in **Table 1** of the appended manuscript. The higher values of protonation constants correspond to the protonation of the primary and secondary amine nitrogens in the acyclic ligands and to the secondary nitrogens in analogous opposing positions in the macrocycle, py[14]aneN<sub>4</sub>. For both  $L^{L/C}$  and  $L^L$ , the protonation constant for the secondary nitrogen is higher than that for the primary nitrogen atom, representing the typically

greater basicity of secondary amines over primary amines<sup>31</sup>. The third and fourth values ( $\log K_3$  and  $\log K_4$ ) for  $L^{L/C}$  and  $L^L$  correspond to the protonation of tertiary nitrogens bearing methyl groups and the pyridine nitrogens, respectively. The last constant for  $L^L$  was not determined because its high acidity prevented a sufficiently accurate determination by potentiometric measurements. The species distribution diagram for  $L^{L/C}$  is shown in **Figure 1**.

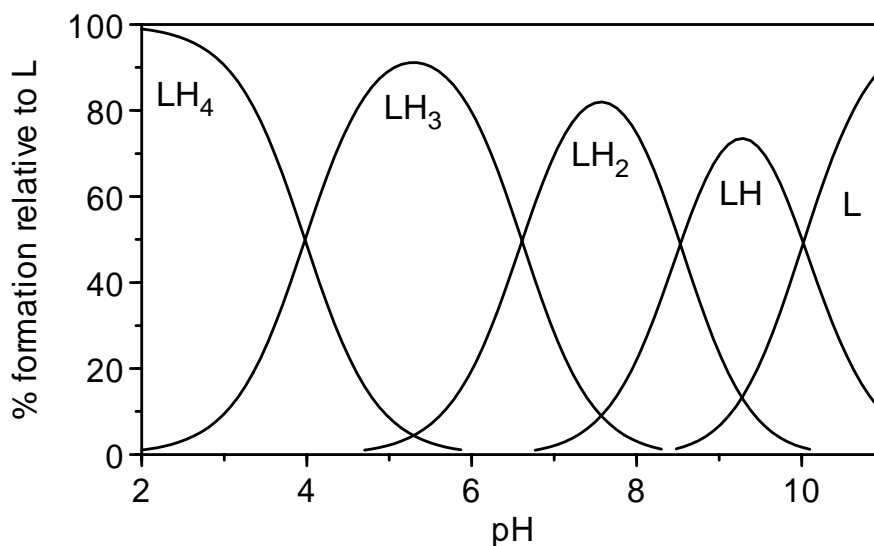
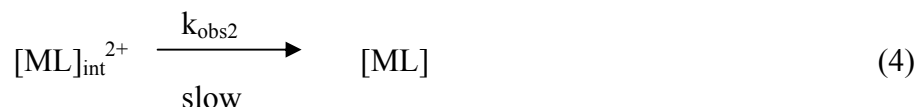
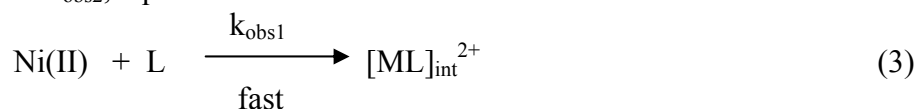


Fig 2. Speciation curves for  $L^{L/C}$ , at 25 °C and  $I = 0.1 \text{ M (KNO}_3\text{)}$ .

Potentiometric titrations (with and without the metal ion present) of the acid salts of  $L^{L/C}$  and  $L^L$  were performed with NaOH. Computer calculations using the titration data revealed the presence of two complex species,  $[\text{MLH}]^{3+}$  and  $[\text{ML}]^{2+}$  for the switch binding ligand,  $L=L^{L/C}$ . Also two complex species are formed by the surrogate ligand ( $L = L^L$ ), the first of which is  $[\text{ML}]^{2+}$  for all metal ions studied and the second varies as the metal ion is changed. Formation constants for these species are given in Table 2 of the appended manuscript.

Kinetic studies--kinetics of formation of  $\text{Ni}(L^{L/C})^{2+}$ . The rate of complexation of nickel(II) with  $L^{L/C}$  was studied both by UV-vis spectrophotometer and with a stopped-flow spectrophotometer at 25°C in the presence of 0.2M  $\text{KNO}_3$  from pH 5 to 7.5. All kinetic measurements were carried out under pseudo first order conditions ( $[L^{L/C}] \geq [\text{Ni(II)}]$ ). Reaction sequences were observed in two distinct time regimes, the first in fractions of seconds and the second in hours. Both processes are accompanied by increasing absorbance ( $\lambda_{\text{max}} = 390 \text{ nm}$ ), as expected for formation of a square planar nickel(II) complex. The two processes can be explained by the pseudo first order rate constants  $k_{\text{obs1}}$  and  $k_{\text{obs2}}$ , eqs 3 and 4.



where  $[\text{ML}]_{\text{int}}^{2+}$  is the intermediate complex species associated with the fast process.

Fast process ( $k_{obs1}$ ). The initial kinetic process between the Ni(II) ion and  $L^{L/C}$  is complex, giving evidence for three apparent sequential steps, the first of which was found to be pH and concentration dependent, whereas the other two steps were overlapping, difficult to separate, and exhibited only small spectral changes. The first events almost certainly involve the usual reversible binding of the first few ligand sites to the metal ion, eq 5,



(As discussion progresses  $T_L$  will be used to represent the sum of all unprotonated and protonated forms of the ligand:  $L$ ,  $HL^+$ ,  $H_2L^{2+}$ , etc.) where  $k_f$  and  $k_d$  are the rate constants for complex formation and the spontaneous dissociation of the nickel(II) complex, respectively.

At constant pH, the reaction kinetics, for the fast reaction were fitted to the differential expression

$$d[NiHL^{3+}]/dt = k_f [Ni^{2+}] [LH_n] - k_d [NiHL^{3+}] \quad (6)$$

Kinetic determinations were carried out at each of several pH values under conditions where  $T_L \gg T_{Ni}$  to yield the pseudo first-order rate expression

$$d[NiHL^{3+}]/dt = k_{obs1} [Ni^{2+}] \quad (7)$$

$$(k_{obs1} = k_d + k_f T_L) \quad (8)$$

for which the observed first-order rate constant,  $k_{obs1}$ , could be obtained from the  $A/t$  data ( $A$  = absorbance;  $t$  = time) computer fitted to eq 9.

$$A = (A_0 - A_\infty) \exp(-k_{obs1}t) + A_\infty \quad (9)$$

( $A_0$  and  $A_\infty$  refer to  $t = 0$  and  $t = \infty$ , respectively)

The pH dependence of  $k_{obs1}$  for the complexation of  $L^{L/C}$  with Ni(II) ion is shown in **Figure 3**.

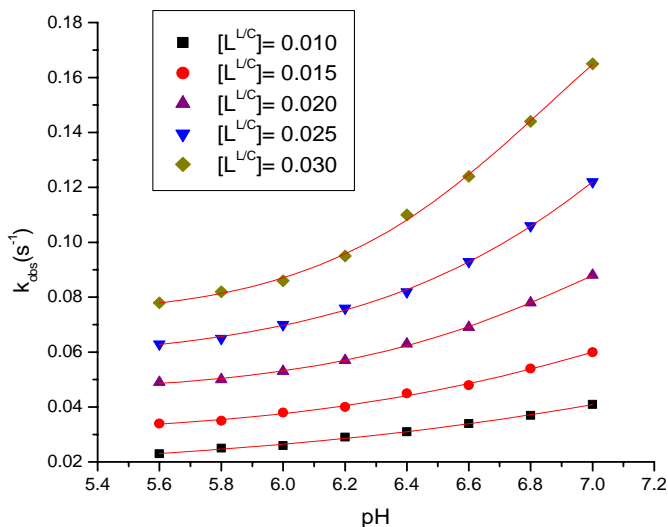


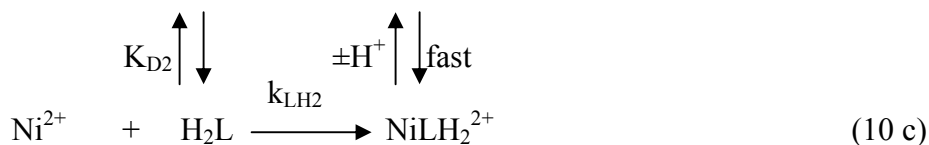
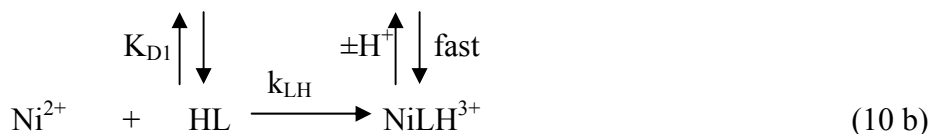
Fig 3. The pH dependence of  $k_{obs1}$ , at various ligand

concentrations, for the initial fast reaction of Ni(II) with  $L^{L/C}$  at 25 °C.

Plots of  $k_{obs1}$  vs the total concentration of  $L^{L/C}$  are linear with slope  $k_f$  and intercept  $k_d$ . Linear regression analysis yielded  $k_d$  values that were not statistically different from zero.

Resolution of Specific Rate Constants. The range of pH values investigated (5.6 – 7.0) was generally limited at the upper end to pH 7-7.4 due to concerns regarding the possible precipitation of  $Ni(OH)_2$ . At low pH values, a very large excess of the one reactant was required to force the reaction to completion. The rates of complex formation between  $L^{L/C}$  and the nickel ion are proportional to  $[L]_T$  and  $[M]_T$ . In addition they are functions of pH. Thus it is presumed that all variations with pH observed for  $k_f$  values are due to varying ratios of the existing species of  $L^{L/C}$  over the pH range of the study:  $L$ ,  $LH^+$  and  $LH_2^{2+}$ . The triprotonated ligand species,  $LH_3^{3+}$  was considered to have no significant kinetic contribution (electrostatic consideration) (see **Figure 2**). A possible kinetic Scheme for the fast complex formation step described by equation 10 could involve the steps:

Scheme 2



where  $K_{D1}$  and  $K_{D2}$  are the first and second deprotonation constants of  $L^{L/C}$  and have the values  $9.55 \times 10^{-11}$  M and  $2.95 \times 10^{-9}$  M, respectively. By appropriate substitution it can be readily shown that

$$k_f = \frac{k_L K_{D1} K_{D2} + k_{LH} K_{D2} [H^+] + k_{LH_2} [H^+]^2}{K_{D1} K_{D2} + K_{D2} [H^+] + [H^+]^2} \quad (11)$$

where  $k_f$  is the experimental second order rate constant and  $k_L$ ,  $k_{LH}$ , and  $k_{LH_2}$  are the resolved specific rate constants. Values of  $k_L$ ,  $k_{LH}$ , and  $k_{LH_2}$  were obtained by curve fitting (using the GRAFIT program<sup>32</sup>, see **Figure 4**) of  $k_f$  to equation 12,

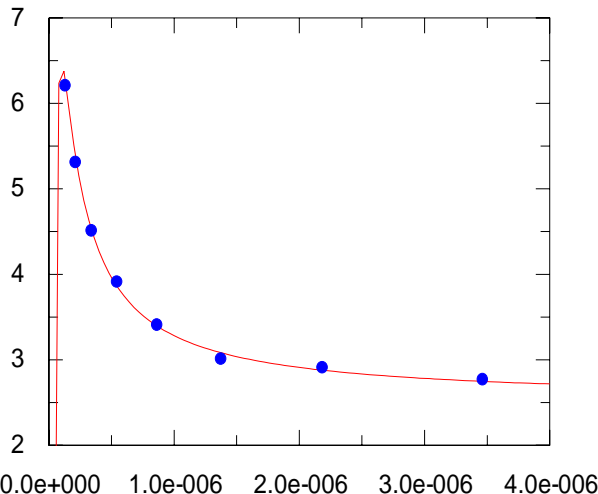
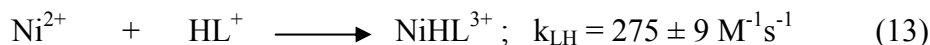


Fig 4. Plot of  $k_f$  vs  $[H^+]$  ( eq 12).The solid line is the calculated curve and the solid points are experimental.

$$k_f = \frac{k_L A + k_{HL} B [H^+] + k_{H_2L} [H^+]^2}{A + B [H^+] + [H^+]^2} \quad (12)$$

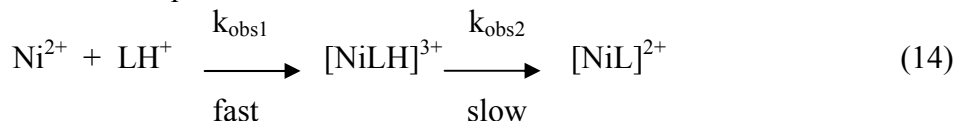
(  $A = K_{D1}K_{D2}$  and  $B = K_{D2}$ )

derived on the basis of eq 11 giving,  $k_L = -832 \pm 184 \text{ M}^{-1} \text{ S}^{-1}$ ,  $k_{LH} = 275 \pm 9, \text{ M}^{-1} \text{ S}^{-1}$  and  $k_{LH_2} = 2.52 \pm 0.03 \text{ M}^{-1} \text{ S}^{-1}$ . This finding indicates that L of the ligand  $L^{L/C}$  makes no kinetic contribution (same as  $LH_3^{3+}$ ) and that the only reactive ligand species are  $LH^+$  and  $LH_2^{2+}$ , with  $LH^+$  being 110 times more reactive than  $LH_2^{2+}$ . As a result, the above **Scheme** can now be approximated by eq 13



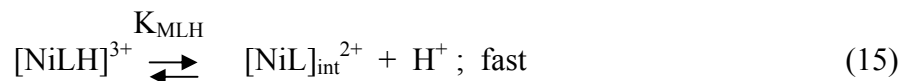
Slow process ( $k_{obs2}$ ). The kinetic measurements for the slow process were made using a conventional spectrophotometer under experimental conditions similar to that used for studying the fast reaction. The pH range was 6.8 to 7.9, with  $[Ni^{2+}] = 1.0 \times 10^{-4} \text{ M}$  in a 12 to 70 fold excess of  $L^{L/C}$  over  $Ni^{2+}$  ( $I = 0.2 \text{ M}$ ,  $25^\circ \text{C}$ ). The kinetics are nicely pseudo first-order and the rate is insensitive to  $[L^{L/C}]$ . A linear increase in rate with pH was observed.

The reaction scheme that can accommodate both the initial fast step and the subsequent slower one is shown in equation 14.



At room temperature this slow reaction proceeds with a half life of 5 hours around neutral pH. The reaction is attributed to the monoprotonated precursor complex,  $NiLH^{3+}$ . Further, because the

equilibrium constant for the deprotonation step (equation 14 ) has been found to be  $1.1 \times 10^{-7}$  M (see below), a substantial amount of  $\text{NiL}^{2+}$  is available for reaction. The conversion of  $[\text{NiLH}]^{3+}$  into  $[\text{NiL}]^{2+}$  is accompanied by a large increase in absorbance. The model that quantitatively describes the slow reaction involves a rapid proton dissociation followed by a rate-determining rearrangement step, equations 15 and 16.



The rate constant  $k_{\text{obs2}}$  can be quantitatively described as a function of the deprotonation constant,  $K_{\text{MHL}}$  ( $K_{\text{MLH}} = [\text{NiL}^{2+}][\text{H}^+]/[\text{NiLH}^{3+}]$ ) and the specific rate constant  $k_{\text{ML}}$  eq 17

$$k_{\text{obs2}} = \frac{k_{\text{ML}} K_{\text{MHL}}}{K_{\text{MHL}} + [\text{H}^+]} \quad (17)$$

Equation 17 can be rearranged to the double reciprocal, eq 18.

$$\frac{1}{k_{\text{obs2}}} = \frac{1}{k_{\text{ML}}} + \frac{1}{k_{\text{ML}} K_{\text{MHL}}} [\text{H}^+] \quad (18)$$

The double reciprocal plot of equation 18 was then applied, using the reciprocal of  $k_{\text{obs2}}$  and the calculated  $\text{H}^+$ . The linear regression analysis of equation 18 yielded  $k_{\text{ML}} = (4.2 \pm 0.2) \times 10^{-5} \text{ s}^{-1}$  and  $K_{\text{MHL}} = 1.1 \times 10^{-7} \text{ M}$ .

Understanding the product of this slow reaction presents a substantial challenge. Very commonly macrocyclic ligands first form complexes in conformations that do not produce the most stable final product. Consequently, slow reactions often follow macrocyclic complex formation. The question then becomes: is the slower reaction observed in this study a rearrangement reaction or is it the ring closure step? Since the rapid and slow processes in the system under study are so well separated in time, mass spectrometric studies were conducted to demonstrate the compositions of the intermediates and products. See **Scheme 1** which shows that the ligand loses a mole of water when macrocyclization occurs. During short reaction times (milliseconds to minutes) the nickel-containing intermediates were shown by mass spectrometry to contain only the beginning ligand,  $\text{L}^{\text{L/C}}$  (the mole of water is still in the ligand composition). On the time scales of hours, the mass spectrometry clearly establishes the appearance and eventual dominance of the macrocyclic complex. Therefore for this system, macrocyclization is slow compared to initial complex formation. The positive ion FAB-MS taken on solutions (pH  $\sim$  7.4) following complexation experiments shows, as the only nickel complex, a peak ( $m/z = 331.3$ ) corresponding to the nickel(II) complex with the fully ring closed macrocycle,  $\text{L}^{\text{C}}$ .

*Kinetics of formation of  $\text{Ni}(\text{L}^{\text{L}})^{2+}$ .* The Kinetics of the formation of  $\text{Ni}(\text{L}^{\text{L}})^{2+}$  were studied in the pH range 6.0-8.5 under conditions where (a) the total Ni(II) concentration is  $\geq 10$  times the total ligand concentration and (b) the total ligand concentration ( $\text{L}^{\text{L}}$ ) is  $\geq 10$  times excess over the total Ni(II) concentration.

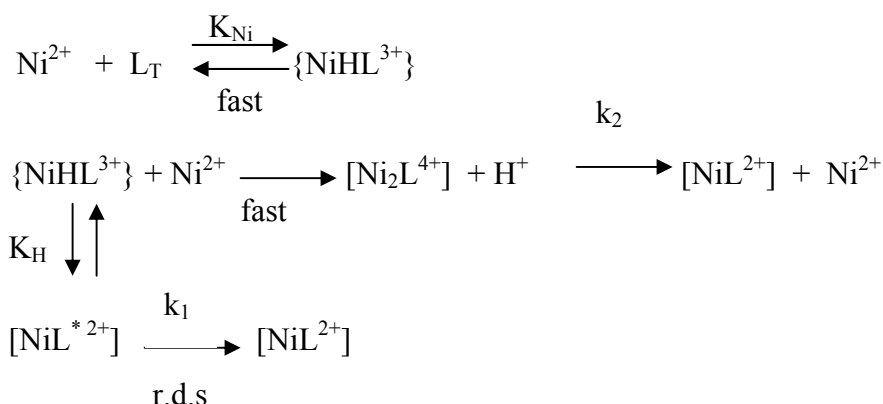
*Kinetics under conditions where  $[\text{Ni(II)}] \geq 10[\text{L}^{\text{L}}]$ .* When  $\text{L}^{\text{L}}$  was mixed with excess  $\text{Ni}^{2+}$  in aqueous solution, a biphasic reaction was observed in all of the experiments ( $\lambda = 360 \text{ nm}$ ). The initial

fast step ( 5 -30 s) is associated with an absorbance increase and the subsequent slower reaction ( 50 - 1000 s) to an absorbance decrease involving a relatively small spectral change. Only the initial fast step is deemed to be significant and therefore the apparent slower step will not be considered further in this work. The dependence of  $k_{\text{obs}}$  on  $[\text{Ni}^{2+}]_{\text{T}}$  was found to be polynomial, conforming to the expression ( at a given pH) given in equation 19.

$$k_{\text{obs}} = a + b[\text{Ni}^{2+}]_{\text{T}} + c[\text{Ni}^{2+}]_{\text{T}}^2 \quad (19)$$

A possible kinetic model for the complex formation described by equation 19 is shown in **Scheme 3**:

**Scheme 3.**



( $\text{L}_{\text{T}} = \text{L}, \text{HL}^+, \text{H}_2\text{L}^{2+}$ , etc)

In the presence of excess nickel(II) ion, the binding of a second nickel ion competes with completion of the chelation process. The second path, completion of chelation, dominates at higher pH where it is accelerated by proton removal. It can be readily shown that the experimentally observed rate constant,  $k_{\text{obs}}$  is that given in equation 20.

$$k_{\text{obs}} = k_0 + k_1 K_{\text{H}} K_{\text{Ni}} [\text{Ni}^{2+}] / [\text{H}^+] + k_2 K_{\text{Ni}} [\text{Ni}^{2+}]^2 \quad (20)$$

(assuming that, under the experimental conditions,  $K[\text{Ni}^{2+}] \ll 1$ )

Where  $k_0$ ,  $K_{\text{H}} K_{\text{Ni}}$ , and  $k_2 K_{\text{Ni}}$  = a, b, and c in equation 19, respectively ( $k_0$  corresponds to the spontaneous dissociation of  $[\text{NiL}^{2+}]$ ).

*Kinetics under conditions where  $[L^L] \geq 10[\text{Ni(II)}]$ .* The observed reaction of Ni(II) with  $L^L$  under the conditions where  $[L^L] \geq 10[\text{Ni(II)}]$  showed, to a large extent, a behavior similar to that observed for the system Ni(II)/ $L^{L/C}$ , as described above. In all cases, graphs of  $k_{\text{obs}}$  versus  $[L^L]$  were linear conforming to the expression given in equation 21.

$$k_{\text{obs}} = k_{\text{f}} [L^L] + k_{\text{d}} \quad (21)$$

The rate constants  $k_{\text{d}}$  (= intercept, Eq 21) were found to be  $\sim$  zero indicating that all reactions proceeded virtually to completion.

If it is assumed that Scheme 3 above also applies to this case, then for each reaction, the rate constant  $k_{\text{f}}$  (= slope, Eq 21) can be expressed as

$$k_f = \frac{k'_L K'_{D1} K'_{D2} + k'_{HL} K'_{D2} [H^+] + k'_{H2L} [H^+]^2}{K'_{D1} K'_{D2} + K'_{D2} [H^+] + [H^+]^2} \quad (22)$$

The equilibrium constants  $K'_{D1}$  and  $K'_{D2}$  are the first and second deprotonation constants of  $L^L$  and have the values  $4.47 \times 10^{-11}$  M and  $2.45 \times 10^{-9}$  M, respectively. Computer fitting of the rate expression, equation 22, yielded  $k'_L = (1.7 \pm 2.2) \times 10^3 \text{ M}^{-1} \text{ S}^{-1}$ ,  $k'_{HL} = 556 \pm 30 \text{ M}^{-1} \text{ S}^{-1}$  and  $k'_{H2L} = 29 \pm 2 \text{ M}^{-1} \text{ S}^{-1}$ . Specific rate constants obtained in this study for nickel(II) reacting with the various species of  $L^{L/C}$  and  $L^L$  in aqueous solution together with some structurally related linear and macrocyclic ligands are given in **Table 1**.

Table 1. Specific rate constants for nickel(II) reacting with various ligand species of  $L^{L/C}$  and  $L^L$  and other structurally related ligands in aqueous solution at 25 °C.

Ligand	specific rate constants ( $\text{M}^{-1} \text{s}^{-1}$ )			
	$k_{LH3}$	$k_{LH2}$	$k_{LH}$	$k_L$
$L^{L/C}$	...	$2.5 \pm 0.03$	$275 \pm 9$	...
$L^L$	...	$29 \pm 2$	$556 \pm 30$	$(1.7 \pm 1) \times 10^3$
trien <sup>a</sup>	...	97	9300	...
cyclam <sup>b</sup>			57	
Py[13]aneN <sub>4</sub> <sup>c</sup>	...	...	73	...

<sup>a</sup> Ref 33; <sup>b</sup>Ref 34; <sup>c</sup>Ref. 35

**Discussion—Equilibrium Studies.** In the absence of a complementary metal ion, the novel ligand,  $L^{L/C}$ , is expected to quickly condense with itself forming both a variety of rings and a variety of linear oligomers. It is a property of ligands of this kind that metal ions that are complementary in size and coordination geometry can serve as templates and cause the ligand to form a single product, a macrocycle that encloses the metal ion.<sup>36</sup> Because Schiff base formation is often rapid,  $L^{L/C}$  was expected to present an ever changing molecular composition during an equilibrium titration. Remarkably, a clean, reproducible titration curve was obtained with equilibration times between base additions of 20-60 seconds. Treatment of that data gave the distinctive set of  $pK_a$  values. The very similar values obtained for the linear ligand  $L^L$  add credibility to the  $pK_a$  values obtained for the self-reacting ligand  $L^{L/C}$ . No complications were expected in the case of the linear ligand  $L^L$ . Another remarkable observation—all four of the values determined for  $L^{L/C}$  are within a few tenths of a  $pK$  unit of those for the linear tetramine, triethylenetetramine (trien).

Formation constants were determined for several metal ions ( $\text{Cu}^{2+}$ ,  $\text{Hg}^{2+}$ ,  $\text{Ni}^{2+}$ ,  $\text{Zn}^{2+}$ ). For pertinence to the rate studies that will be discussed later, it must be remembered that the titrations were all carried out with 20-60s equilibration times. Under the conditions of the experiments,

LL/C forms two kinds of complexes,  $[M(LL/C)]^{2+}$  and  $[M(LL/CH)]^{3+}$ . The surrogate ligand LL, forms the expected complex with the neutral ligand  $[M(LL)]^{2+}$ , but the monoprotonated complex is found only for copper(II).

The binding constants  $\beta_{110}$  are remarkably similar for the two ligands, LL/C and LL, so it is apparent that both ligands chelate as linear tetradentate molecules on the time scale of the titrations. Clearly the ligand LL/C has not cyclized prior to binding to the metal ion in any case.

Kinetic Studies. Detailed kinetic investigations have been carried out only for the reactions of the nickel(II) ion with the two ligands LL/C and LL. The study of the LL/C system, reveals a pattern that is, in general, common for reactions between metal ions and macrocyclic ligands, but in detail the pattern is unusual. As would be expected, kinetic events occur in two time regimes, fractions of seconds and hours. A single well-behaved process on the fast time scale is accompanied by what appear to be two additional, but poorly resolved processes that involve only small color changes. The first rapid process is well behaved and reveals that, under conditions of these experiments, nickel(II) undergoes complex formation with only two of the possible ligand species,  $L^{L/C}H_2^{2+}$  and  $L^{L/C}H^+$ , and that reaction with the monoprotonated ligand is dominant. Significant concentrations of the fully deprotonated ligand species are not present at pH values sufficiently low to assure the solubility of  $Ni(OH)_2$ . The additional unexplained rate processes mentioned above may be associated with binding steps subsequent to the linking of the first  $L^{L/C}$  donor atom to the metal ion, however, there is a second likely source. These processes might reflect parallel reactions by partially self-condensed ligands; this additional possibility is unique to self-condensable ligands. Since the surrogate ligand does not show these complications, this second explanation is favored.

At neutral pH the fast reaction is solely due to the monoprotonated ligand,  $L^{L/C}H^+$ , forming the intermediate complex,  $[Ni(L^{L/C}H)]^{3+}$ . That species converts to the final product  $[Ni(L^C)]$  by what appears to be a classic pre-equilibrium proton dissociation step followed by rate determining ligand rearrangement (equation 12). Analysis of the data reveals a half life of about 5 hours and a proton ionization constant of  $1.1 \times 10^{-7} M$ . The acidity of this last proton (from  $L^{L/C}H^+$ ) has been increased by about 3 orders of magnitude by chelation of the ligand to the metal ion. From the equilibrium data, it is reasonable to suggest that the ligand has not undergone ring formation during the rapid reaction steps, but such a conclusion, based on those results alone, must be regarded as tentative at best. If the macrocycle had already formed, it would not be unusual to observe a very slow rearrangement reaction. Often the initial kinetic product of complex formation with macrocyclic ligands is not the thermodynamic product. A common readjustment is the slow inversion of coordinated quarternary nitrogen atoms. The strongest support, from the rate studies, for macrocyclization during the slow step is the large increase in absorbance in the region normally found for low spin square planar nickel(II) complexes.

The kinetics of binding of the surrogate ligand,  $L^L$ , supports the view that the slow reaction in the case of  $L^{L/C}$  involves ring closure. The ligand  $L^L$  displays only relatively rapid kinetic processes. For experiments conducted under the same conditions as those used in the study of  $L^{L/C}$ , i.e., in the presence of excess ligand, the  $L^L$  system behaved in a similar fashion to the rapid reaction in the  $Ni/L^{L/C}$  system. The specific rate constants for the ligand,  $L^L$ , are both larger than those for the more complicated ligand,  $L^{L/C}$ . For the simpler surrogate ligand, kinetic studies were also carried out in the presence of a large excess of nickel(II) ion. The excess nickel fostered formation of a 2:1 nickel:ligand complex at lower pH values.

Mass spectrometry has provided definitive proof that the macrocyclization occurs during the slow kinetic time regime. The difference in mass between the nickel(II) complexes with the linear tetradentate precursor ligand,  $L^{L/C}$ , and the macrocyclic ligand,  $L^C$ , is  $\sim 18$  mass units due to the loss of one water molecule. The dominant nickel(II) species at times approximating the completion of the rapid and slow processes, respectively, differ in mass by just that amount (see Figures 11 and 12 in attached manuscript). Therefore the slow reaction is ring closure, and it produces the macrocyclic complex within a precursor complex containing the switch binding ligand. It should be recalled that there is no corresponding slow kinetic process in the case of the ligand  $L^C$ . *These results prove the switch binding concept based on metal ion templating of specially designed ligands. Further, the dynamics of this first case have been revealed in substantial detail.*

Whereas no one has previously suggested the possible advantages of switch binding for ultra tight-binding ligands, a small number of examples exist in the literature where similar topological changes in ligand structure (linear to macrocyclic) have been observed.<sup>37-43</sup> In fact, these constitute examples of what we labeled the kinetic template effect many years ago.<sup>44</sup>

From the results reported here and the observations recorded in the literature it is clear that a slow macrocyclization reaction can be fostered following rapid binding of linear polydentate ligands. Thus the switch binding principle enjoys substantial generality. This opens the way to many new uses for the chemistry of ultra tight-binding ligands. Among the perceived advantages peculiar to these novel switch binding ligands is the ability of the rapidly binding ligand to invade strong metal ion binding sites and eventually remove metal ions as transportable species in which the metal ion is sequestered by a ligand of extreme binding affinity

## Switch Release

**Introduction.** Ultra tight-binding ligands, such as polyether cryptands, display fascinating coordination and host-guest chemistry.<sup>45,46</sup> The ability to selectively encapsulate guest atoms or molecules or to selectively extract specific metal ions has attracted considerably current attention,<sup>52,54</sup> particularly for potential applications in catalysis, analytical chemistry, separation techniques, and environmental remediation.<sup>5-7</sup> These powerful ligands can capture ionic and/or molecular guests under the most competitive circumstances such as selectively sequestering ions dispersed within mineralized sites, thereby separating certain metal ions from others, even capturing them at extremely low concentrations in dilute solution. However, applications of ultra tight-binding ligands for separations and for isolation procedures are limited by the very slow rates of ion release from the bound metal cryptate. The binding constants exceed those of ordinary ligands by  $10^6 - 10^9$ . However, they release their guest ion or molecule very slowly.<sup>52-54</sup> Furthermore, the time to reach equilibria may be even more lethargic since the rate of binding may also be slow.

The design of functional chemical devices is a major contemporary theme of supramolecular chemistry.<sup>55,56</sup> New molecular designs, based on structural modifications and functional group integration within a supramolecular architecture invite new dynamic features such as photo-, electro-, or iono-activity.<sup>57</sup> In order to make the best use of tight-binding receptors, such as cryptands, a photolabile group capable of fracturing the host cage might be introduced into the cryptand. Such a feature would be an o-nitrobenzyl moiety attached to one of the cryptand bridges, which will make it susceptible to rapid, irreversible conversion of the cryptand to a lariat macrocycle—within its metal complex. The newly formed ligand releases the encapsulated metal ion by accelerating the dissociation and association rates of the ligand and decreasing the equilibrium constant for metal ion/ligand binding. The o-nitrobenzyl group is well known for applications as a photoactivated deprotection group.<sup>58-66</sup> Generally, photochemically removable protecting groups are chromophores

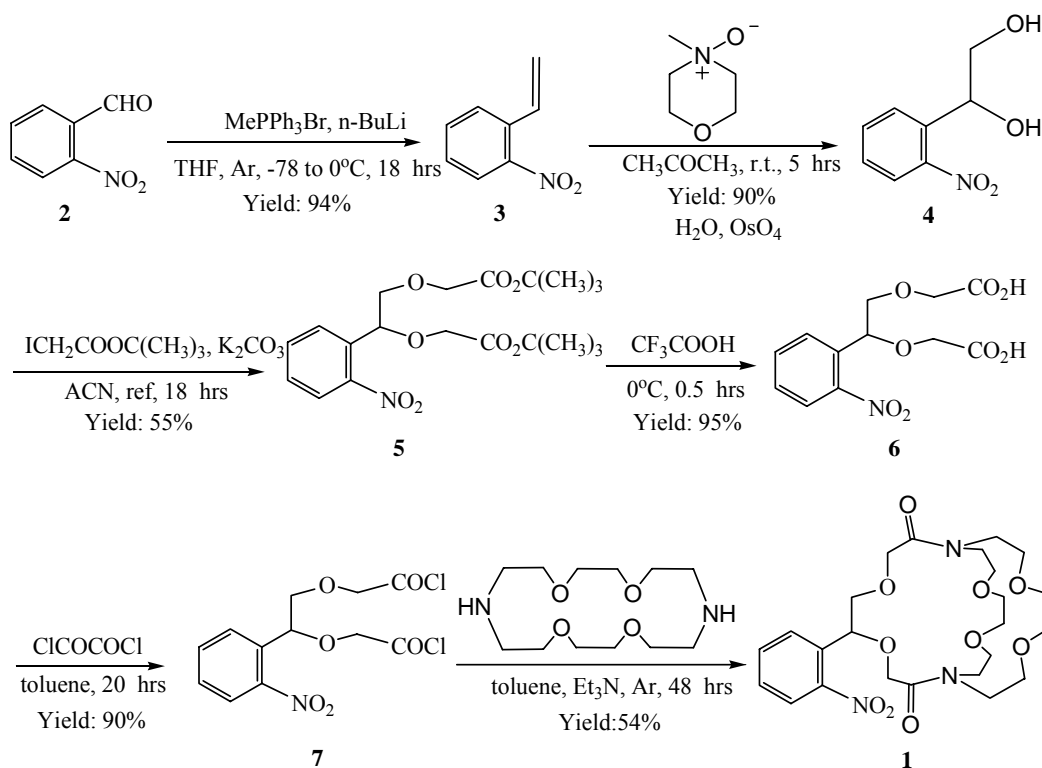
that are covalently bonded to a molecule as a means of releasing the protected moiety upon irradiation.<sup>23</sup> The photolabile groups are rapidly and irreversibly divested of the substrate moiety upon exposure to UV light. Such protecting groups find use not only in multistep syntheses but also in biophysical studies where they are often called “caged molecules” or “phototriggers”.<sup>59-62</sup> The o-nitrobenzyl group is the most frequently employed member of this type of cage or “phototriggers”.<sup>59,60,63-67</sup>

We have completed two syntheses of a photo-cleavable, ultra tight-binding polyether cryptand, originally designed by Lehn and Quinkert,<sup>68</sup> in which a photoactive o-nitrobenzyl group has been strategically placed on one of the bridges of the macrobicyclic structure. We have employed these photolabile cryptands to capture selected target metal ions to form cryptates and followed this by the photorelease of the metal ions from the cryptates by UV irradiation. The cryptand and its derivative cryptates are shown to be capable of rapid release of tightly bound metal ions through a “molecular switch” that replaces the normal metal-cryptand equilibration process with irreversible photolytic fragmentation of one of the cryptates bridging arms, producing an altered ligand that binds the metal ion less strongly.

**Results.** Cryptand **1** was synthesized according to the strategy outlined by Lehn and Quinkert<sup>68</sup>. A second synthetic strategy was also explored. The first involved a stepwise construction of the photo-cleavable bridge from 1-(2'-nitrophenyl)ethane-1,2-diol (**4**) by Williamson synthesis of the diacetyl *tert-butyl* ester **5**. Conversion of the diester to the diacid chloride **7** followed by coupling of the bridge to a 1,10-diaza-24-crown-8 macrocycle gave the cryptand **1**. A second strategy, where the capture of the metal is concomitant with the closure to produces the identical metal cryptate **16**. We have termed the macrocycle **8** a “lariat” macrocycle because of its ability to capture free metal ions (*vide infra*).

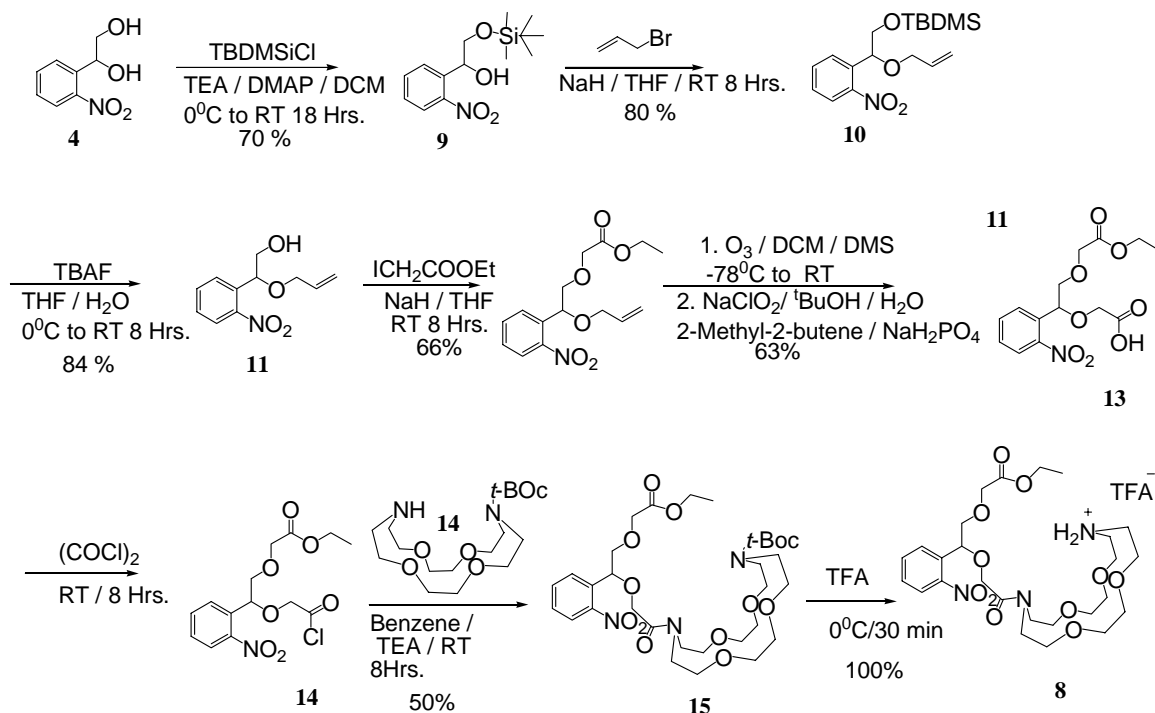
**Synthesis of tight-binding cryptand.** The cryptand 5-(2-nitrophenyl)-4,7,13,16,21,24-hexaoxa-1,10-diazabicyclo[8,8,8] hexacosane-2,9-dione (**1**) was synthesized as shown in Scheme 1 starting with the conversion of 2-nitrobenzaldehyde (**2**) to 2-nitrostyrene (**3**) by a Wittig<sup>69</sup> reaction with methyltriphenylphosponium bromide and nBuLi. Osmium tetraoxide dihydroxylation yielded 1-(2-nitrobenzyl)ethane-1,2-diol (**3**) in quantitative yield.<sup>70</sup> Alkylation of diol **4** with excess *tert-butyl* iodoacetate using K<sub>2</sub>CO<sub>3</sub> in acetonitrile yielded the di-*tert-butyl* ester **5**. Hydrolysis to the diacid **6** with TFA followed by reaction with oxylyl chloride gave the diacid chloride **7**, which was immediately coupled to 1,4,10,13-tetraoxa-7,16-diazacyclooctadecene in benzene/triethylamine to form cryptand **1** in an overall yield of 21% from **2**.

**Scheme 4.** The synthetic strategy for ultra tight-binding light-sensitive cryptands.



The synthesis of the dissymmetrically bridged “lariat” cryptand, 16-{2-[2-ethoxycarbonylmethoxy-1-(2-nitrophenyl)-ethoxy]-acetyl}-1,4,10,13-tetraoxa-7,16-diazacyclooctadecane (**8**), required a modified strategy (Scheme 5). The primary hydroxyl group of 1-(2-nitrobenzyl)ethane-1,2-diol (**4**) was protected as its TBDMSiCl monosilylated ether **9**. Allylation of the remaining secondary hydroxyl group with allyl bromide in THF gave the allyl TBDMS diether **10** in quantitative yield. Removal of the TBDMS protecting group with TBAF followed by etherification of the hydroxyl group on **11** with ethyl iodoacetate/NaH yielded the allyl ester **12**. The allyl group was converted to an aldehyde with ozone at  $-78^\circ\text{C}$  in dichloromethane followed by DMS to yield the aldehyde. This was then directly oxidized with sodium chlorite to give the mono acid **13**. The acid was converted to its acid chloride with oxlyl chloride and immediately coupled to the mono N-boc protected macrocycle, 1,4,10,13-tetraoxa-7,16-diaza-cyclooctadecane-7-carboxylic acid *tert*-butyl ester (prepared separately) in dichloromethane to yield **15**. The N-Boc protecting group on **15** was removed using trifluoroacetic acid (TFA) to give **8** in an overall yield of 10% from **4**.

**Scheme 5.** The synthetic strategy for light-sensitive “Lariat” macrocycle.



In principle, there are eight stereoisomeric cryptands, e.g., four diastereoisomeric pairs, for the unsymmetrical structure **1** due to the stereo center  $\alpha$  to the phenyl group and the four conformational arrangements of the carbonyl carbon-amide nitrogen (CO-N) bond. Both carbonyls may be oriented inward or both outward or one carbonyl inward and the other outward (two isomers). A mixture of stereoisomers was observed by  $^1\text{H}$  NMR indicating that the conformational interconversion is slow relative to the  $^1\text{H}$  NMR measurement timescale. However, the conformers could not be separated by conventional chromatographic methods. The benzylic methine protons for cryptand conformers appear as resolvable sets of doublets between 5.0-5.5 ppm but were not assigned to specific conformers. However, it is clear that the ratio of conformers varied with the solvent. This suggests that the cryptand is not a rigid, fixed structure, but may be somewhat malleable.

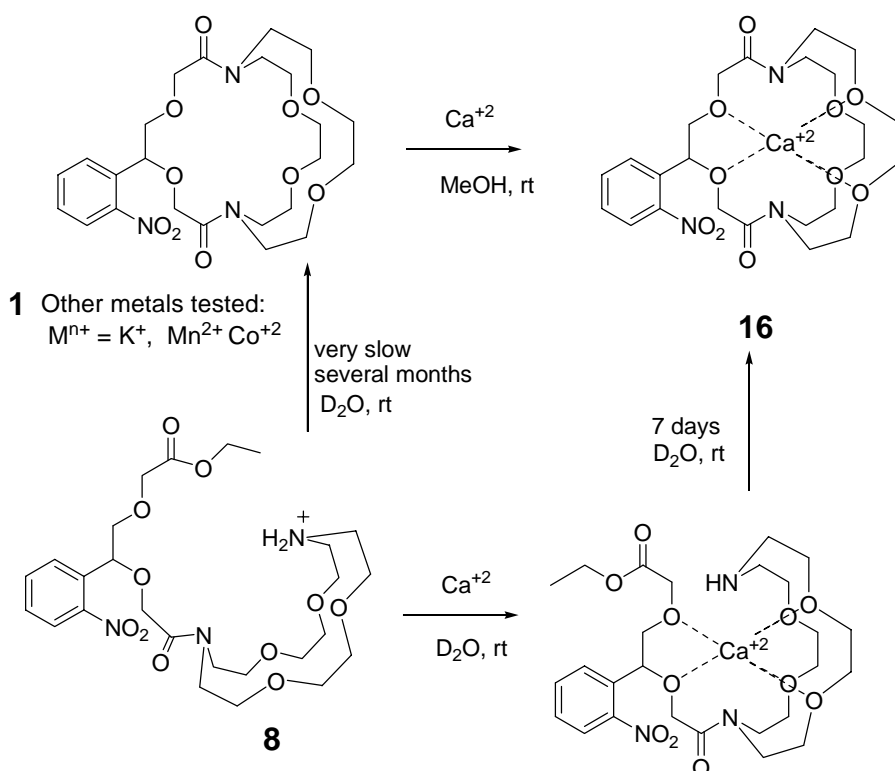
To test the flexibility of the cryptand, the effect of temperature on the position, appearance, and intensity of the signals for the individual conformers in  $^1\text{H}$  NMR was examined. The thermal interconversion of the conformers was observed beginning at 60 °C, where the methine and aromatic signals broadened finally merging at 100 °C to a much simpler spectrum. At this temperature, the spectrum indicates the presence of rapidly interconverting conformers. Cooling the sample to room temperature regenerated the original spectrum. These results clearly demonstrate the flexibility of the cryptand motif, an important and necessary feature for the encapsulation of guest metal ions in solution or similar environments.

Capturing of metals by cryptand:  $^1\text{H}$  NMR studies of the synthesis of calcium cryptate **16**. The addition of  $\text{Ca}(\text{SCN})_2$  to a solution of the cryptand was monitored by  $^1\text{H}$  NMR. When  $\sim 1$  eq. of  $\text{Ca}^{+2}$  was added, the  $^1\text{H}$  NMR simplified to a much less complex spectrum as noted above for 100 °C suggesting almost complete incorporation in less than 30 min. The subsequent spectra showed no change, indicating that equilibrium had been reached for the cryptate/cryptand complex (Scheme 6). Addition of 3 eq. of  $\text{Ca}^{+2}$  caused no further change as well. The  $\text{Ca}(\text{BF}_4)_2$  cryptate (115 mg, 14.3 mM) was also prepared by slow addition (24 h) of one equivalent of  $\text{Ca}(\text{BF}_4)_2$  and the cryptand in methanol at 25 °C into a solution of 5 mL  $\text{D}_2\text{O}$  containing 10  $\mu\text{L}$  acetonitrile as the internal standard ( $^1\text{H}$  NMR).<sup>71,72</sup> The molar absorption coefficient ( $\epsilon$ ) of  $\text{Ca}(\text{BF}_4)_2$  cryptate **16** in water at 265 nm was

determined to be  $3920 \text{ M}^{-1} \text{ cm}^{-1}$ .

Formation of the  $\text{Ca}^{+2}$  cryptate by the lariat macrocycle **8** was much slower. When **8** was dissolved in  $\text{D}_2\text{O}$  and two equivalents of  $\text{Ca}^{2+}$  were added, the  $^1\text{H-NMR}$  signals of the  $\text{Ca}^{+2}$  cryptate **16** slowly appeared ( $^1\text{H NMR}$ ). The conversion of **8** to **16** took seven days to complete! The cryptate, characterized by  $^1\text{H-NMR}$ ,  $^{13}\text{C-NMR}$  and mass spectral analysis, was identical to the cryptate **16** derived from **1**. The cyclization to the cryptand **1** in the absence of  $\text{Ca}^{2+}$  was even more sluggish. After several months at room temperature, only a trace of the cryptand was formed.

**Scheme 6:** Cryptand capture of  $\text{Ca}^{+2}$  and template closure of the “lariat” macrocycle **8** to cryptate **16** in  $\text{D}_2\text{O}$  at  $25^\circ\text{C}$ .

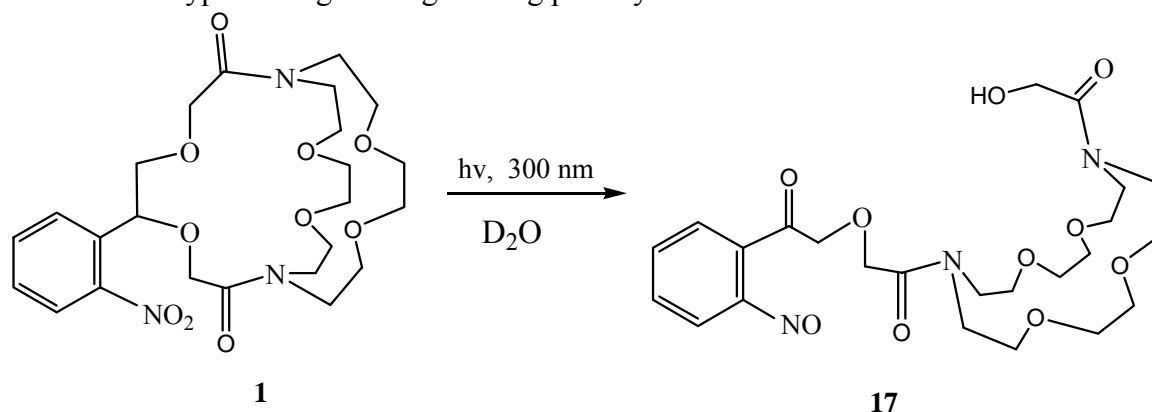


Photochemistry of the cryptand and the  $\text{Ca}^{+2}$  cryptate: Product studies. A 1.0 mM aqueous solution of cryptand **1** was photolyzed at 300 nm and the progress of the reaction monitored periodically by the  $^1\text{H NMR}$ . At partial conversion, the separation of the photoproducts from the starting cryptand by silica-gel column chromatography or HPLC was unsuccessful. However, at complete conversion the photoproducts could be analyzed by their  $^1\text{H-NMR}$ , IR and UV-visible spectra. During the photolysis, the  $^1\text{H NMR}$  signals for the four diastereomeric benzylic proton signals between 5.0-5.5 ppm (*vide supra*) decreased and new signals at 4.77, 4.2, and 4.1 ppm appeared. The new signals were assigned to the three methylene peaks of the photodegraded macrocycle **17** (a, b, and c in Scheme 4), consistent with those expected for the ring opened cryptand.

A 1 mM  $\text{D}_2\text{O}$  solution of the  $\text{Ca}^{+2}$  cryptate **16** was also photolyzed at 300 nm and the  $^1\text{H NMR}$  recorded every 30 min of photolysis. The decrease in the benzylic peaks at 5.2 ppm of the cryptand was used to determine the reaction efficiency. The ring cleavage proceeded to completion at approximately the same rate with or without  $\text{Ca}^{2+}$  present (i.e., **1** and **16**) and the reactions proceeded with very nearly the same efficiencies. Mass spectral studies further supported the release of calcium

from the cage after the photolysis by the disappearance of the 652 amu of the  $\text{Ca}(\text{BF}_4)_2$  cryptate and the appearance of a new peak at 544 amu which corresponds to the photoproduct, macrocycle **17** (Scheme 7). The IR spectra of the products recorded after photolysis clearly showed the formation of a new carbonyl absorption ( $1711\text{ cm}^{-1}$ ) and the presence of a hydroxyl group ( $3407\text{ cm}^{-1}$ ) also, in accord with the structure of the ring-opened photolysis product. During photolysis, the UV absorption at 265 nm decreased and a new peak appeared at 310 nm, further supporting the formation of the nitroso keto alcohol of the photoproduct (Scheme 7).

**Scheme 7:** Cryptand ring cleavage during photolysis in water at 300 nm.



Mechanistic studies of calcium cryptate photolysis. A 3 mL solution of 0.1 mM  $\text{Ca}(\text{BF}_4)_2$  cryptate in  $\text{D}_2\text{O}$  was photolyzed at 300 nm and aliquots analyzed every minute for 10 min by UV-visible spectroscopy. As the photolysis time increased the peak at 265 nm decreased in intensity and a new peak at 310 nm appeared (Table 2)

Photolyses that were carried out with more intense exposures produced a new absorption at 250 nm along with a more rapid disappearance of the primary photoproduct signal at 311 nm. The absence of an isosbestic point suggested that there is at least one additional, UV-silent intermediate in the reaction pathway.

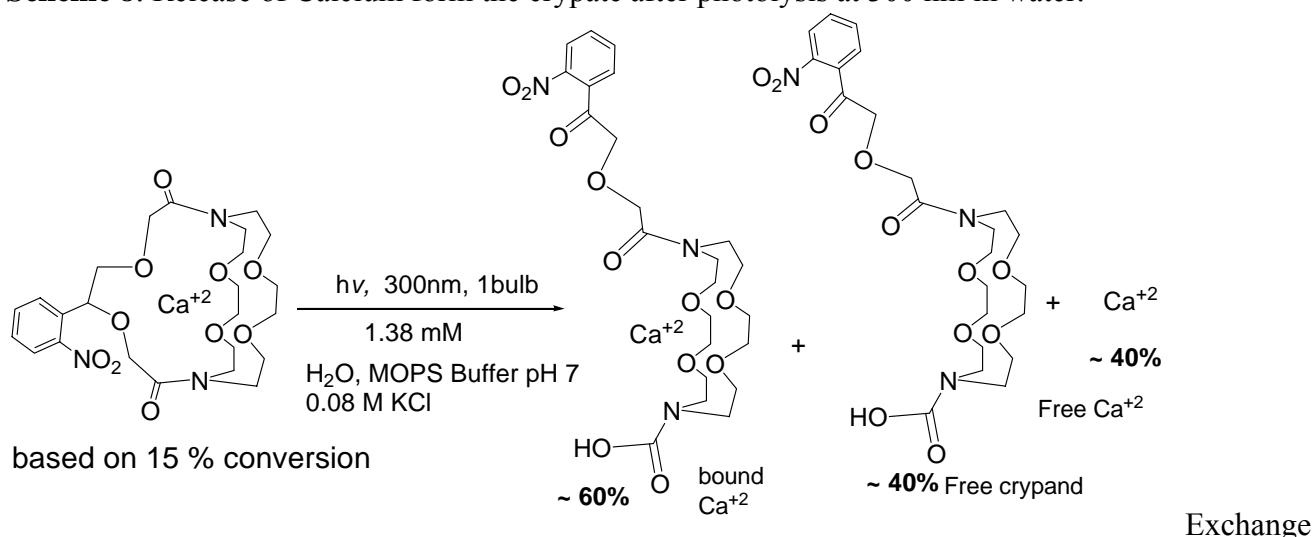
**TABLE 2:** UV-visible absorptivity of  $\text{Ca}(\text{BF}_4)_2$  cryptate ( $10^{-4}\text{ M}$ ) photolysis mixtures of **17** irradiated at 300 nm for 400 s and monitored at 30 sec. intervals.

Time (s)	A at $\lambda_{265\text{ nm}}$	A at $\lambda_{310\text{ nm}}$
0	1.148	0.40
30	1.132	0.43
90	1.101	0.50
160	1.073	0.56
210	1.046	0.60
270	1.022	0.65
330	0.992	0.70
400	0.971	0.73

Quantum efficiencies for  $\text{Ca}(\text{BF}_4)_2$  cryptate disappearance. The quantum efficiency of  $\text{Ca}(\text{BF}_4)_2$  cryptate disappearance was determined in water at 300 nm using the potassium ferrioxalate ( $\text{K}_3\text{Fe}(\text{C}_2\text{O}_4)_3^{2-}$ ) actinometry (0.02 mE /h).<sup>73</sup>

Quantitative determination of  $\text{Ca}^{+2}$  release using a calcium-specific electrode. When one equivalent of  $\text{Ca}(\text{BF}_4)_2$  is stirred in the presence of the cryptand, 95% of the  $\text{Ca}^{+2}$  is incorporated rapidly into the cryptand. The calcium cryptate was photolyzed in  $\text{D}_2\text{O}$  at 300 nm and the release of calcium was monitored using a calcium electrode. A 2 mL solution of  $\text{Ca}(\text{BF}_4)_2$  cryptate (13.8 mM  $\text{Ca}(\text{BF}_4)_2$ ) was added to a solution of cryptand; MW 740) in 17.6 mL of MOPS buffer solution (pH 7) containing 0.4 mL of 4M KCl (ionic strength adjustor). A 3mL aliquot of the cryptate solution was placed in a cuvette and photolyzed at 300nm (one lamp in the Rayonet chamber) for 0, 1, 2, 4, and 6 min and the calcium electrode signal in mV was recorded. The  $[\text{Ca}^{+2}]$  released from the cryptate was determined along with the quantum efficiency of the  $\text{Ca}^{+2}$  release. Potassium ferrioxalate was used as an actinometer for determining the light output<sup>73</sup> From these measurements, it was determined that, 40% of the  $\text{Ca}^{+2}$  was released relative to the total disappearance of the cryptate. The remaining 60% of calcium was bound to the opened macrocycle crown ether as depicted in the Scheme 8.

**Scheme 8:** Release of Calcium form the cryptate after photolysis at 300 nm in water.



of calcium for potassium was also explored. When  $\text{Ca}^{+2}$  cryptate was dissolved in a solution containing KCl and MOPS buffer at pH 7 and stirred for 24 hrs at room temperature in the dark, an equilibrium was established in which 19% of the calcium was replaced (Scheme 9).

**Scheme 9:** Ion displacement of potassium for calcium at pH 7 in MOPS buffer at 25°C.

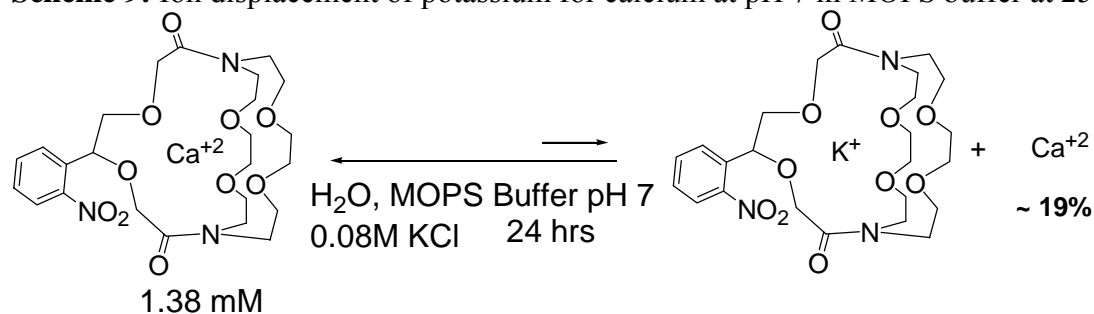


**TABLE 3:** Photochemical release of Calcium from its cryptate (300 nm).

Time (min.)	mV	$\text{Ca}^{+2}$ released in $\mu\text{moles}$	% of $\text{Ca}^{+2}$ released (dark)	% of $\text{Ca}^{+2}$ released (photolysis)
0	-8	0.088	0	0
1	-7	0.098	0.7	14.70

2	-5	0.120	2.4	22.53
4	-3	0.147	4.5	27.60
6	-2	0.163	5.8	37.47

A 1.38 mM cryptate buffer solution was photolyzed at 300 nm and the signal from the  $\text{Ca}^{+2}$  electrode was recorded in mV.  $\text{CaCl}_2$  was used to calibrate the electrode; the slope of the calibration curve ( $22.5 \text{ mV}^{-1}$ ) was determined from a plot of  $\log [\text{conc}]$  vs. electrode signal in mV.

A 200 mL aliquot of the photolyzed solution was added to 2.8 mL of water and the OD at 265 nm was determined. The concentration of the cryptate was calculated using the absorptivity ( $\epsilon$ ) value of  $3920 \text{ M}^{-1}\text{cm}^{-1}$ . The conversion and quantum efficiency were determined.

**TABLE 4:** Photochemical opening of the calcium cryptate (300 nm).

Time (min.)	A at $\lambda_{265 \text{ nm}}$	Remaining Cryptate (mmoles)	Ring-opened cryptate ( $\mu\text{mole}$ )	% of cryptate disappearance
0	0.361	1.38	0.266	0
1	0.344	1.31	0.294	4.70
2	0.324	1.23	0.361	10.24
4	0.305	1.16	0.440	15.50
6	0.308	1.17	0.490	14.54

A 1.38 mM cryptate buffer solution at pH 7 was photolyzed at 300 nm and the absorption changes monitored at 265 nm.

The quantum efficiency for the disappearance of cryptate and the appearance of the  $\text{Ca}^{+2}$  were determined using potassium ferrioxalate actinometry.<sup>73</sup> A plot of concentration of the cryptate (disappearance) and  $\text{Ca}^{+2}$  (appearance) were linear versus the irradiation time (Figure 5). The photolysis was carried out in such way that the conversion never exceeded 20%.

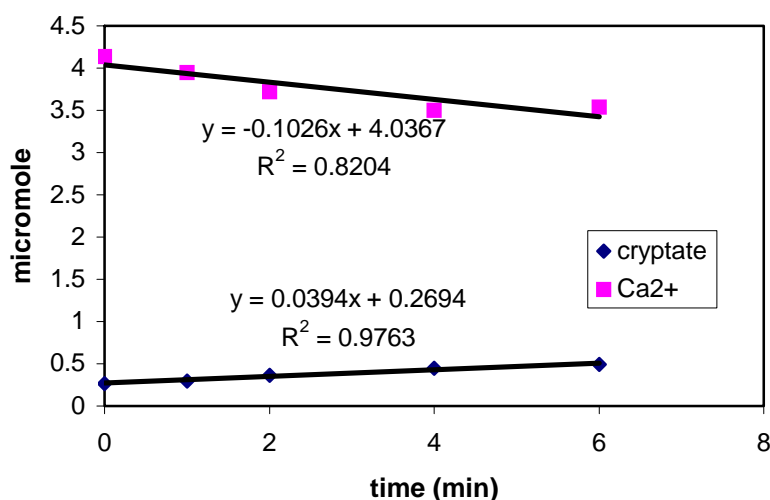


**FIGURE 5:** Measurement of quantum efficiencies for the disappearance of cryptate and release of calcium for photolysis at 300 nm.  $\phi_{\text{dis}}$  (disappearance of cryptate) =  $0.0062\text{mM}/\text{min}/0.022 \text{ mE}/\text{min} = \mathbf{0.28}$ ;  $\phi_{\text{release}}$  ( $\text{Ca}^{+2}$  release) =  $0.0024\text{mM}/\text{min}/0.022\text{mE}/\text{min} = \mathbf{0.12}$ .

<sup>1</sup>H NMR study of calcium cryptate. Quantum efficiencies were measured by NMR in methanol. A solution of  $6.35 \times 10^{-2}$  mM  $\text{Ca}^{+2}$  cryptate was prepared in methanol-d<sub>4</sub>, irradiated for 40 min (Fig. 6). The quantum efficiency of the appearance of the product, the opened macrocycle **19**, was determined to be 0.060 and the disappearance of the cryptate was 0.080.

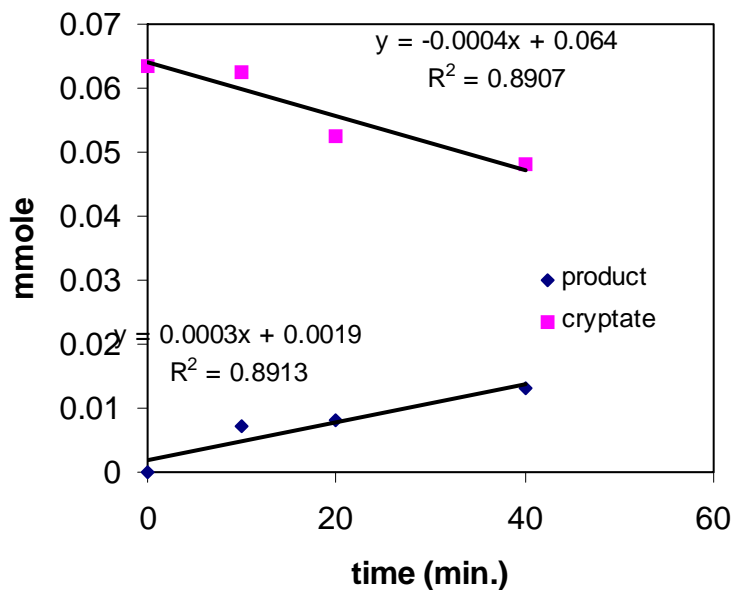
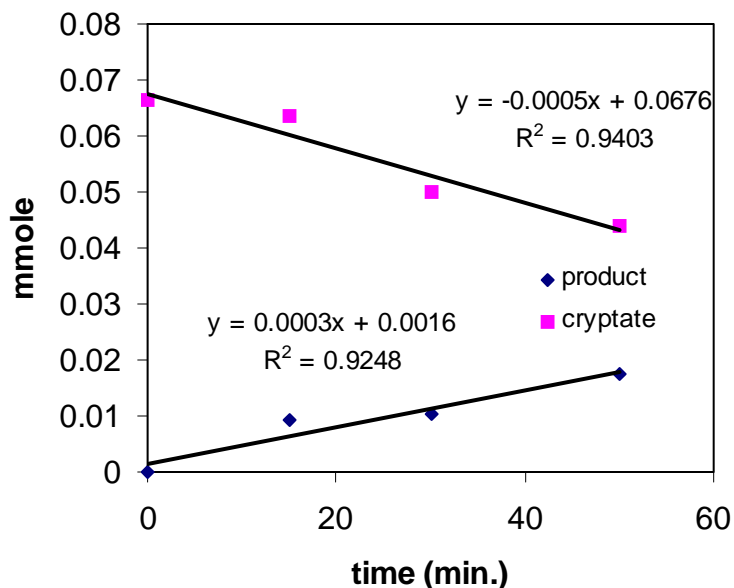


Figure 6. Quantum efficiency in Methanol

Quantum efficiencies were also measured by <sup>1</sup>H NMR in D<sub>2</sub>O  $6.65 \times 10^{-2}$  mM solution of  $\text{Ca}^{+2}$  cryptate was prepared in D<sub>2</sub>O, irradiated for 50 min. The quantum efficiency of the appearance of the product, the opened macrocycle **19**, was determined to be 0.060 while disappearance of the cryptate was 0.099 (Fig. 7).



**Figure 7.** Quantum efficiency of disappearance of cryptate in water.

The quantum efficiency was also determined by  $^1\text{H}$  NMR in methanol.  $6.35 \times 10^{-2}$  mM Ca-cryptate was prepared in methanol- $d_4$ , irradiated and monitored for 40 min. The quantum efficiency of the disappearance of the cryptate was 0.18 from the plot of concentration change vs irradiation time (Fig. 8).

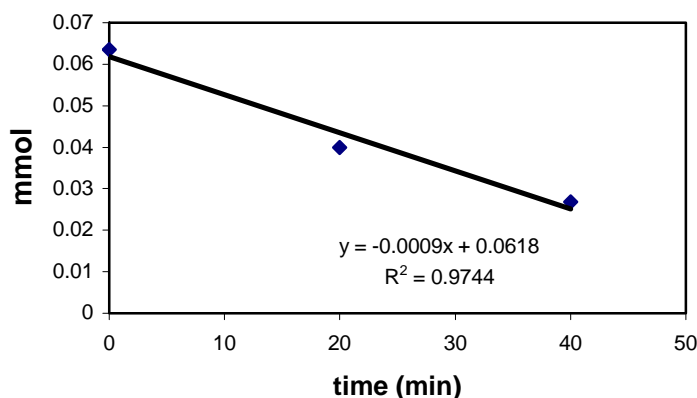


**Figure 8.** Quantum efficiency of disappearance of cryptate by HPLC

### Discussion.

The stepwise synthesis of a photo-cleavable, switch-release polyether cryptand 5-(2-nitrophenyl)-4,7,13,16,21,24-hexaoxo-1,10-diazabicyclo[8,8,8]hexacosane-2,9-dione (**1**) is shown in Scheme 4. This strategy places a photoactive *o*-nitrobenzyl group in a position to serve as the photoactivator for cleavage of one of the bridges of the macrobicyclic structure. This strategy closely follows that reported earlier by Lehn and Quinkert.<sup>68</sup>

A second strategy is also reported in which a true “catch and release” protocol is employed for capture of selected metal ions. In this strategy, the metal ion participates in the closure of the *N*-substituted 7,16-diazacyclo[8.8] macrocycle (**8**) by a template closure of the third bridge to produce the identical cryptate (i.e., **16**) formed from metal ion sequestering by cryptand **1**.

*Synthesis of the Lariat macrocycle.* Synthesis of the lariat macrocycle, 16-{2-[2-ethoxycarbonylmethoxy-1-(2-nitrophenyl)-ethoxy]-acetyl}-1,4,10,13-tetraoxa-7,16-diazacyclooctadecane (**8**) began with the same nitrophenyl ethan-1,2-diol employed in the synthesis of **1**. To differentiate the two sides of the glycol, selective protection of the  $1^\circ$  alcohol was performed using TBDMSiCl followed by allylation of the  $2^\circ$  alcohol. The allyl ether was obtained in quantitative yield. Removal of the silyl protecting group followed by etherification with ethyl iodoacetate gave an allyl ester, which was converted with ozone at  $-78^\circ\text{C}$  to an acid-ester. By introducing dissymmetry to the bridging arm, single sided attachment to the macrocycle could be accomplished. Thus, the acid group was coupled to 1,4,10,13-tetraoxa-7,16-diaza-cyclooctadecane to yield the lariat macrocycle **8**.

*Structural features of the cryptand-cryptate system.* The four diastereoisomeric pairs possible for the racemic cryptand **1** were observable by  $^1\text{H}$  NMR indicating that conformational interconversions are relatively slow on the  $^1\text{H}$  NMR timescale. It is clear that the ratio of conformers varies with solvent and temperature. Raising the temperature causes the isomers to interconvert more rapidly and at  $100^\circ\text{C}$  the position and intensity of the individual signals coalesce in the  $^1\text{H}$  NMR spectrum. The mixture returns to the original ratio of isomers upon cooling to room temperature.

*Effects of metal on the structure and chemistry.* When one equivalent of Ca (BF<sub>4</sub>)<sub>2</sub> is stirred in the presence of the cryptand, 95% of the Ca<sup>+2</sup> is incorporated rapidly into the cryptand. Furthermore, introduction of the metal ion collapses the mixture of isomeric cryptands to a single structure or conformer of the metal cryptate as shown by <sup>1</sup>H NMR. That conformer has both carbonyls oriented away or “out” relative to the metal ion.

Capture of Ca<sup>+2</sup> by the N-substituted 7,16-diazacyclo[8.8] macrocycle **8** was also examined. When **8** was dissolved in D<sub>2</sub>O containing two equivalents of Ca<sup>2+</sup> the product cryptate appear slowly requiring seven days for complete conversion to the same cryptate obtained from Ca<sup>+2</sup> and **1** as shown by <sup>1</sup>H-NMR, <sup>13</sup>C-NMR and mass spectral analysis. In the absence of Ca<sup>2+</sup> cyclization was extremely slow, taking months to form any measurable quantities of the cryptate.

*Photochemistry.* Photolysis of the Ca<sup>+2</sup> cryptates in water result in only 40% release of the Ca<sup>+2</sup> based on the disappearance of the cryptate. The remaining 60% of Ca<sup>+2</sup> is bound to the opened macrocyclic crown ether. This observation indicates that the metal ion has been made available for precipitation, binding to stronger ligands, diffusion through MEMBRANES, etc.

The quantum efficiencies for the disappearance of the cryptate and cryptand are solvent dependent. Thus, in MeOH, the disappearance efficiency of the cryptand is 0.18 whereas the quantum efficiencies for appearance of the opened macrocycle are 0.060 and the disappearance of the cryptate, 0.099 in H<sub>2</sub>O. On the other hand, the efficiencies were the same for both the cryptate and cryptand under otherwise identical conditions. Thus, the metal ion does not appear to influence the efficiency of ring opening, at least for Ca<sup>+</sup>

## RELEVANCE, IMPACT AND TECHNOLOGY TRANSFER

### The Soil Poultice.

- a) **Relationship to Critical DOE EM problems.** Many of the multitude of DOE contamination issues specifically involve compounds or ions of the metallic elements, ranging over actinides, fission products, RCRA metals, and including strontium and cesium. In extreme cases, contamination involves circumstances that are unmanageable with the tools based on existing technologies. This program focused on fundamental molecular principles that are expected to be foundational to the development of new scientific tools that will overcome this limitation. They will spawn powerful new science-based tools and new technologies that will greatly facilitate the management of these hazardous wastes. The broad category of new molecular tools includes the molecules, called ligands, that are most powerful at binding to metal ions. The known versions and modes of application of these most powerful, or tight-binding, ligands react too slowly to be broadly useful in, for example, environmental cleanup. This program explored two pathways to making slowly reacting, tight-binding ligands useful in separations: the soil poultice and the use of molecular switching in place of the natural slow rates of reaction of metal ion derivatives of tight-binding ligands.

As explained in the discussion of the Soil Poultice in the Introduction, by copying the way bacteria extract iron from the soil, we have shown how to design a 2-component material that, when applied to a contaminated surface (e.g., wall, floor, or the soil), will selectively adsorb the contaminating substance for which it is designed. Then the material is mechanically removed (e.g., scrape it off), leaving a decontaminated surface. This is a seminal separations science design and it has been necessary to create the underlying foundations by fundamental research on the properties of special

polymers called MIPs (molecularly imprinted polymers) that bind by non-covalent (so-called supramolecular) interactions. MIPs are imprinted when the polymers are made by letting them polymerize around the species for which they are to be imprinted. One then removes the imprint, leaving a “site” in the polymer that will recognize the imprinting molecule or ion when one comes along. The trick is making non-covalent interactions strong enough to pick up significant amounts of the imprint. Work in this project has successfully achieved proof of concept, and first steps were taken in an effort to apply early results to the sequestration of mercuric ion.

Accomplishments in this work include:

- ✓ Learning how to organize simple hydrogen bonds so that they rebind imprints to MIPs significantly.
- ✓ Learning how to make minor coordinate bonds rebind imprints to MIPs significantly
- ✓ Exploiting the simultaneous use of hydrogen bonds and complementary electrostatic charges to get very high rebinding of imprints to MIPs through synergism
- ✓ Exploiting the simultaneous use of hydrogen bonds and minor coordinate bonds to get very high rebinding of imprints to MIPs through synergism
- ✓ Learning the relationships between MIPs polymer composition and morphology for systems of these kinds
- ✓ Proving that imprint rebinding can be effective when using water as the solvent during the waste removal process
- ✓ Demonstrating the dual selectivity that comes from using a ligand that selectively binds to the contaminating metal ion and using MIPs that select for the corresponding metal/ligand complex.
- ✓ Found the MIPs to be extremely durable, giving promise of extended lifetimes while in use.
- ✓ Demonstrated the selectivity in binding Hg(II) by a ligand suitable for soil poultice studies.
- ✓ Discovered a geometrically specific selectivity between metal complexes with ligands that chelate as geometric isomers.

In conclusion, the scientific foundations have been laid for the design of specific soil poultice applications. Prior to the expiration of the program reporting here, it was only possible to demonstrate the first stage of the dual selectivity for the first metal ion of specific interest, mercury(II)

- b) **How Can These Results Be Used?** It will be possible to use the principles uncovered in these studies to design MIPs with strong rebinding capacities for contaminating ions of interest to DOE. Further, use can be made of insights obtained in these studies into the molecular structures most likely to enjoy strong rebinding abilities. As indicated above, the proposed new technology should open new avenues to the treatment of contaminated surfaces.
- c) **Bridging the Fundamental Science/Applications Gap.** This work has involved fundamental science, but it has been directed at building the understanding necessary to apply MIPs to contamination problems, following a model found in nature—the extraction of iron from the soil by microbes. The results show how to optimize polymer properties that are very important to the building of applications on MIPs. A gap remains because no prototypic application has been taken to completion.
- d) **Impact of Work on Individuals, Institutions, Etc.** There are broad interests in using Molecularly Imprinted Polymers, mostly in separations science, catalysis, or molecular devices. The

fundamental science revealed in these studies will benefit all areas where applications might be attempted, because we have shown how to design MIPs having large rebinding capacities using only supramolecular interactions with their target molecules. The fact that these supramolecular interactions form and let go fast makes them especially useful in such applications as chemical separations.

- e) **Is Scaleup Needed? Applied Impact?** Since the work has been, for the most part, limited to the fundamental science, issues of scaleup are not appropriate.
- f) **Improved Capabilities of Scientists.** The scientists involved have gained a deep appreciation for a relatively young sub-field of polymer science (MIPs) and they will doubtless use this knowledge in future work. For example, a postdoc who worked on this project is considering using MIPs in chiral catalysis—the field recognized in the 2002 Nobel Prize in Chemistry.
- g) **Advanced Understanding of Area.** This work has made a very substantial contribution to the understanding of the binding capacity and selectivity of non-covalent (supramolecular) MIPs. This provides foundations that can be used to develop new separations technologies and similar applications. Previously, the area did not look promising because no one knew how to get substantial rebinding of imprints to non-covalent MIPs.
- h) **What are the Remaining Hurdles?** To apply these results to DOE EM problems it would be necessary to focus on a specific carefully chosen separations problem, such as removing mercury, first from controlled surfaces and eventually from the soil. That prototypic system should be pursued to the stage of bench top applications at the very least. The issue least understood is selectivity of the MIPs and it may be necessary to do basic science on that issue.
- i) **Have Others Shown Interest?** No government agencies or private enterprises have expressed interest in the results

## Molecular Switching to Provide Rapid Rates

### j) **Relationship to Critical DOE EM problems**

As pointed out in the Introduction and in the Methods and Results sections, the most powerful ligands could be applied to separations technologies if it were possible to make the reactions of those ligands proceed substantially more rapidly. This should make it possible to extract selected target ions (e.g., actinides,  $\text{Cs}^+$ ,  $\text{Sr}^{+2}$ ,  $\text{Hg}^{+2}$ , etc.) from mineral deposits, surface contaminants, very dilute media or under other challenging conditions. The overcoming of this challenge requires the replacement of the natural equilibration process in which any ligand ordinarily binds with a metal ion under any conditions. The work summarized here has pursued the replacement of that natural equilibrium process with molecular switching processes. The issue is a fundamental science matter—how can something that naturally happens very slowly be made to happen rapidly? We have used the principles of coordination chemistry and supramolecular chemistry to define fundamental research that promised to accomplish this task. The underlying challenge is proving that such molecular switching mechanisms exist and we have accomplished this task for both the switch binding and switch-release processes. That is, proof of concept has been achieved. Further the two processes (switch binding and switch release) have been combined and demonstrated in a specific individual ligand system.

Detailed studies of two generations of ligand types have been studied in the case of Switch binding, (1) a linear tetradentate ligand that closes on itself around the targeted metal ion by the Schiff base reaction to form a macrocycle, an example of a tight-binding ligand, and (2) a lariat macrocycle

that closes a second ring around a targeted metal ion by amide formation, forming a cage-type of ligand called a cryptate. Both of these systems have proven the concept that relatively weak, but rapidly reacting ligands, can be made to react around a targeted metal ion to form slow reacting, but more tightly binding ligands of greater topological complexity (linear to big ring in example (1) and ring with arm to cage in (2)). The generation 2 ligand system has been the subject of Switch-release studies and it has been shown that a specially designed cage-like cryptate ligand bound to a metal ion can be broken photolytically to a lariat macrocycle, leading to release of the metal ion. In a highly significant example, a lariat macrocycle has been designed to undergo both molecular switching processes. In the presence of a metal ion, the lariat arm reacts and closes to form a cage enclosing the metal ion. Upon exposure to light, the cage is broken and returned to a lariat macrocycle structure. These studies have very clearly proven the reality of the concept.

Specifically achievements are:

- ✓ Two examples, generations 1 and 2, have proven the concept that ligands can be specifically designed to convert from weaker, rapidly binding structures to stronger, slow binding, so-called tight-binding, ligands upon linking to specific metal ions.
- ✓ One example, generation 2, has proven the concept that ligands having the tightest binding structures can be converted to weaker binding ligands while bound to metal ions.
- ✓ The photo switch-release of calcium ion from a cryptate ligand is rapid and the metal ion has no noticeable effect on the photo release.
- ✓ The expectations of photo-release are fully realized in experiments showing that the product lariat macrocycle complex of  $\text{Ca}^{+2}$  has an equilibrium constant of approximately unity whereas the (unmeasured) equilibrium constant for the parent cryptate of  $\text{Ca}^{+2}$  would be expected to be several factors of ten under the same conditions.
- ✓ For both generations 1 and 2, the so-called template switch binding does indeed involve rapid chelation of the lower affinity starting complex followed by slow conversion, in situ, to the tighter-binding ligand.
- ✓ But for both generations 1 and 2, the rate of the in situ ligand conversion is surprisingly slow and more rapid intramolecular ring closure would be good.
- ✓ The synthesis, characterization and demonstration of a single molecular system that undergoes both switch binding and switch-release constitutes complete success in demonstrating the concept—albeit each step can only be performed one time in this particular system

- k) **How Can These Results Be Used?** Because of the success of these “proof of concept” switch binding and/or release studies, new conceptual capabilities have been created. The concepts can be used in any circumstance where the relative rates of binding and/or release of metal ions (or more generally guests) need to be accelerated in order to facilitate a ligand/metal ion interaction. This can have value for separations methodologies, sequestering of contaminants, and other scenarios wherein metal ion (guest) control is necessary.
- l) **Bridging the Fundamental Science/Applications Gap.** This research and the corresponding results are fundamental science. As such, the results do not cross the gap between basic science and its applications. In order to bridge the gap, the scientific results need to be applied to specific examples, such as the switch binding of ligands to contaminants in the field and switch release at the point of disposal.
- m) **Impact of Work on Individuals, Institutions, Etc.** These results provide new scientific tools to be used by the scientists involved as they solve chemical problems, both basic and applied, in the future.

- n) **Is Scaleup Needed? Applied Impact?** Since this research has been basic, scaleup is not appropriate.
- o) **Improved Capabilities of Scientists.** Increased understanding of basic chemistry by the involved scientists is empowering as they continue research in related areas.
- p) **Advanced Understanding of Area.** The capability of replacing the ‘natural’ equilibration rates of ligand/metal ion binding and ligand/metal complex dissociation with molecular switching methodologies constitutes a substantial contribution to the understanding in the area of coordination chemistry.
- q) **What are the Remaining Hurdles?** To apply these results to problems of interest to DOE it will be necessary to identify specific target metal ions in circumstances demanding these special methodologies. Specifically the sequestering of  $\text{Cs}^+$ ,  $\text{Sr}^{+2}$ , or even actinide ions might be targeted for the application of molecular switching techniques.
- r) **Have Others Shown Interest?** Others have not shown interest in this program.

## PROJECT PRODUCTIVITY

The project goals for the development of seminal methodologies dependent on the unraveling of chemical principles, be they ever so minor, is a sequential process. Proof of concept comes first and proceeds through exploratory stages. How these relate to the progress of this program is summarized in the following brief sections.

### Soil Poultice

The objectives stated at the beginning of this report substantially reproduce those of the original proposal. They are sequential as just stated and, if all aspects had been completed, would have proceeded more or less as follows: (a) the detailed study of the factors and techniques that lead to good rebinding capabilities and selectivities of non-covalent MIPs, (b) the selection of early, most promising examples for demonstration of the success of the new separations methodology, (c) application to increasing interesting examples. Such a sequence would easily span a decade and the summation of actual supported research periods was somewhat less than six years, extended over some 8 calendar years. The objectives described in (a) above have been fully achieved, and those of (b) were well under way, but the ultimate applications weren't attempted because of the rate of progress of the fundamental studies. The goals were not all accomplished simply because the program did not last long enough. As is characteristic of basic research, the work plan was under constant revision. For example, as we learned that factors improving rebinding affected polymer morphology, we redesigned the polymer composition to preserve morphology; when we discovered that pairs of supramolecular interactions favored rebinding, we refocused on those binary pairs.

### Molecular Switching to Provide Rapid Rates.

The objectives reflect a long term mission, beginning with basic research to establish new scientific tools, leading to applications of increasingly demanding and promising natures. The design, synthesis and demonstration of ligand/metal ion systems dedicated to proofs of concept constituted the first 3 bullets of Switch binding and the first 5 bullets of Switch-release. In the case of this chemistry, even the more advanced objectives have strong fundamental science aspects. Most of the more basic objectives were achieved, leading to strong contributions to the field of coordination chemistry.

## PERSONNEL SUPPORTED

Personnel associated with the project were: Faculty -- Co-PIs, Professors Richard S. Givens and Daryle H. Busch; Post Doctoral Research Associates – Drs. Stephen J. Archibald, K. Mani Bushan, Abdulhameed M. Hassan, Jong-Il Lee, Donnati Mosha, Chi Zhang, and Xiaobin Zuo; Graduate Student – Ann K. McCasland; Undergraduate Student – Galen S. Loving.

## PUBLICATIONS

*Mansour M Hassan, Chi Zhang, Jong-ill Lee, K. Mani Bushan, Anne McCasland, Richard S. Givens, Daryle H. Busch*, “Dynamics of Switch binding by a linear ligand that transforms to a macrocycle upon chelation to a metal ion: synthesis, kinetics and equilibria,” ACS Symposium Volume, submitted; copy of manuscript appended.

*Xiaobin Zuo, Donnati Mosha, Stephen J. Archibald, Anne K. McCasland, Abdulhameed M. Hassan, Richard S. Givens, and Daryle H. Busch*, “Toward the Soil Poultrice and a New Separations Methodology: Rebinding of Macrocyclic Metal Complexes to Molecularly Imprinted Polymers Specifically Templated via Non-covalent Interactions,” Journal of Coordination Chemistry, Issue dedicated to Professor Arthur Martell, in press; copy of manuscript appended.

## INTERACTIONS

R.S.Givens, D.H.Busch, C. Zhang, J-I.Lee, K.M. Bushan, G.S.Loving, “Capture and Release: Managing Tight-binding Receptors,” presented at 228<sup>th</sup> National ACS Meeting, Philadelphia, PA, August 22-26, 2004.

X.Zuo, D.Mosha, M.M.Hassan, R.S.Givens, D.H. Busch, “Novel Methodology for Metal Ion Separation Based on Molecular Imprinting,” presented at the 227<sup>th</sup> National ACS Meeting, Anaheim, CA, March 28-April 1, 2004.

D.H.Busch, R.S.Givens, X. Zuo, C. Zhang, D. Mosha, J-I. Lee, K.M.Bushan, M.M.Hassan, G.S.Loving, “Exploiting Ultra Tight-binding Ligands for Separations Technologies,” presented at EMSP Symposium at the 226<sup>th</sup> National ACS Meeting, New York, NY, September 10, 2003.

X.Zuo, D.Mosha, M.M. Hassan, D.H.Busch, “Molecularly Imprinted Polymers for Specific Rebinding of Macrocyclic Metal Complexes via Noncovalent Interactions, presented at 225<sup>th</sup> National ACS Meeting, New Orleans, LA, March 23-27, 2003.

D.H.Busch, “Managing Tight-binding Ligands for New Separations Technologies,” plenary lecture, DOE Symposium, 221<sup>st</sup> National ACS Meeting, San Diego, CA, April 2, 2001.

D.H.Busch, “Basic Science for Tough Applications: Strategies to Use the Strongest Ligands in Metal Ion Separations, DOE EMSP Symposium at 222<sup>nd</sup> National ACS Meeting, Chicago, IL, August 28, 2001

D.H.Busch, R.S.Givens, X. Zuo, C. Zhang, D. Mosha, J-I. Lee, K.M.Bushan, M.M.Hassan, A.K.McCasland, G.S.Loving, "Exploiting Ultra Tight-binding Ligands for Separations Technologies," poster presented at DOE EMSP Workshop, Atlanta, GA, April 24-27, 2000.

A.K.McCasland, D.H.Busch, "Making Tight-binding Ligands React Rapidly: Mechanistic Studies on Macrocyclization of a Linear Ligand upon complexation to Nickel(II)," presented at 217<sup>th</sup> National ACS Meeting, Anaheim, CA, March 21-25, 1999.

A.K.McCasland, D.H.Busch, "Accelerated Binding Rates for Tightly Bound Adducts," presented at 216<sup>th</sup> National ACS Meeting, Boston, MA, August 23-27 (1998)

D.H.Busch, A.K.McCasland, S.J.Archibald, "Tight-binding Ligands for New Separations Technologies," presented at the 213<sup>th</sup> National ACS Meeting, San Francisco, CA, April 13-17, 1997.

### TRANSITIONS

None has been accomplished to date.

### PATENTS

None

### LITERATURE CITED

1. Telford, J. R.; Raymond, K. N. In *Supramolecular Chemistry*; Gokel, G. ed.; Permagon: Oxford, **1996**; pp 245. (b) Telford, J. R.; Raymond, K. N. In *Bioinorganic Chemistry, An Inorganic Perspective of Life*; Kluwer: Dordecht, **1995**; pp 25.
2. Busch, D. H. "The Compleat Coordination Chemistry--What a Difference A Century Makes", Werner Centennial Volume, ACS Symposium Series 565, **1994**; pp. 148-164. (b) Busch, D. H. "Ligand Design for Enhanced Molecular Organization--Selectivity and Specific Sequencing in Multiple Receptor Ligands, and Orderly Molecular Entanglements", in *Transition Metal Ions in Supramolecular Chemistry*; Fabbrizzi, L. ed.; Kluwer: Dordecht, **1994**; pp 55-79.
3. (a) Wulff, G; Sarhan, A. *Angew. Chem. Int. Ed. Engl.* **1972**, *11*, 341. (b) Wulff, G; Sarhan, A; Zabrocki, K. *Tetrahedron Lett.* **1973**, *14*, 4329-4332.
4. For reviews see: (a) Wulff, G. *Chem. Rev.* **2002**, *102*, 1-28. (b) Mosbach, K. *Anal. Chim. Acta* **2001**, *435*, 3-8. (c) Sellergren, B. *Angew. Chem. Int. Ed. Engl.* **2000**, *39*, 1031-1037. (d) Whitcombe, M. J.; Alexander C.; Vulfson, E. N. *Synlett.* **2000**, 911-923. (e) Andersson, L. I. *J. Chromatogr. B* **2000**, *745*, 3-13. (f) Wulff, G. *Angew. Chem. Int. Ed. Engl.* **1995**, *34*, 1812-1834.
5. (a) Sellergren, B. *Makromol. Chem.* **1989**, *190*, 2703-2711. (b) Kempe M.; Mosbach, K. *Anal.*

- Lett.* **1991**, *24*, 1137-1145. (c) Sellergren B.; Shea, K. J. *J. Chromatogr.* **1993**, *635*, 31-49.
6. Nishide, N.; Tsuchida, E. *Makromol. Chem.* **1976**, *177*, 2295-2310.
  7. Kuchen, W.; Schram, J. *Angew. Chem. Int. Ed. Engl.* **1988**, *27*, 1695-1697.
  8. Garcia, R.; Pinel, C.; Madic C.; Lemaire, M. *Tetrahedron Lett.* **1998**, *39*, 8651-8654.
  9. Chen, H.; Olmstead, M. M.; Albright, R. L.; Devenyi, J.; Fish, R. H. *Angew. Chem. Int. Ed. Engl.* **1997**, *36*, 642-645.
  10. Sharma, A. C.; Joshi, V.; Borovik, A. S. *J. Polym. Sci. A: Polym. Chem.* **2001**, *39*, 888-897.
  11. The DOTAM (a cyclen-based ligand with four pendant groups  $-\text{CH}_2\text{CONH}_2$ ) complexes of  $\text{Cd}^{2+}$  were described as six-coordinate with secondary coordination of the other two oxygen donors. Maumela, H.; Hancock, R. D.; Carlton, L.; Reibenspies, J. H.; Wainwright, K. P. *J. Am. Chem. Soc.* **1995**, *117*, 6698-6707.
  12. (a) Warner, L. G.; Busch, D. H. *J. Am. Chem. Soc.* **1969**, *91*, 4092-4101. (b) Warner, L. G.; Rose, N. J.; Busch, D. H. *J. Am. Chem. Soc.* **1967**, *89*, 703-704.
  13. O'Shannessy, D. J.; Anderson, L. I.; Mosbach, K. *J. Mol. Recognit.* **1989**, *2*, 1-5.
  14. Yu, C.; Mosbach, K. *J. Org. Chem.* **1997**, *62*, 4057-4064.
  15. Nicholls, I. A.; Adbo, K.; Anderson, H. S.; Anderson, P. O.; Ankarloo, J.; Hedin-Dahlström, J.; Jokela, P.; Karlsson, J. G.; Olofsson, L.; Rosengren, J.; Shoravi, S.; Svenson, J.; Wikman, S. *Anal. Chim. Acta* **2001**, *435*, 9-18.
  16. O'Shannessy, D. J.; Ekberg, B.; Mosbach, K. *Anal. Biochem.* **1989**, *177*, 144-151.
  17. Anderson, L. I.; Müller, R.; Vlatakis, G.; Mosbach, K. *Proc. Natl. Acad. Sci. USA* **1995**, *92*, 4788-4792.
  18. Adbo, K.; Anderson, H. S.; Ankarloo, J.; Karlsson, J. G.; Norell, M. C.; Olofsson, L.; Rosengren, J.; Svenson, J.; Örtengren, U.; Nicholls, I. A. *Bioorg. Chem.* **1999**, *27*, 363-371.
  19. Freeman, G. M.; Barefield, E. K.; Van Derveer, D. G. *Inorg. Chem.* **1984**, *23*, 3092-3103.
  20. Svenson, J.; Nicholls, I. A. *Anal. Chim. Acta* **2001**, *435*, 19-24.
  21. The control polymer was selected to avoid the complication caused by the nitrogen-containing residue imprint (*ca.* 3% of the starting material) in the imprinted polymer.
  22. The nitrogen content of **P1** is 1.59%. After the treatment with concentrated hydrochloric acid and concentrated nitric acid, the values are 1.40% and 2.08%.
  23. (a) Cox, B.G.; Schneider, H.; Stroka, J. *J. Am. Chem. Soc.*, **1978**, *100*, 4746; (b) Liesegang, G.W.; Eyring, E.M. in "Synthetic Multidentate Macrocyclic Compounds,"

- Ed. by Izatt, R.M.; Christensen, J.J. Academic press, Inc., London, **1978**, pp 245-289;
- (c) Eyring, E.M.; Petrucci, S. In "Cation Binding by macrocycles," Ed. by Inoue, Y.; Goekel, G.W. Marcel Dekker, Inc., New York, **1990**, pp. 179-203.
24. *Biological Applications of Photochemical Switches*, Ed. By Morrison, H., John Wiley, NY **1993**: Lester, H. A.; Gurney, A. M. *Physiol. Rev.* **1987**, *67*, 583.; Givens, R. S.; Weber, J. J. F.; Jung, A. H.; Park, C.-H. "New Photoprotecting Groups: Desyl and p-Hydroxyphenacyl Phosphate Carboxylate Esters" in *Methods in Enzymology on Caged Compounds: Chemistry, Instrumentation, and Applications*, Ed. By Gerard Marriott, **1998**, *291*, 1- 29).
25. (a) Busch, D.H. "Ligand Design for Enhanced Molecular Organization--Selectivity and Specific Sequencing in Multiple Receptor Ligands, and Orderly Molecular Entanglements," in *Transition Metal Ions in Supramolecular Chemistry*, Ed by Fabbri, L., Kluwer, **1994**, pp. 55-79; (b) Busch, D.H. "The Complete Coordination Chemistry -- What a Difference A Century Makes", *Werner Centennial Volume*, ACS Symposium Series, Vol. 565, , pp. 148-164.; (c) Busch, D.H. *Chem.Rev.*, 93, **1993**, 847-860; (d) Busch, D.H. *Chem. Eng. News*, June 29, **1970**, p. 9.
26. Barefield, E.K.; Lovecchio, F.V.; Tokel, N.E.; Ochiai, E.; Busch, D.H. *Inorg. Chem.*, **1972**, *11*, 283.
27. Atwell, G. J.; Denny, W. A. *Synthesis*, 1984, 1032.
28. Moffett, R. B.; Leonard, N. J.; Miller, L. A. Synthesis of *N*-methyl-1,2-diphenylethylamine and hydrochloride., *Organic Synthesis*, Coll. Vol. 4, p 605.
29. (a) Abdel-Magid, A. F.; Carson, K. G.; Harris, B. D.; )b) Maryanoff, C. A.; Shah, R. D. *J. Org. Chem.* **1996**, *61*, 3849; (c) Abdel-Magid, A. F.; Maryanoff, C. A.; (d) Carson, K. G. *Tetrahedron Lett.* **1990**, *31*, 5595.
30. Ben-Ishai, D.; Berger, A. *J. Org. Chem.* **1952**, *17*, 1564.
31. McCasland, A.K., Ph.D. Dissertation, University of Kansas, **1999**.
32. Erithacus Software Limited © 1988.
33. Moss, D. B.; Lin, Chin-tung.; Rorabacher, D. B., *J. Am. Chem. Soc.*, **1973**, *8*, 5179.
34. Wu, Y.; Kaden, T.A.; *Helv. Chim. Acta*, **1984**, *67*, 1868.
35. Hassan, M. M, Marafie, H. M., and El-Ezaby, M. S.; *Coordination Chemistry*, **2003**, *8*, 709.

36. Hubin, T. J. and Busch, D. H.; *Coord. Chem. Rev.* **2000**, 200-202, 5.
37. Bormans, G.; Peters, O. M.; Vanbilloen, H.; Blaton, N.; Verbruggen, A. *Inorg. Chem.* **1996**, 35, 624.
38. Grummon, G.; Rajagopalan, R.; Palenik, G. J.; Koziol, A. E.; Nosco, D. L. *Inorg. Chem.* **1995**, 34, 1764.
39. Nosco, D. L.; Beaty-Nosco, J. A. *Coord. Chem. Rev.* **1999**, 184, 91.
40. Reichert, D.E.; Lewis, J.S.; Anderson C.J. *Coord. Chem. Rev.* **1999**, 184, 3.
41. Thunus, L; Lejeune, R. *Coord. Chem. Rev.* **1999**, 184, 125.
42. Hay, R. W.; Danby, A.; Miller, S.; Lightfoot, P. *Inorg. Chim. Acta.* **1996**, 246, 395.
43. Danby, A. M., Ph.D. Dissertation, St. Andrews University, 1996.
44. (a) Thompson, M.C.; Busch, D. H. *Chem. Eng. News*, September 17, **1962**.p. 57; (b) Thompson, M.C.; Busch, D.H. *J. Am. Chem. Soc.*, **1964**, 86, 3651.
45. Jasat, A., Sherman, J. C., *Chem. Rev.*, (**1999**) 99, 931
46. Zhang, X. X., Iosos, R. M.; Bradshaw, J. S.; Krakowiak, K. E. *Coord. Chem. Rev.* (**1998**) 174, 179.
47. Ikeda, A. et al. ( **1997**) *Chem. Rev.*, 97, 173.
48. Beer, P.D., G Gale, P. A, Chen, Z., ( **1998**) *Adv. Phys. Org. Chem.*, 31, 1.
49. Lindoy, L.F., *The chemistry of Macrocyclic Ligand Complexes*. 1989
50. Dietrich, B.V., Lehn, J. M., *Macrocyclic Chemistry*. 1993.
51. Zolotov, Y.A., *Macrocyclic Compounds in Analytical Chemistry*. 1997.
52. Busch, D. H., ed., Fabrizzi, L., Kluwer., *Ligand Design for Enhanced Molecular Organization - Selectivity and Specific Sequencing in Multiple Receptor Ligands, and Orderly Molecular Entanglements, in Transition Metal Ions in Supramolecular Chemistry*. 1994: p. 55.
53. Busch, D.H., *The Complete Coordination Chemistry - What a Difference A Century Makes*. Werner Centennial Volume, ACS Symposium Series, 1994(565): p. 148.
54. Busch, D.H., *Metals and Enzymes - Multiple Juxtapositional Fixedness*. *Chem. Eng. News*, 1970, June 29: p. 9.
55. Lehn, J.M., *Supramolecular Chemistry - Concepts and Perspectives*. 1995: p. 89.
56. Steed, J. W., et al., *Supramolecular Chemistry*. 2000: p. 573
57. Barboiu, M., Lehn, J. M., (**2002**) *Proc. Natl. Acad. Sci.*, 99, 5201.
58. Pillai, V.N.R., (**1987**) *Organic Photochemistry* , Padwa, A., Ed. vol. 9, 225.

59. Willner, I.W., B., in *Biological Applications of Photochemical Switches*, Morrison, H., Ed. (1993), 1.
60. Corrie, J.E.T., Trentham, D. R., in *Biological Applications of Photochemical Switches*, Morrison, H., Ed. (1993), 243.
61. Givens, R.S. Kueper, L. W. III, (1993) *Chem. Rev.*, 93, 55.
62. Givens, R.S. Conrad, P. G.; Yousef, A. L.; Lee J. I., *Photoremovable Protecting Groups* (2004) **CRC Handbook on Photochemistry and Photobiology**, Horspool W. M. and Song, P. S.,(Ed.), 69/1-69/46.
63. Houlihan, F.M.N., O.; Kometani, J. M.; Reichmanis, E., J. (1997), *Imaging. Sci. Technol*, 41, 35.
64. **Caged Compounds**, Marriott, G. Ed. (1998) *Methods in Enzymology*, vol. 291.
65. Ellis-Davies, G.C., et al., (1988), *J. Org. Chem.*, 53, 1966.
66. Hibino, S., et al., (1987), *Heterocycles*, 26,1883 -9.
67. Greene, T.W., et al., *Protective Groups in Organic Synthesis*, 2nd ed. (1991)
68. Warmuth, R.G., E.; Lehn, J. M.; Bats, J. W.; Quinkert, G., (1991) *Helv. Chim. Acta*, 74, 671.
69. VanRheenen, V.K., Cha, D. Y., (1976), *Tetrahedron Lett*, 1973.
70. Metz, B.M., Weiss, R., (1971) *J. Am. Chem. Soc.*, 93, 1806.
71. Abdel-Magid, A.F.C., K. G.; Harris, B. D.; Maryanoff, C. A.; Shah, R. D., (1996) *J. Org. Chem.*, 61, 3849.
72. Abdel-Magid, A.F.; Carson, K. G., (1990) *Tetrahedron Lett.*, 31, 5595.
73. Hatchard, C.G., Parker, C. A., (1956) *Proc. R. Soc. London. A-235*, 518-522.

## FEEDBACK

Continuity, even persistence, is critical to major advances in both basic and applied research. This is especially true when the application depends on successful basic science research and is sequentially related to that basic research. This specific project does involve sequential basic and applied science. After much hard work the greatest basic science challenges have been met and the new knowledge is nearing the point where applications can reasonably be expected. At the point of entry of these investigators into this project it was understood that DOE had finally recognized the need to perform research basic to confronting the waste treatment challenges that cannot be met by the tractor and backhoe components of known chemistry. In general terms it remains true that the need still exists. Is EM making progress in this essential programmatic development?

## APPENDICES

The two (2) manuscripts identified above as undergoing the publication process are appended here.

### **Dynamics of Switch binding by a linear ligand that transforms to a macrocycle upon chelation to a metal ion: synthesis, kinetics and equilibria**

*Mansour M Hassan\**, *Chi Zhang\*\**, *Jong-ill Lee\*\**, *K. Mani Bushan\*\**, *Anne McCasland\*\**, *Richard S. Givens\*\**, *Daryle H. Busch\*\**

*\*Department of chemistry, Faculty of higher education-Aden, University of Aden, Aden Yemen.*

*\*\*Department of Chemistry, 1251 Wescoe Hall Dr. University of Kansas, Lawrence, KS 66045-7582*

## Abstract

It is proposed that for chemical processes in which equilibration is too slow to achieve certain goals, switch binding and switch-release reactions may be used to accelerate complex formation. Whereas photo triggers are well known for switch-releasing, switch binding is first described here for notably slow complex formation reactions between metal ions and macrocyclic ligands. A linear tetradentate ligand,  $L^{L/C}$ , was designed with functional groups that will react with each other (primary amine, carbonyl) at its extremities. Upon complexation the metal ion is predicted to cause reaction between these functional groups, producing a macrocyclic ligand that encircles the metal ion. Equilibrium studies were made with the metal ions  $Cu^{2+}$ ,  $Hg^{2+}$ ,  $Ni^{2+}$ , and  $Zn^{2+}$  both with the switch binding ligand,  $L^{L/C}$ , and with a ligand,  $L^L$ , that is very similar except it cannot undergo the switching process. The formation constants were very similar for the two ligands, with the metal ion affinities decreasing in the order  $Cu^{2+} \gg Ni^{2+} \approx Zn^{2+} > Hg^{2+}$ . The kinetics of reaction were studied for formation of the nickel(II) complexes of both ligands. Results gave a first indication that nickel very rapidly chelates to the switch binding ligand before forming the macrocycle. The nickel(II) reacts with  $L^{L/C}$  in a complicated rapid set of processes on the fractional second time scale, followed by a process in the hour time regime. In contrast, under the same conditions, only a single rapid rate process was observed for the reaction of nickel(II) with  $L^L$ . The specific rate constants for  $L^L$  are greater than those for  $L^{L/C}$ . Detailed analysis, strongly augmented by mass spectrometric studies, proved that the rapid process produces a nickel complex of the linear ligand and that intramolecular ring closure takes place relatively slowly and under the control of the metal ion. This proof of concept for switch binding, using the template effect, completes the model for replacing equilibration for the reversible formation of metal complexes with a switch binding and release process.

## Introduction

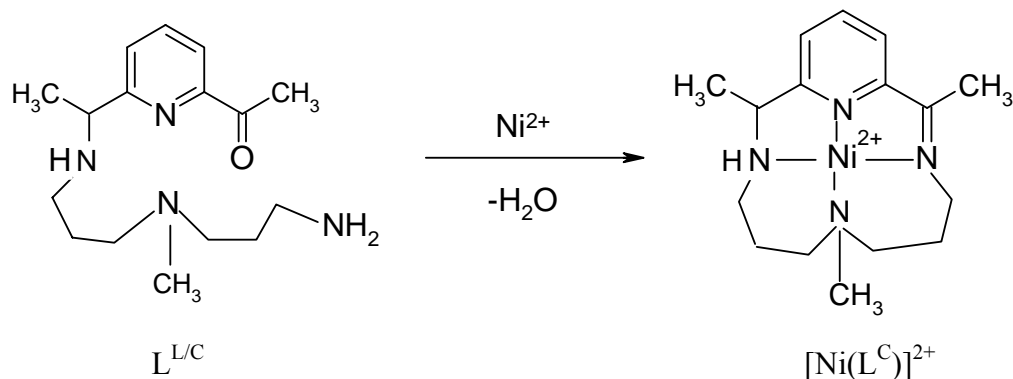
In principle the most powerful known ligands can capture metal ions in the most competitive of circumstances, for example from mineralized sites, from lesser ligands, and even from extremely dilute solutions; i.e., under circumstances where ordinary ligands, such as those used in well-known separations technologies, are completely ineffective. Clearly there are compelling incentives for finding ways to apply these tight-binding ligands to the management of the metallic elements under many conditions, but there are major hurdles that must be overcome.

The applications of such tight-binding ligands have been limited by the slow rates at which their equilibria are established. It is an experimental fact that the equilibrium constants for the binding

of any kind of receptee (e.g., a metal ion) to its complementary receptor (i.e., ligand) commonly vary monotonically with the rates at which the receptee is liberated from the receptee/receptor complex.<sup>1</sup> Consequently, ultra tight-binding ligands, whose equilibrium constants for binding exceed ordinary values by factors of millions or billions, will release their complement at least that many millions or billions of times slower. Most often, the slowness is even more lethargic since the rate of binding is also retarded and  $K_{\text{equil}} = k_{\text{binding}}/k_{\text{release}}$ . In order to make best use of tight-binding receptors it is, therefore, necessary to either accommodate any specific methodology to these slow kinetic processes or to find means of accelerating the formation and dissociation rates associated with complexation.

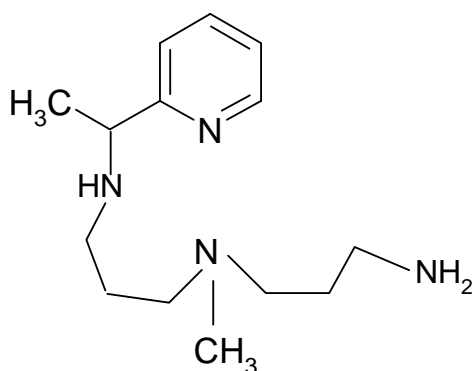
Here we present the concept of replacing slow rates of complex formation by a chemical switching process that we will refer to as *switch binding*. The combined chemical processes of ligand binding and release constitute metal ion/ligand equilibration and complete replacement of that natural process with chemical switching requires both switch binding and switch-release. Switch-release is broadly used to generate immediate sizeable infusions of biological substrates, including metal ions, in life science studies.<sup>2</sup> Switch-release is the subject of other work in these laboratories. The concept of switch binding and switch-release is in step with the goals of science to move beyond what nature gives to us spontaneously.

Here switch binding is accomplished by a change in the structure of the ligand in accompaniment to its binding to the metal. The structural change is from a rapidly reacting, more weakly binding ligand structure in the free state to a more slowly reacting, more strongly binding ligand structure in the target metal complex. *Complementarity* and *ligand constraints* determine the stabilities of metal complexes.<sup>3</sup> Complementarity, a necessary but not sufficient condition for maximum affinity, implies a consonance between metal ion and ligand in bond type (often including charge), geometry, and size. Given equal complementarity, the constraints built into the structure of the ligand determine just how strong its complexes will be. For the example presented here, the topological constraint built into the ligand changes from that of a linear tetradentate ligand to that for a macrocycle (Scheme 1). Given equal complementarity, the stabilities of complexes increase dramatically with increasing topological constraint: (simple ligand < chelate < macrocycle < cryptand). Further, as described above, the rates of their binding to and dissociation from metal ions decrease as complex stability increases.



**Scheme I.** Switch binding process in which a rapidly reacting linear chelate becomes an inert macrocyclic ligand coordinated to a nickel(II) ion.

The switch binding ligand investigated in this work,  $L^{L/C}$ , was designed to have complementary functional groups at its ends, primary amino and ketone groups, which react to close the macrocycle,  $L^C$ , about the metal ion. This Schiff base condensation, produces a macrocyclic ligand that is known to be nicely complementary to the nickel(II) ion. The square planar complex,  $[Ni(L^C)]^{2+}$ , has been prepared by a more traditional route and characterized<sup>4</sup>. Because the expected product of the complete switch binding process has been characterized, this is a good system to test the switch binding concept. For comparison, a very similar ligand ( $L^L$ , Structure I) that is not capable of undergoing cyclization was also synthesized, and details of the syntheses are reported. Detailed kinetic and mechanistic information has been obtained for the complexation reactions of both ligands,  $L^{L/C}$  and  $L^L$ , with nickel(II). The work also includes the determination of the protonation and complex formation constants for the two ligands.



Structure I

## Experimental

### Synthesis of L<sup>L/C</sup> and L<sup>L</sup>

*a) {3-[(3-Amino-propyl)-methyl-amino]-propyl}-carbamic acid benzyl ester*<sup>5</sup> 3,3'-Diamino-N-methyldipropylamine (14.53 g, 0.10 mol) was dissolved in water (25 ml) containing bromocresol green (0.01%) as the indicator. Methanesulfonic acid (~ 19.2 g, 0.20 mol) in water (15 ml) is added slowly until the blue to yellow color transition is just achieved. The mixture was then diluted with ethanol (70 mL) and vigorously stirred at room temperature, while a solution of benzyl chloroformate (15.2 g, 0.089 mol) in dimethoxyethane (25mL) and 25% w/v aqueous potassium acetate (~ 60 mL) is added dropwise simultaneously at rates which maintain the correct reaction pH (yellow-green indicator coloration). After the additions are complete, the mixture is stirred for an additional 4 hr. at room temperature. The volatiles are then removed under vacuum and the residue is extracted with water (250 ml) and filtered to remove small quantities of the bis-derivative that is formed as a byproduct. The filtrate is washed with methylene chloride (3 × 100 ml), made basic with excess 40% aqueous NaOH solution and extracted with methylene chloride (2 × 150 ml). The organic layer is washed once with saturated aqueous sodium chloride (100 ml) and dried over magnesium sulfate. The solution is filtered to remove the drying agent and the solvent is removed by rotary evaporation to yield a yellow oil which is dried under vacuum overnight. Yield: 8.6 g (35 %). <sup>1</sup>H NMR (CDCl<sub>3</sub>, 400 MHz): δ 7.37(m, 5H), 5.96(s, 1H), 5.09(s, 2H), 3.27(m, 2H), 2.73(t, 2H), 2.39(m, 4H), 2.18(s, 3H), 1.63(m, 6H) ppm.

*b) [3-({3-[1-(6-Acetyl-pyridin-2-yl)-ethylideneamino]-propyl}-methyl-amino)-propyl]-carbamic acid ester*<sup>6</sup>. A solution of {3-[(3-amino-propyl)-methylamino]-propyl}-carbamic acid benzyl ester (2.79 g, 10 mmol) in 30 ml of dry benzene is added to a solution of 2,6-diacetylpyridine (DAP) (1.64 g, 10 mmol) in dry benzene (20 ml). The reaction mixture is heated to reflux overnight under N<sub>2</sub> with stirring. During the heating at reflux, the solution gradually becomes bright orange with cooling and concentration of the benzene layer under vacuum, a light orange oil is obtained. Yield: 1.96 g (46%). <sup>1</sup>H NMR (CDCl<sub>3</sub>, 400 MHz): δ 8.21(m, 1H), 8.03(m, 1H), 7.83(t, 1H), 7.37(m, 5H), 5.94(s, 1H), 5.08(s, 2H), 3.57(t, 2H), 3.30(d, 2H), 2.80(d, 3H), 2.40(m, 4H), 2.26(s, 3H), 1.95(m, 2H), 1.69(d, 2H), 1.60(s, 3H) ppm.

*c) 3-({3-[1-(6-Acetyl-pyridin-2-yl)-ethylamino]-propyl}-methyl-amino)-propyl]-carbamic acid benzyl ester*<sup>7</sup> [3-({3-[1-(6-Acetylpyridin-2-yl)-ethylamino]-propyl}-methylamino)-propyl]-carbamic acid benzyl ester (1.50 g, 3.54 mmol) is dissolved in 1,2-dichloroethane (20 ml), and then sodium triacetoxyborohydride (1.05 g, 4.95 mmol) is added slowly under N<sub>2</sub> atmosphere. Upon completing of the addition of the solid, the reaction mixture is stirred for 24 hr. at rt. The reaction is quenched by adding an excess of 40% aqueous NaOH (30 ml), followed by extraction with methylene chloride (3 × 50 ml), washed with brine solution (100 ml), and dried over magnesium sulfate. The inorganic salts are filtered and the filtrate evaporated under vacuum. The resulting yellowish-orange oil is dried on the vacuum line overnight. Yield: 1.05 g (70%). The crude product is purified by flash column chromatography (hexane/EtOAc = 1/3, then EtOAc/MeOH = 1/1) to give the purified product as a yellow oil. <sup>1</sup>H NMR (CDCl<sub>3</sub>, 400 MHz): 7.85(d, 1H), 7.70(s, 1H), 7.40(d, 1H), 7.31(m, 5H), 5.99(s, 1H), 5.08(s, 2H), 3.85(m, 1H), 3.22(m, 2H), 2.70(s, 3H), 2.56(m, 1H), 2.41(m, 1H), 2.36(m, 4H), 2.15(s, 3H), 2.05(s, 1H), 1.64(m, 4H), 1.36(d, 3H) ppm. <sup>13</sup>C NMR (CDCl<sub>3</sub>, 100 MHz): 200.97, 164.65, 156.88, 153.50, 137.61, 137.30, 128.87, 128.70, 128.43, 128.38, 125.05, 120.07, 66.75, 59.47, 56.73, 56.34, 46.73, 42.47, 42.17, 41.32, 40.72, 28.25, 27.51, 26.91, 26.16, 23.20 ppm. Major infrared absorbances (cm<sup>-1</sup>): 3333(N-H stretch), 1398(C=O), 1530(N-H bend), 1452, 1357(-CH<sub>3</sub> bend). FAB-MS: 427.2.

*d) 1-[6-(1-{3-[1-(6-acetylpyridin-2-yl)-ethylamino]-propyl}-methylamino)-propylamino}-ethyl)-pyridin-2-yl]-ethanone, L<sup>L/C</sup>*<sup>8</sup>. A saturated solution (15 ml) of dry hydrogen bromide in acetic acid (30%) is added to cleave the N-carbobenzyloxy protecting group from [3-({3-[1-(6-acetylpyridin-2-yl)-ethylamino]-propyl}-methylamino)-propyl]-carbamic acid benzyl ester (0.60 g, 1.42 mmol), stirred in a three-necked, 50 mL round bottomed flask. Evolution of carbon dioxide is evident upon acidification, indicative of effective decarboxylation. The resulting deep orange-red solution is allowed to stir for 2 hrs at rt. Dry ethyl ether (120 ml) is subsequently added directly to the flask and the yellow-white hydrobromide salt separates from the solution. Due to the extremely hygroscopic nature of the product, a syrupy material forms upon standing during vacuum filtration. The crude product is recrystallized by precipitating the solid by addition of ether to a solution of a minimal amount of dry ethanol. The purified product is dried under vacuum for 2 d to give a white-yellow solid. Yield: 0.485 g (59%). <sup>1</sup>H NMR (CDCl<sub>3</sub>, 400 MHz): δ 8.08(m, 2H), 7.70(t, 1H), 4.73(m, 1H), 3.25(m, 6H), 3.09(t, 4H), 2.91(m, 4H), 2.76(s, 3H), 2.12(m, 4H), 1.95(m, 1H), 1.66(d, 3H) ppm. <sup>13</sup>C NMR (D<sub>2</sub>O, 100 MHz): 203.35, 165.09, 155.26,

139.87, 126.87, 123.13, 58.27, 53.51, 53.37, 42.85, 39.95, 39.87, 36.71, 26.03, 22.30, 21.50 ppm.

FAB-MS: 293.2. HRMS: 293.2333 (calc.: 293.2341).

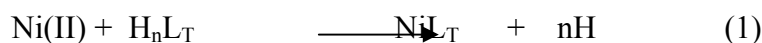
**a) {3-[(3-Aminopropyl)-methylamino]-propyl}-carbamic acid benzyl ester.** 3,3'-Diamino-N-methyldipropylamine (14.53 g, 0.10 mol) is dissolved in water (25 ml) containing bromocresol green (0.01%) as the indicator. Methane sulfonic acid (~ 19.2 g, 0.20 mol) in water (15 ml) is added slowly from a dropping funnel until the blue to yellow color transition is just achieved. The mixture is then diluted with ethanol (70 mL) and vigorously stirred with a magnetic stir bar at rt, while a solution of benzyl chloroformate (15.2 g, 0.089 mol) in dimethoxyethane (25mL) and 25% w/v aqueous potassium acetate (~ 60 mL) is added dropwise simultaneously at rates which maintained the correct reaction pH (yellow-green indicator coloration). After the additions are completed, the mixture is stirred for an additional 4 hrs at rt. The volatiles are then removed under vacuum and the residue is extracted with water (250 ml), and filtered to remove small quantities of the bis-derivative formed in the reaction. The filtrate is washed with methylene chloride (3 × 100 ml), made basic with excess 40% aqueous NaOH solution, and extracted with methylene chloride (2 × 150 ml). The organic layer is washed once with saturated aqueous sodium chloride (100 ml) and dried with magnesium sulfate. The solution is filtered to remove the drying agent and the solvent is removed by rotary evaporation to yield a viscous, faintly yellow oil which is dried under vacuum overnight. Yield: 8.71 g (36 %). <sup>1</sup>H NMR (CDCl<sub>3</sub>, 400 MHz): δ 7.37(m, 5H), 5.96(s, 1H), 5.09(s, 2H), 3.27(m, 2H), 2.73(t, 2H), 2.39(m, 4H), 2.18(s, 3H), 1.63(m, 6H) ppm.

**b) [3-({3-[1-(pyridin-2-yl)-ethylideneamino]-propyl}-methylamino)-propyl]-carbamic acid benzyl ester.** A solution of {3-[(3-aminopropyl)-methylamino]-propyl}-carbamic acid benzyl ester (4.74 g, 17 mmol) in 30 ml of dry benzene is added to a solution of 2-acetylpyridine (2.08 g, 17 mmol) in dry benzene (30 ml). The reaction mixture is heated to reflux overnight under N<sub>2</sub> with stirring. During this time the solution gradually becomes bright orange. Heating is stopped when no more water formed. Upon cooling and concentrating the benzene layer under vacuum, a light orange oil is obtained. Yield: 5.67 g (87%). <sup>1</sup>H NMR (CDCl<sub>3</sub>, 400 MHz): δ 8.59(d, 1H), 8.05(d, 1H), 7.69(t, 1H), 7.36(m, 5H), 7.30(t, 1H), 5.93(s, 1H), 5.08(s, 2H), 3.54(t, 2H), 3.30(t, 2H), 2.50(m, 4H), 2.33(s, 3H), 2.26(s, 3H), 1.95(m, 2H), 1.70(m, 2H). <sup>13</sup>C NMR (CDCl<sub>3</sub>, 100 MHz): 166.70, 157.79, 156.49, 149.00, 148.25, 136.86, 136.29, 128.45, 128.02, 127.11, 124.02, 121.67, 120.82, 66.37, 55.96, 50.31, 42.07, 40.79, 28.41, 26.46, 25.83, 14.03 ppm. FAB-MS: 383.2.

*c) [3-({3-[1-(pyridin-2-yl)-ethylamino]-propyl}-methylamino)-propyl]-carbamic acid benzyl ester.* [3-({3-[1-(pyridin-2-yl)-ethylamino]-propyl}-methyl-amino)-propyl]-carbamic acid benzyl ester (5.67 g, 14.83 mmol) is dissolved in 1,2-dichloroethane (40 ml), and then sodium triacetoxyborohydride (4.63 g, 20.76 mmol) is added slowly under N<sub>2</sub> atmosphere. Upon completing of the addition of the solid, the reaction mixture is stirred for 24 hrs at room temperature. The reaction is quenched by addition of an excess of 40% aqueous NaOH (50 ml), followed by extraction with methylene chloride (3 × 50 ml), washed with saturated aqueous sodium chloride (150 ml), and dried over magnesium sulfate. The inorganic salts are filtered and the filtrate evaporated under vacuum. The resulting yellowish-orange oil is dried on the vacuum line overnight. The crude product is purified by flash column chromatography (hexane/EtOAc = 1/3, then EtOAc/MeOH = 1/1) to give the purified product (4.67 g, Yield: 82%). <sup>1</sup>H NMR (CDCl<sub>3</sub>, 400 MHz): 8.49(d, 1H), 7.54(t, 1H), 7.28(m, 5H), 7.24(d, 1H), 7.06(t, 1H), 6.31(s, 1H), 5.03(s, 2H), 4.48(s, 1H), 3.82(m, 1H), 3.18(m, 2H), 2.59(m, 1H), 2.32(m, 5H), 2.12(s, 3H), 1.62(m, 4H), 1.34(d, 3H) ppm. <sup>13</sup>C NMR (CDCl<sub>3</sub>, 100 MHz): 163.13, 156.42, 149.15, 136.73, 136.41, 128.20, 127.78, 127.68, 121.88, 121.23, 66.06, 58.91, 56.59, 55.16, 46.32, 41.60, 39.55, 26.41, 26.33, 23.75, 22.09 ppm. FAB-MS: 385.1. HRMS: 385.2602 (calc.: 385.2604).

*d) 3-({3-[1-(Pyridin-2-yl)-ethylamino]-propyl}-N-methyl)-1-aminopropane, L<sup>L</sup>.* A saturated solution (20 ml) of dry hydrogen bromide in acetic acid (30%) is added to cleave the N-carbobenzyloxy protecting group from [3-({3-[1-(pyridin-2-yl)-ethylamino]-propyl}-methylamino)-propyl]-carbamic acid benzyl ester (2.43 g, 6.31 mmol), stirred in a 100 mL round bottomed flask. Evolution of carbon dioxide is evident upon acidification, indicative of effective decarboxylation. The deep orange-red solution is allowed to stir for 2 hrs. at room temperature. Dry ethyl ether (80 ml) is subsequently added directly to the flask and the yellow-white hydrobromide salt separates from the solution. Due to the extremely hygroscopic nature of the product, a syrupy material forms upon standing during vacuum filtration. The crude product is recrystallized by precipitating the solid from a minimal amount of dry ethanol with the addition of ether. The purified product is dried under vacuum for 2 d to give a white-yellow solid. Yield: 2.89 g, (86%). <sup>1</sup>H NMR (CDCl<sub>3</sub>, 400 MHz): δ 8.70(d, 1H), 8.17(t, 1H), 7.75(t, 1H), 7.68(d, 1H), 4.72(m, 1H), 3.26(m, 6H), 3.09(m, 4H), 2.92(s, 3H), 2.18(m, 4H), 2.07(s, 3H), 1.73(d, 3H) ppm. <sup>13</sup>C NMR (D<sub>2</sub>O, 100 MHz): 153.03, 148.22, 141.69, 125.99, 124.23, 58.08, 53.51, 53.32, 43.12, 40.01, 36.78, 22.33, 21.42, 17.94 ppm. FAB-MS: 251.3 [M+H]<sup>+</sup>. HRMS: 251.2244 [M+H]<sup>+</sup> (calc.: 251.2236); 331.1489 [M+HBr]<sup>+</sup> (calc.: 331.1497).

**Kinetic Measurements.** The kinetics of the reaction of nickel(II) with the ligands  $L^{L/C}$  and  $L^L$  were measured spectrophotometrically at the absorption maxima, 390 and 360 nm, respectively, using a Hi Tech MG-6000 Rapid Diode Array Stopped Flow Spectrophotometer (Model SF-41) interfaced with an IBM PC. Data acquisition and processing was carried out using Hi Tech systems kinetics software. Rate constants were calculated by the computer programs IS- software from HI-Tech. The ionic strength was adjusted to 0.2 M with  $KNO_3$  in all of the reactions, and the temperature was kept constant at  $25 \pm 0.1$  °C. MES (2-[N-Morpholino]ethane sulfonic acid) buffer (0.05M) was used to maintain a constant pH. Pseudo-first order conditions ( $[L^{L/C}]_{tot} \geq 10[Ni(II)]_{tot}$  or  $[Ni(II)]_{tot} \geq 10[L^L]_{tot}$ ) were maintained in all of the reactions. The reaction monitored is shown in eq 1.



Where  $H_nL_T$  is the total ligand concentration of  $L^{L/C}$  or  $L^L$ . The kinetics were fit to the rate expression

$$Rate = k_f [Ni(II)] [H_nL_T]$$

where  $k_f$  is the rate constant for complex formation. For each of the systems studied, a series of kinetic runs were carried out at several pH values ( 5.6 – 8.5) under conditions where  $[L_T] \gg [Ni(II)]$  or  $[Ni(II)] \gg [L_T]$  to give the first order expression

$$d[NiL_T]/dt = k_{obs} [Ni(II)]$$

or

$$d[NiL_T]/dt = k_{obs} [L_T] \text{ for}$$

The observed first order rate constants  $k_{obs}$  were obtained from the  $A/t$  data (  $A$  = absorbance;  $t$  = time) which could be computer- fitted to eq 2 very well ( least-squares method).

$$A = (A_o - A_\infty) \exp(-k_{obs}t) + A_\infty \quad (2)$$

$A_0$  and  $A_\infty$  refer to  $t = 0$  and  $t = \infty$ , respectively.

### **Potentiometric Equipment and Measurements.**

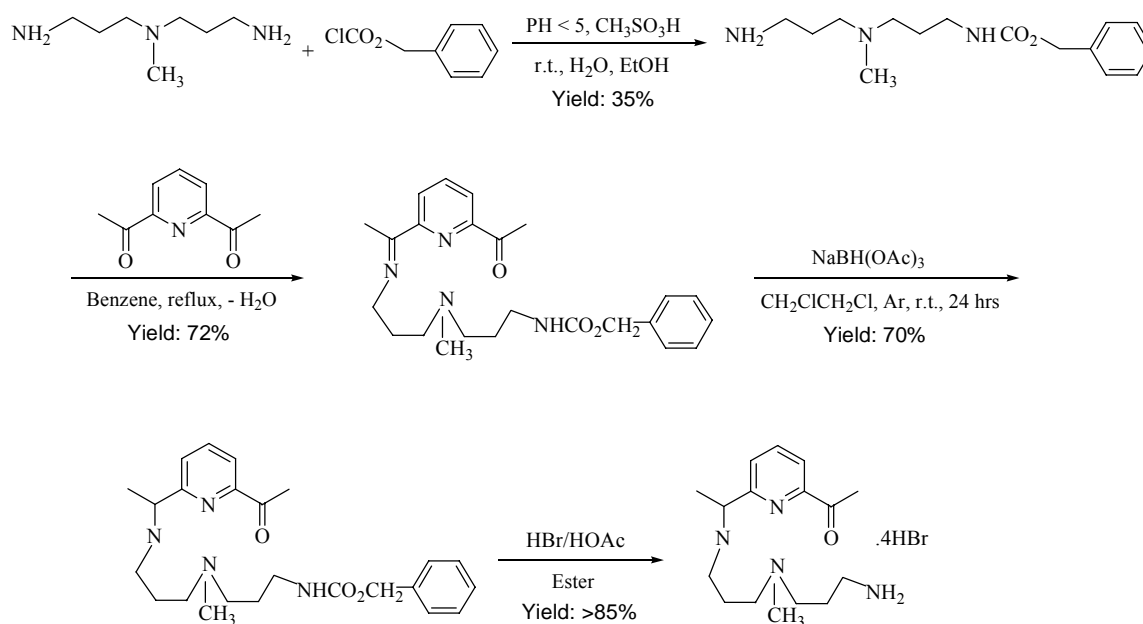
**Reagents and Standard Solutions.** Analytical grade metal nitrates were used and solutions were prepared in doubly distilled water and standardized against EDTA (AR, Aldrich) using a copper-selective electrode and calomel reference electrode. The ligand stock solution was standardized potentiometrically against a copper(II) nitrate solution using the copper/calomel electrode system. The titration was carried out in ammonia buffer at pH 10. The NaOH solution (0.201M; Aldrich) was standardized potentiometrically against KHP (potassium hydrogen phthalate, Fisher) and stored under solid mixture of anhydrous  $\text{CaCl}_2$  and sodium hydroxide to minimize carbonate formation.

**Potentiometric titrations.** These were performed under  $\text{N}_2$  at  $25.0^\circ\text{C}$  on a Brinkmann Metrohm 736GB Titrino equipped with an ORION Ross combination electrode (model 81-02). The electrode was standardized by three-buffer calibration using the Titrino's internal standardization method. The potentiometric equilibrium measurements were made on 50.0 ml of ligand ( $0.5 \times 10^{-3}$  M), first in the absence of metal ions and then in the presence of each metal ion for which  $[\text{L}]:[\text{M}]$  ratios were 1:1. The ionic strength was maintained constant at 0.1 M ( $\text{KNO}_3$ ). The pH data were collected after 0.01 ml incremental additions of standard NaOH solution (with a 20 – 60 s equilibration time) while the titration data (pH vs ml base) were captured in the Titrino's built-in software. Direct pH meter readings were used for calculation of the protonation and stability constants. The constants determined are mixed constants (also known as Brønsted constants) which involve the hydrogen ion activity and the concentrations of the other species. The protonation and stability constants were calculated by fitting the potentiometric data with the SUPERQUAD program<sup>9</sup>. Species distribution diagrams were generated with the aid of the program Hyss<sup>10</sup>.

## **RESULTS**

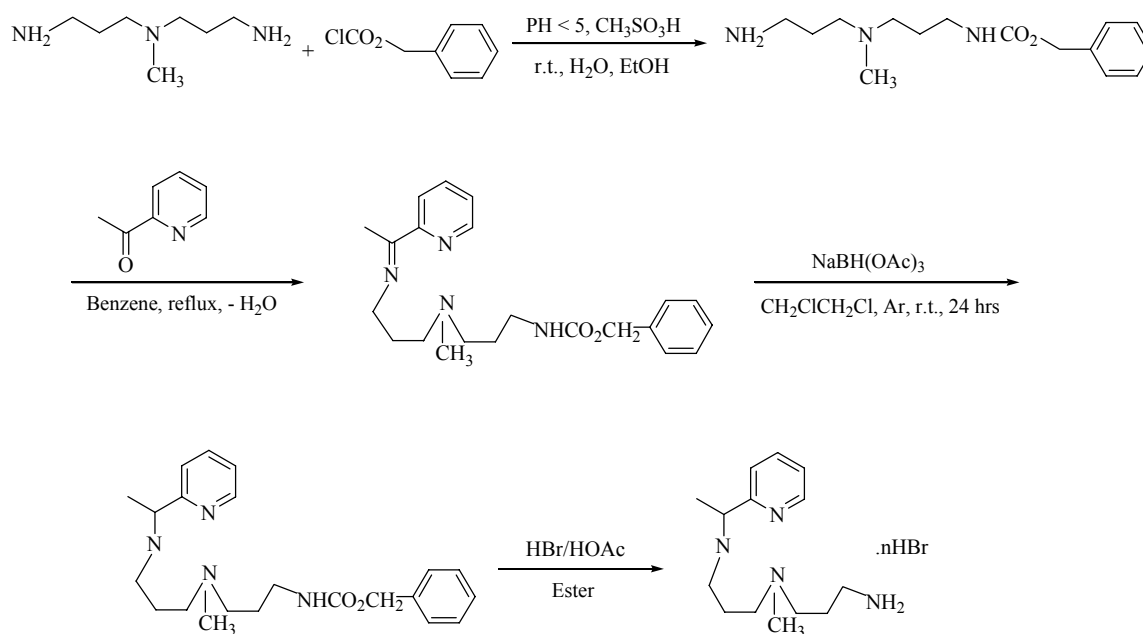
**Strategies for the synthesis of the switch binding ligand 1-[6-{3-[(3-amino-propyl)-methyl-amino]-propylamino}ethyl]-pyridin-2-yl]ethanone,  $\text{L}^{\text{L/C}}$ , and 3-({3-[pyridine-2-yl]-ethylamino}-propyl)-N-methyl-1-amino)propane,  $\text{L}^{\text{L}}$ , as the hydrobromide salts.**

The strategy is outlined in Schemes II and III.



**Scheme II.** Strategy for preparation of the switch binding ligand  $L^{\text{L/C}}$

*N*-Methyl-3,3'-*N,N*-dipropylamine was coupled<sup>5</sup> with benzyl chloroformate in a pH controlled solution of ethanol- $\text{H}_2\text{O}$  to generate {3-[(3-aminopropyl)-methylamino]-propyl}-carbamic acid benzyl ester whose unprotected primary amine was converted to the imine<sup>6</sup> of [3-({3-[1-(6-acetylpyridin-2-yl)-ethylideneamino]-propyl}-methylamino)-propyl]-carbamic acid benzyl ester by reacting with 2,6-diacetylpyridine. Sodium triacetoxyborohydride reduced<sup>7</sup> selectively the imine to an amine of [3-({3-[1-(6-acetylpyridin-2-yl)-ethylamino]-propyl}-methylamino)-propyl]-carbamic acid benzyl ester without reduction of acetyl group. The carbobenzyloxy group was removed by treatment with hydrobromic acid to get the ligand,  $L^{\text{L/C}}$ .<sup>8</sup>



Scheme III. Strategy for the synthesis of the unreactive surrogate ligand  $L^L$

*N*-Methyl-3,3'-*N,N*-dipropylamine was coupled<sup>5</sup> with benzyl chloroformate in pH controlled solution of ethanol- $H_2O$  to generate {3-[(3-amino-propyl)-methylamino]-propyl}-carbamic acid benzyl ester whose unprotected primary amine was converted to imine<sup>6</sup> of [3-({3-[1-(pyridin-2-yl)-ethylideneamino]-propyl}-methyl-amino)-propyl]-carbamic acid ester by reacting with 2-acetylpyridine. Sodium triacetoxyborohydride reduced<sup>7</sup> the imine to the amine of [3-({3-[1-(pyridin-2-yl)-ethylamino]-propyl}-methylamino)-propyl]-carbamic acid benzyl ester. The carbobenzyloxy group was removed by hydrobromic acid to get  $L^L$ .  $xHBr$

**Equilibrium studies.** Protonation constants for  $L^L$  and  $L^{L/C}$  for formation of their acid salts and their complex stability constants were calculated by computer fitting of the potentiometric data. The initial results of the computations were obtained in the form of overall protonation constants

$$\beta_i^H = [H_i L] / [L] [H]^i$$

or overall stability constants

$$\beta_{pqr} = [MpLqHr] / [M]^p [L]^q [H]^r$$

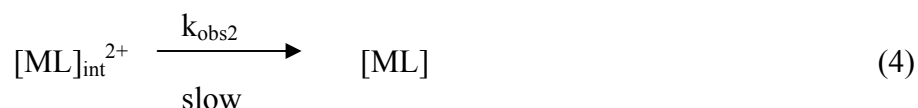
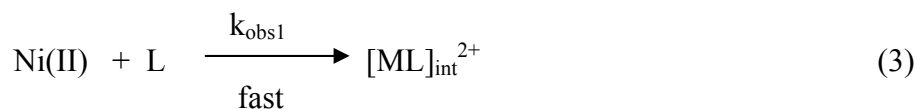
Differences between the various  $\log \beta_i^H$  or the  $\log \beta_{pqr}$  give the stepwise protonation constants or the stepwise formation and protonation constants of the complex reactions.

Typical titration curves of  $L^L$  and  $L^{L/C}$  with NaOH are shown in **Figure 1**. The titration curve for  $L^{L/C}$  was found to be reproducible and reversible despite the expectation that it would quickly form a variety of products in solutions, due to its innate ability to condense inter- or intramolecularly at a variety pH levels. The anticipated variety of products and intermediates was expected to greatly complicate the potentiometric measurements since the identity of the ligand might constantly shift among numerous linear and cyclic structures. The protonation constants for  $L^L$  and  $L^{L/C}$ , together with literature data for related ligands, are summarized in **Table 1**. The higher values of protonation constants correspond to the protonation of the primary and secondary amine nitrogens in the acyclic ligands and to the secondary nitrogens in analogous opposing positions in the macrocycle, py[14]aneN<sub>4</sub>. For both  $L^{L/C}$  and  $L^L$ , the protonation constants for the secondary nitrogen is higher than that for the primary nitrogen atom, representing the typically greater basicity of secondary amines over primary amines<sup>13</sup>. The third and fourth values ( $\log K_3$  and  $\log K_4$ ) for  $L^{L/C}$  and  $L^L$  correspond to the protonation of tertiary nitrogens bearing methyl groups and the pyridine nitrogens, respectively. The last constant for  $L^L$  was not determined because its high acidity prevented a sufficiently accurate determination by potentiometric measurements. The species distribution diagram for  $L^{L/C}$  is shown in **Figure 2**.

Potentiometric titration curves (with and without the metal ion present) of the acid salts of  $L^{L/C}$  and  $L^L$  with NaOH are shown in **Figures 3a** and **3b**. Computer calculations revealed the presence of two complex species,  $[MLH]^{3+}$  and  $[ML]^{2+}$  for the switch binding ligand,  $L=L^{L/C}$ . Also two complex species are formed by the surrogate ligand ( $L = L^L$ ), the first of which is  $[ML]^{2+}$  for all metal ions studied and the second varies as the metal ion is changed. Formation constants for these species are given in **Table 2**. It is noteworthy that in the titration of  $L^{L/C}$  with base in presence of Cu(II) ion, a color change from blue to violet took place as the pH value exceeded 6.5. It is believed that at this pH the copper first complexes with the acyclic ligand (< pH 6) and that the resulting complex ( $CuL^{L/C}$ ) then slowly transforms into the corresponding macrocyclic complex ( $CuL^C$ ). The conversion to the macrocyclic derivative accelerates as the pH increases. Cu(II) solutions that have been titrated with base can be reversibly titrated with acid, completely removing the ligand from the metal ion, a result that is unlikely for macrocyclic complexes. The fact that the  $L^{L/C}/Cu(II)$  formation constant for the 1:1 complex is lower than expected is attributed to complications that follow from the uncertainty over whether equilibrium had been completely attained at each titration point (specifically above pH 6.5). The same uncertainty is associated with results for the other metal ions.

## Kinetic studies

**Kinetics of formation of  $Ni(L^{L/C})^{2+}$ .** The rate of complexation of nickel(II) with  $L^{L/C}$  was studied both by UV-vis spectrophotometer and with a stopped-flow spectrophotometer at 25 °C in the presence of 0.2M  $KNO_3$  from pH 5 – 7.5. All kinetic measurements were carried out under pseudo first order conditions ( $[L^{L/C}] \geq [Ni(II)]$ ) over the pH range 5.0 to 7.5. Reaction sequences were observed in two distinct time regimes, the first in fractions of seconds and the second in hours. Both processes are accompanied by increasing absorbance ( $\lambda_{max} = 390 \text{ nm}$ ), as expected for formation of a square planar nickel(II) complex, **Figure 4**. The two processes can be explained by the pseudo first order rate constants  $k_{obs1}$  and  $k_{obs2}$ , eqs 3 and 4.



where  $[ML]_{int}^{2+}$  is the intermediate complex species associated with the fast process.

**Fast process ( $k_{obs1}$ ).** The initial kinetic process between the Ni(II) ion and  $L^{L/C}$  is complex, giving evidence for three apparent sequential steps (see **Figure 5**), the first of which was found to be pH and concentration dependent, whereas the other two steps were overlapping, difficult to separate, and exhibited only small spectral changes. The first events almost certainly involve the usual reversible binding of the first few ligand sites to the metal ion, eq 5,



(As discussion progresses  $T_L$  will be used to represent the sum of all unprotonated and protonated forms of the ligand:  $L, HL^+, H_2L^{2+}$ , etc)

where  $k_f$  and  $k_d$  are the rate constants for complex formation and the spontaneous dissociation of the nickel(II) complex, respectively.

At constant pH, the reaction kinetics, for the fast reaction were fitted to the differential expression

$$d[\text{NiHL}^{3+}]/dt = k_f [\text{Ni}^{2+}] [\text{LH}_n] - k_d [\text{NiHL}^{3+}] \quad (6)$$

Kinetic determinations were carried out at each of several pH values under conditions where  $T_L \gg T_{\text{Ni}}$  to yield the pseudo first-order rate expression

$$d[\text{NiHL}^{3+}]/dt = k_{\text{obs1}} [\text{Ni}^{2+}] \quad (7)$$

$$(k_{\text{obs1}} = k_d + k_f T_L) \quad (8)$$

for which the observed first-order rate constant,  $k_{\text{obs1}}$ , could be obtained from the  $A/t$  data ( $A =$  absorbance;  $t =$  time) computer fitted to eq 9

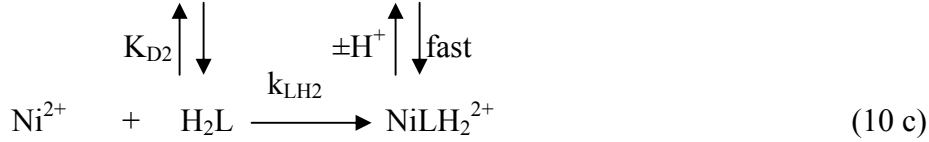
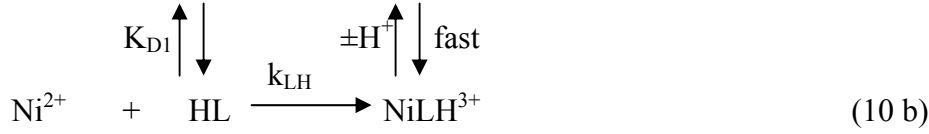
$$A = (A_0 - A_\infty) \exp(-k_{\text{obs1}}t) + A_\infty \quad (9)$$

( $A_0$  and  $A_\infty$  refer to  $t = 0$  and  $t = \infty$ , respectively)

The pH dependence of  $k_{\text{obs1}}$  for the complexation of  $L^{L/C}$  with Ni(II) ion is shown in **Figure 6**. Plots of  $k_{\text{obs1}}$  vs the total concentration of  $L^{L/C}$  are linear, **Figure 7**, with slope  $k_f$  and intercept  $k_d$ . Linear regression analysis yielded  $k_d$  values that were not statistically different from zero.

**Resolution of Specific Rate Constants.** The range of pH values investigated (5.6 – 7.0) was generally limited at the upper end to pH 7-7.4 due to concerns regarding the possible interference caused by precipitation of  $\text{Ni}(\text{OH})_2$ . At low pH values, a very large excess of the one reactant was required to force the reaction to completion. The rates of complex formation between  $L^{L/C}$  and the nickel ion are proportional to  $[\text{L}]_T$  and  $[\text{M}]_T$ . In addition they are functions of pH. Thus it is presumed that all variations with pH observed for  $k_f$  values are due to varying ratios of the existing species of  $L^{L/C}$  over the pH range of the study:  $L$ ,  $\text{LH}^+$  and  $\text{LH}_2^{2+}$ . The triprotonated ligand species,  $\text{LH}_3^{3+}$  was considered to have no significant kinetic contribution (electrostatic consideration) (see **Figure 2**). A possible kinetic Scheme for the fast complex formation step described by equation 10 could involve the steps:

Scheme IV



where  $K_{D1}$  and  $K_{D2}$  are the first and second deprotonation constants of  $L^{L/C}$  and have the values  $9.55 \times 10^{-11}$  M and  $2.95 \times 10^{-9}$  M, respectively ( see **Table 1**). By appropriate substitution it can be readily shown that

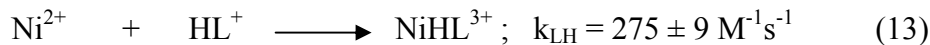
$$k_f = \frac{k_L K_{D1} K_{D2} + k_{HL} K_{D2} [H^+] + k_{H2L} [H^+]^2}{K_{D1} K_{D2} + K_{D2} [H^+] + [H^+]^2} \quad (11)$$

where  $k_f$  is the experimental second order rate constant and  $k_L$ ,  $k_{LH}$ , and  $k_{LH2}$  are the resolved specific rate constants. Values of  $k_L$ ,  $k_{LH}$ , and  $k_{LH2}$  were obtained by curve fitting (using the GRAFIT program<sup>14</sup>, see **Figure 8**) of  $k_f$  to equation 12,

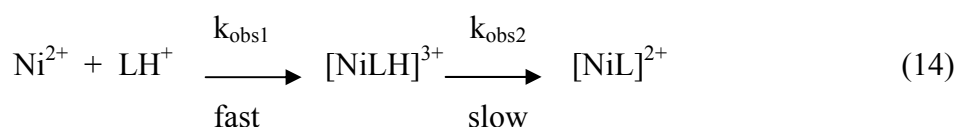
$$k_f = \frac{k_L A + k_{HL} B [H^+] + k_{H2L} [H^+]^2}{A + B [H^+] + [H^+]^2} \quad (12)$$

$$(A = K_{D1} K_{D2} \text{ and } B = K_{D2})$$

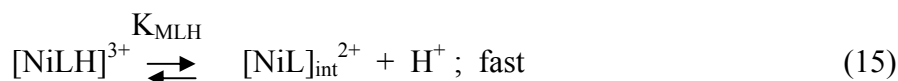
derived on the basis of eq 11 giving,  $k_L = -832 \pm 184 \text{ M}^{-1} \text{ S}^{-1}$ ,  $k_{LH} = 275 \pm 9, \text{ M}^{-1} \text{ S}^{-1}$  and  $k_{LH2} = 2.52 \pm 0.03 \text{ M}^{-1} \text{ S}^{-1}$ . This finding indicates that L of the ligand  $L^{L/C}$  makes no kinetic contribution (same as  $LH_3^{3+}$ ) and that the only reactive ligand species are  $LH^+$  and  $LH_2^{2+}$ , with  $LH^+$  being 110 times more reactive than  $LH_2^{2+}$ . As a result, the above **Scheme** can now be approximated by eq 13



**Slow process ( $k_{obs2}$ ).** The kinetic measurements for the slow process were made using a conventional spectrophotometer under experimental conditions similar to that used for studying the fast reaction. The pH range was 6.8 to 7.9, with  $[Ni^{2+}] = 1.0 \times 10^{-4}$  M in a 12 to 70 fold excess of  $L^{L/C}$  over  $Ni^{2+}$  ( $I = 0.2$  M,  $25$  °C). The kinetics are nicely pseudo first-order and the rate is insensitive to  $[L^{L/C}]$ . A linear increase in rate with pH was observed, **Figure 9**. The reaction **Scheme** that can accommodate both the initial fast step and the subsequent slower one is



At room temperature this slow reaction proceeds with a half life of 5 hours around neutral pH. The reaction is attributed to the monoprotonated precursor complex,  $NiLH^{3+}$ . Further, because the equilibrium constant for the deprotonation step (equation 14) has been found to be  $1.1 \times 10^{-7}$  M (see below), a substantial amount of  $NiL^{2+}$  is available for reaction. The conversion of  $[NiLH]^{3+}$  into  $[NiL]^{2+}$  is accompanied by a large increase in absorbance (see **Figure 4**). The model that quantitatively describes the slow reaction involves a rapid proton dissociation followed by a rate-determining rearrangement step, equations 15 and 16.



The rate constant  $k_{obs2}$  can be quantitatively described as a function of the deprotonation constant,  $K_{MHL}$  ( $K_{MLH} = [NiL^{2+}][H^+]/[NiLH^{3+}]$ ) and the specific rate constant  $k_{ML}$  eq 17

$$k_{obs2} = \frac{k_{ML} K_{MHL}}{K_{MHL} + [H^+]} \quad (17)$$

Equation 17 can be rearranged to the double reciprocal, eq 18.

$$\frac{1}{k_{\text{obs}2}} = \frac{1}{k_{\text{ML}}} + \frac{1}{k_{\text{ML}} K_{\text{MHL}}} [\text{H}^+] \quad (18)$$

The double reciprocal plot of equation 18 was then applied, using the reciprocal of  $k_{\text{obs}2}$  and the calculated  $\text{H}^+$ , **Figure 10**. The linear regression analysis of equation 18 yielded  $k_{\text{ML}} = (4.2 \pm 0.2) \times 10^5 \text{ s}^{-1}$  and  $K_{\text{MHL}} = 1.1 \times 10^{-7} \text{ M}$ .

Understanding the product of this slow reaction presents a substantial challenge. Very commonly macrocyclic ligands first form complexes in conformations that do not produce the most stable final product. Consequently, slow reactions often follow macrocyclic complex formation. The question then becomes: is the slower reaction observed in this study a rearrangement reaction or is it the ring closure step? Since the rapid and slow processes in the system under study are so well separated in time, mass spectrometric studies were conducted to demonstrate the compositions of the intermediates and products; see Scheme I. This Scheme shows that the ligand loses a mole of water when macrocyclization occurs. During short reaction times ( milliseconds to minutes) the nickel-containing intermediates were shown to contain only the beginning ligand,  $\text{L}^{\text{L}^{\text{C}}}$  (the mole of water is still in the ligand composition). On the time scales of hours, the mass spectrometry clearly establishes the appearance and eventual dominance of the macrocyclic complex. Therefore for this system, macrocyclization is slow compared to initial complex formation. The positive ion FAB-MS taken on solutions (pH  $\sim$  7.4) following complexation experiments shows, as the only nickel complex, a peak ( $m/z = 331.3$ ) corresponding to the nickel(II) complex with the fully ring closed macrocycle,  $\text{L}^{\text{C}}$  (**Figure 11**). At earlier times, the complex of the ring-open ligand is also detected (**Figure 12**).

#### ***Kinetics of formation of $\text{Ni}(\text{L}^{\text{L}})^{2+}$***

The Kinetics of the formation of  $\text{Ni}(\text{L}^{\text{L}})^{2+}$  were studied in the pH range 6.0-8.5 under conditions where (a) the total Ni(II) concentration is  $\geq 10$  times the total ligand concentration and (b) the total ligand concentration ( $\text{L}^{\text{L}}$ ) is  $\geq 10$  times excess over the total Ni(II) concentration.

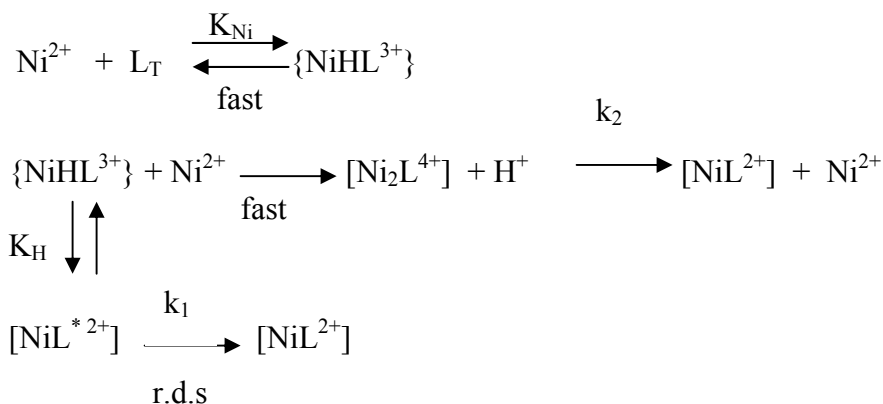
*Kinetics under conditions where  $[\text{Ni}(\text{II})] \geq 10[\text{L}^{\text{L}}]$ .* When  $\text{L}^{\text{L}}$  was mixed with excess  $\text{Ni}^{2+}$  in aqueous solution, a biphasic reaction was observed in all of the experiments ( $\lambda = 360 \text{ nm}$ ). The initial fast step ( 5 -30 s) is associated with an absorbance increase and the subsequent slower reaction ( 50 - 1000 s) to an absorbance decrease involving a relatively small spectral change (**Figure 13**). Only the initial fast step is deemed to be significant and therefore the apparent slower step will not be considered further in this work.

The dependence of the pseudo first-order rate constant,  $k_{\text{obs}}$  on pH at various nickel(II) concentrations is shown in **Figure 14**. The plot of  $k_{\text{obs}}$  vs  $[\text{Ni}^{2+}]_{\text{T}}$  was found to be polynomial, (**Figure 15**) conforming to the expression ( at a given pH) given in equation 19.

$$k_{\text{obs}} = a + b[\text{Ni}^{2+}]_{\text{T}} + c[\text{Ni}^{2+}]_{\text{T}}^2 \quad (19)$$

A possible kinetic model for the complex formation described by equation 19 is shown in **Scheme V**:

**Scheme V.**



( $\text{L}_{\text{T}} = \text{L}, \text{HL}^+, \text{H}_2\text{L}^{2+}$ , etc)

In the presence of excess nickel(II) ion, the binding of a second nickel ion competes with completion of the chelation process. The second path, completion of chelation, dominates at higher pH where it is accelerated by proton removal. It can be readily shown (**Scheme V**) that the experimentally observed rate constant,  $k_{\text{obs}}$  is that given in equation 20.

$$k_{\text{obs}} = k_0 + k_1 K_{\text{H}} K_{\text{Ni}} [\text{Ni}^{2+}] / [\text{H}^+] + k_2 K_{\text{Ni}} [\text{Ni}^{2+}]^2 \quad (20)$$

(assuming that, under the experimental conditions,  $K[\text{Ni}^{2+}] \ll 1$ )

Where  $k_0$ ,  $K_{\text{H}} K_{\text{Ni}}$ , and  $k_2 K_{\text{Ni}}$  = a, b, and c in equation 19, respectively ( $k_0$  corresponds to the spontaneous dissociation of  $[\text{NiL}^{2+}]$ ).

*Kinetics under conditions where  $[L^L] \geq 10[Ni(II)]$ .* The observed reaction of Ni(II) with  $L^L$  under the conditions where  $[L^L] \geq 10[Ni(II)]$  showed, to a large extent, a behavior similar to that observed for the system Ni(II)/ $L^{L/C}$ , as described above. The dependencies of  $k_{obs}$  on pH ( at fixed  $[L^L]$ ) and on  $L^L$  concentration (at a given pH) are shown in Figures 16 and 17 respectively. In all cases, graphs of  $k_{obs}$  versus  $[L^L]$  were linear conforming to the expression given in equation 21.

$$k_{obs} = k_f [L^L] + k_d \quad (21)$$

The rate constants  $k_d$  (= intercept, Eq 21) were found to be  $\sim$  zero indicating that all reactions proceeded virtually to completion.

If it is assumed that Scheme IV above also applies to this case, then for each reaction, the rate constant  $k_f$  (= slope, Eq 21 ) can be expressed as

$$k_f = \frac{k'_L K'_{D1} K'_{D2} + k'_{HL} K'_{D2} [H^+] + k'_{H2L} [H^+]^2}{K'_{D1} K'_{D2} + K'_{D2} [H^+] + [H^+]^2} \quad (22)$$

The equilibrium constants  $K'_{D1}$  and  $K'_{D2}$  are the first and second deprotonation constants of  $L^L$  and have the values  $4.47 \times 10^{-11}$  M and  $2.45 \times 10^{-9}$  M, respectively (Table 1). Computer fitting of the rate expression, equation 22, yielded  $k'_L = (1.7 \pm 2.2) \times 10^3 \text{ M}^{-1} \text{ S}^{-1}$ ,  $k'_{HL} = 556 \pm 30 \text{ M}^{-1} \text{ S}^{-1}$  and  $k'_{H2L} = 29 \pm 2 \text{ M}^{-1} \text{ S}^{-1}$ . Specific rate constants obtained in this study for nickel(II) reacting with the various species of  $L^{L/C}$  and  $L^L$  in aqueous solution together with some structurally related linear and macrocyclic ligands are given in **Table 3**.

## Discussion

**Equilibrium Studies.** In the absence of a complementary metal ion, the novel ligand,  $L^{L/C}$ , is expected to quickly condense with itself forming both a variety of rings and a variety of linear oligomers. It is a property of ligands of this kind that metal ions that are complementary in size and coordination geometry can serve as templates and cause the ligand to form a single product, a macrocycle that encloses the metal ion.<sup>18</sup> Because Schiff base formation is often rapid,  $L^{L/C}$  was expected to present an ever changing molecular composition during an equilibrium titration. Remarkably, a clean, reproducible titration curve was obtained with equilibration times between base additions of 20-60 seconds. Treatment of that data gave the distinctive set of  $pK_a$  values listed in Table 1. The very similar values obtained for the linear ligand  $L^L$  add credibility to the  $pK_a$  values obtained

for the self-reacting ligand  $L^{L/C}$ . No complications were expected in the case of the linear ligand  $L^L$ . Another remarkable observation—all four of the values determined for  $L^{L/C}$  are within a few tenths of a pK unit of those for the linear tetramine, triethylenetetramine (trien).

The protonation pattern for the free ligand anticipates the early events in the binding of  $L^{L/C}$  to a metal ion. The last proton to be removed from  $L^{L/C}H_4^{4+}$  is the secondary amine between the pyridine moiety and the tertiary amine. Internal hydrogen bonding may be expected to augment the inductive effects that make this amine most basic. These considerations, and the resulting relative isolation of the primary amine, point to that group as the nucleophilic center that first binds to the metal ion in the complex formation process, assuming (vide infra) that  $L^{L/C}H^+$  is the dominant reacting ligand species.

Formation constants were determined for several metal ions ( $Cu^{2+}$ ,  $Hg^{2+}$ ,  $Ni^{2+}$ ,  $Zn^{2+}$ ). For pertinence to the rate studies that will be discussed later, it must be remembered that the titrations were all carried out with 20-60s equilibration times. Under the conditions of the experiments,  $L^{L/C}$  forms two kinds of complexes,  $[M(L^{L/C})]^{2+}$  and  $[M(L^{L/C}H)]^{3+}$ . The surrogate ligand  $L^L$ , forms the expected complex with the neutral ligand  $[M(L^L)]^{2+}$ , but the monoprotonated complex is found only for copper(II).

The binding constants  $\beta_{110}$  are remarkably similar for the two ligands, LL/C and LL, so it is apparent that both ligands chelate as linear tetradentate molecules on the time scale of the titrations. Clearly the ligand LL/C has not cyclized prior to binding to the metal ion in any case.

Detailed kinetic investigations have been carried out only for the reactions of the nickel(II) ion with the two ligands LL/C and LL. The study of the LL/C system, reveals a pattern that is, in general, common for reactions between metal ions and macrocyclic ligands, but in detail the pattern is unusual. As would be expected, kinetic events occur in two time regimes, fractions of seconds and hours. A single well-behaved process on the fast time scale is accompanied by what appear to be two additional, but poorly resolved processes that involve only small color changes. The first rapid process is well behaved and reveals that, under conditions of these experiments, nickel(II) undergoes complex formation with only two of the possible ligand species,  $LL/CH_2^{2+}$  and  $LL/CH^+$ , and that reaction with the monoprotonated ligand is dominant. Significant concentrations of the fully deprotonated ligand species are not present at pH values sufficiently low to assure the solubility of  $Ni(OH)_2$ . The additional unexplained rate processes mentioned above may be associated with binding steps subsequent to the linking of the first LL/C donor atom to the metal ion, however, there is a second likely source. These processes might reflect parallel reactions by partially self-condensed ligands; this

additional possibility is unique to self-condensable ligands. Since the surrogate ligand does not show these complications, this second explanation is favored.

At neutral pH the fast reaction is solely due to the monoprotinated ligand,  $LL/CH^+$ , forming the intermediate complex,  $[Ni(LL/CH)]^{3+}$ . That species converts to the final product  $[Ni(Lc)]$  by what appears to be a classic pre-equilibrium proton dissociation step followed by rate determining ligand rearrangement (equation 12). Analysis of the data reveals a half life of about 5 hours and a proton ionization constant of  $1.1 \times 10^{-7} M$ . The acidity of this last proton (from  $LL/CH^+$ ) has been increased by about 3 orders of magnitude by chelation of the ligand to the metal ion. From the equilibrium data, it is reasonable to suggest that the ligand has not undergone ring formation during the rapid reaction steps, but such a conclusion, based on those results alone, must be regarded as tentative at best. If the macrocycle had already formed, it would not be unusual to observe a very slow rearrangement reaction. Often the initial kinetic product of complex formation with macrocyclic ligands is not the thermodynamic product. A common readjustment is the slow inversion of coordinated quaternary nitrogen atoms. The strongest support, from the rate studies, for macrocyclization during the slow step is the large increase in absorbance in the region normally found for low spin square planar nickel(II) complexes.

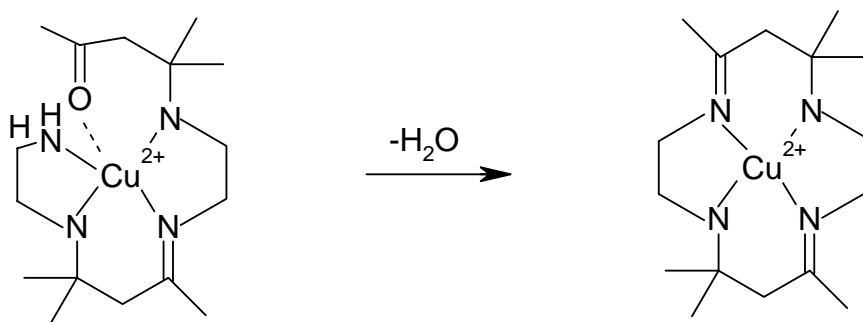
The kinetics of binding of the surrogate ligand,  $L^L$ , supports the view that the slow reaction in the case of  $L^{L/C}$  involves ring closure. The ligand  $L^L$  displays only relatively rapid kinetic processes. For experiments conducted under the same conditions as those used in the study of  $L^{L/C}$ , i.e., in the presence of excess ligand, the  $L^L$  system behaved in a similar fashion to the rapid reaction in the  $Ni/L^{L/C}$  system. The specific rate constants for the ligand,  $L^L$ , are both larger than those for the more complicated ligand,  $L^{L/C}$ . For the simpler surrogate ligand, kinetic studies were also carried out in the presence of a large excess of nickel(II) ion. The excess nickel fostered formation of a 2:1 nickel:ligand complex at lower pH values.

Mass spectrometry has provided definitive proof that the macrocyclization occurs during the slow kinetic time regime. The difference in mass between the nickel(II) complexes with the linear tetradentate precursor ligand,  $L^{L/C}$ , and the macrocyclic ligand,  $L^C$ , is  $\sim 18$  mass units due to the loss of one water molecule. The dominant nickel(II) species at times approximating the completion of the rapid and slow processes, respectively, differ in mass by just that amount (see Figures 11 and 12). Therefore the slow reaction is ring closure, and it produces the macrocyclic complex within a precursor complex containing the switch binding ligand. It should be recalled that there is no corresponding

slow kinetic process in the case of the ligand L<sup>C</sup>. These results prove the switch binding concept based on metal ion templating of specially designed ligands. Further, the dynamics of this first case have been revealed in substantial detail.

Whereas no one has previously suggested the possible advantages of switch binding for ultra tight-binding ligands, a small number of examples exist in the literature where similar topological changes in ligand structure (linear to macrocyclic) have been observed. In fact, these constitute examples of what we labeled the kinetic template effect many years ago.<sup>19</sup>

The first example was found as Verbruggen *et al* explored numerous peptide derivatives as ligands for complexes with technetium(IV) in radiopharmaceutical development.<sup>20-24</sup> Curious *in situ* chemistry was observed when the tetramer of L-alanine was reacted with technetium(IV), yielding an unstable complex that converted into a monooxotechnetium(V) complex of the cyclic tetra-L-alanine as shown in **Scheme VI**.



Scheme VI. Cyclization of [Tc(IV)(tetra-L-alanine)] complex.

In this complex, the carboxyl group was forced in the vicinity of the free amino group, thereby facilitating amide formation and cyclization. Formation of the complex with the tetraamide in aqueous solution was fast but ring closure was quite slow ( $4.9 \times 10^{-3} \text{ min}^{-1}$  at 25 °C, typically), being most rapid at pH 6. The acyclic complex was characterized by HPLC analysis; this intermediate complex was not isolated.

In their investigations on base-catalyzed imine formation, Danby and Hay successfully isolated and determined the crystal structure of the copper(II) complex of the non-cyclized  $\alpha$ -aminoketone in Scheme VII.<sup>25</sup> Scheme VII. Base-catalyzed imine formation of trans-[14]-diene In basic solution, the complex undergoes ring closure to give the macrocyclic copper(II) complex of 5,7,7,12,14,14-hexamethyl-1,4,8,11-tetra-azacyclotetradeca-4,11-diene (trans-[14]-diene). The observed rapid ring

closure occurs via an intramolecular reaction involving the hydroxocomplex  $[\text{Cu}(\text{L})\text{OH}]^+$  at a kobs of  $4.98 \times 10^4 \text{ s}^{-1}$  at  $30.1 \text{ }^\circ\text{C}$ .<sup>26</sup>

From the results reported here and the observations recorded in the literature it is clear that a slow macrocyclization reaction can be fostered following rapid binding of linear polydentate ligands. Thus the switch binding principle enjoys substantial generality. This opens the way to many new uses for the chemistry of ultra tight-binding ligands. Among the perceived advantages peculiar to these novel switch binding ligands is the ability of the rapidly binding ligand to invade strong metal ion binding sites and eventually remove metal ions as transportable species in which the metal ion is sequestered by a ligand of extreme binding affinity. These and many other possibilities remain to be investigated.

**Acknowledgement:** Support of this research by the DOE EMSP Grant DE-FG07-96ER14708 IS deeply appreciated.

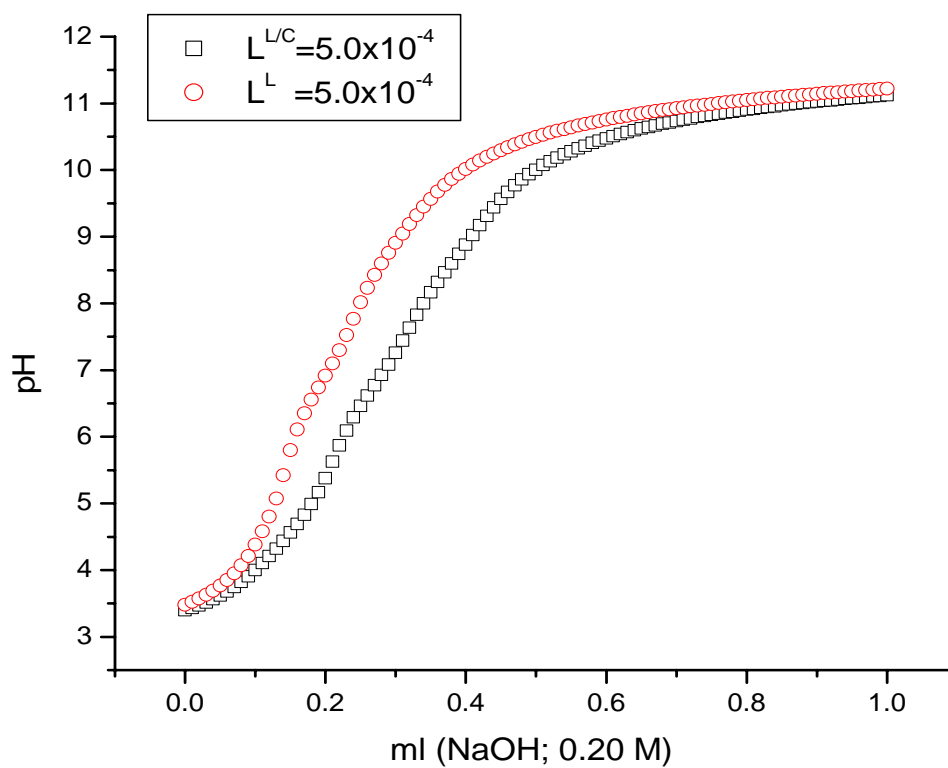
---

## References

1. (a) Cox, B.G.; Schneider, H.; Stroka, J. *J. Am. Chem. Soc.*, **1978**, *100*, 4746; (b) Liesegang, G.W.; Eyring, E.M. in "Synthetic Multidentate Macrocyclic Compounds," Ed. by Izatt, R.M.; Christensen, J.J. Academic press, Inc., London, **1978**, pp 245-289; (c) Eyring, E.M.; Petrucci, S. In "Cation Binding by macrocycles," Ed. by Inoue, Y.; Goekel, G.W. Marcel Dekker, Inc., New York, **1990**, pp. 179-203.
2. *Biological Applications of Photochemical Switches*, Ed. By Morrison, H., John Wiley, NY **1993**: Lester, H. A.; Gurney, A. M. *Physiol. Rev.* **1987**, *67*, 583; Givens, R. S.; Weber, J. J. F.; Jung, A. H.; Park, C.-H. "New Photoprotecting Groups: Desyl and p-Hydroxyphenacyl Phosphate Carboxylate Esters" in *Methods in Enzymology on Caged Compounds: Chemistry, Instrumentation, and Applications*, Ed. By Gerard Marriott, **1998**, *291*,1-29).
3. (a) Busch, D.H. "Ligand Design for Enhanced Molecular Organization--Selectivity and Specific Sequencing in Multiple Receptor Ligands, and Orderly Molecular Entanglements," in *Transition Metal Ions in Supramolecular Chemistry*, Ed by Fabbrizzi, L.,Kluwer, **1994**, pp. 55-79; (b) Busch, D.H. "The Compleat Coordination Chemistry -- What a Difference A Century Makes", *Werner Centennial Volume*, ACS

- Symposium Series, Vol. 565, , pp. 148-164.; (c)Busch, D.H. *Chem.Rev.*, 93, **1993**, 847-860; (d) Busch, D.H. *Chem. Eng. News*, June 29, **1970**, p. 9.
4. Barefield, E.K.; Lovecchio, F.V.; Tokel, N.E.; Ochiai, E.; Busch, D.H. *Inorg. Chem.*, **1972**, *11*, 283.
  5. Atwell, G. J.; Denny, W. A. *Synthesis*, 1984, 1032.
  6. Moffett, R. B.; Leonard, N. J.; Miller, L. A. Synthesis of *N*-methyl-1,2-diphenylethylamine and hydrochloride., *Organic Synthesis*, Coll. Vol. 4, p 605.
  7. Abdel-Magid, A. F.; Carson, K. G.; Harris, B. D.; Maryanoff, C. A.; Shah, R. D. *J. Org. Chem.* **1996**, *61*, 3849; Abdel-Magid, A. F.; Maryanoff, C. A.; Carson, K. G. *Tetrahedron Lett.* **1990**, *31*, 5595.
  8. Ben-Ishai, D.; Berger, A. *J. Org. Chem.* **1952**, *17*, 1564.
  9. Gans, P.; Sabatini, A.; Vaca, A. *J. Chem. Soc., Dalton Trans.* **1985**, 1195.
  10. Alderighi, L. ;Gans, P. ;Ienco, A. ;Peters, D. ;Sabatani, A. ;Vacca, A. *Coord. Chem. Rev.*, **1999**,*184*, 311.
  11. Martell, A. E. ;Smith, R. M. *Critical Stability Constants*. New York: Plenum Press, **1982**.
  12. Costa, J. ;Delgado, R. *Inorg. Chem.*, **1993**, *32*, 5257.
  13. McCasland, A,K., Ph.D. Dissertation, University of Kansas, **1999**.
  14. Erithacus Software Limited © 1988.
  15. Moss, D. B.; Lin, Chin-tung.; Rorabacher, D. B., *J. Am. Chem. Soc.*, **1973**, *8*, 5179.
  16. Wu, Y.; Kaden, T.A.; *Helv. Chim. Acta*, **1984**, *67*, 1868.
  17. Hassan, M. M, Marafie, H. M., and El-Ezaby, M. S.; *Coordination Chemistry*, **2003**, *8*, 709.
  18. Hubin, T. J. and Busch, D. H.; *Coord. Chem. Rev.* **2000**, *200-202*, 5.
  19. Thompson, M.C.; Busch, D. H. *Chem. Eng. News*, September 17, **1962**.p. 57;  
Thompson, M.C.; Busch, D.H. *J. Am. Chem. Soc.*, **1964**, *86*, 3651.
  20. Bormans, G.;Peters, O. M.; Vanbilloen, H.;Blaton, N.; Verbruggen, A. *Inorg. Chem.* **1996**, *35*, 624.
  21. Grummon, G.; Rajagopalan, R.; Palenik, G. J.; Koziol, A. E.; Nosco, D. L. *Inorg. Chem.* **1995**, *34*, 1764.
  22. Nosco, D. L.; Beaty-Nosco, J. A. *Coord. Chem. Rev.* **1999**, *184*, 91.

23. Reichert, D.E.; Lewis, J.S.; Anderson C.J. *Coord. Chem. Rev.* **1999**, 184, 3.
24. Thunus, L; Lejeune, R. *Coord. Chem. Rev.* **1999**, 184, 125.
25. Hay, R. W.; Danby, A.; Miller, S.; Lightfoot, P. *Inorg. Chim. Acta.* **1996**, 246, 395.
26. Danby, A. Ph.D. Dissertation. St Andrews University, **1996**.



titration curves for the acid salts of  $L^{L/C}$  and  $L^L$  at 25 °C and  $I = 0.1 \text{ KNO}_3$ .

Fig 1. pH

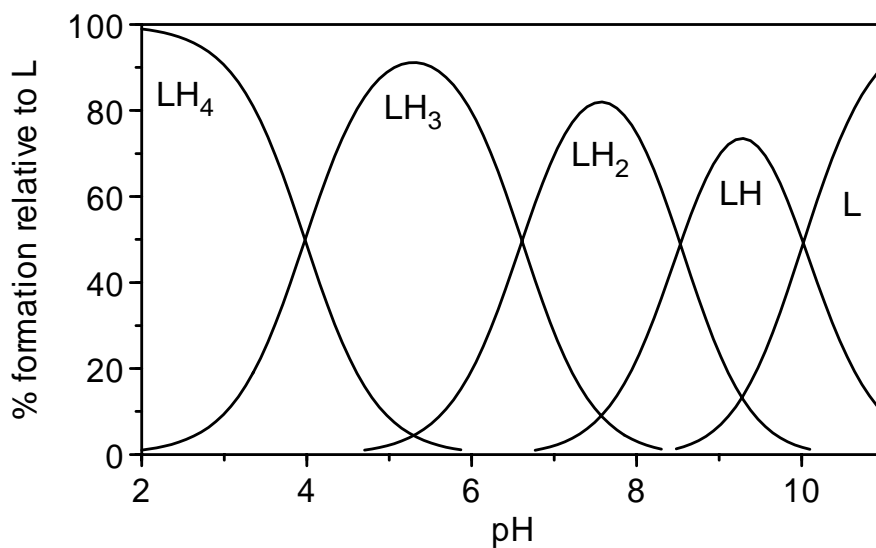
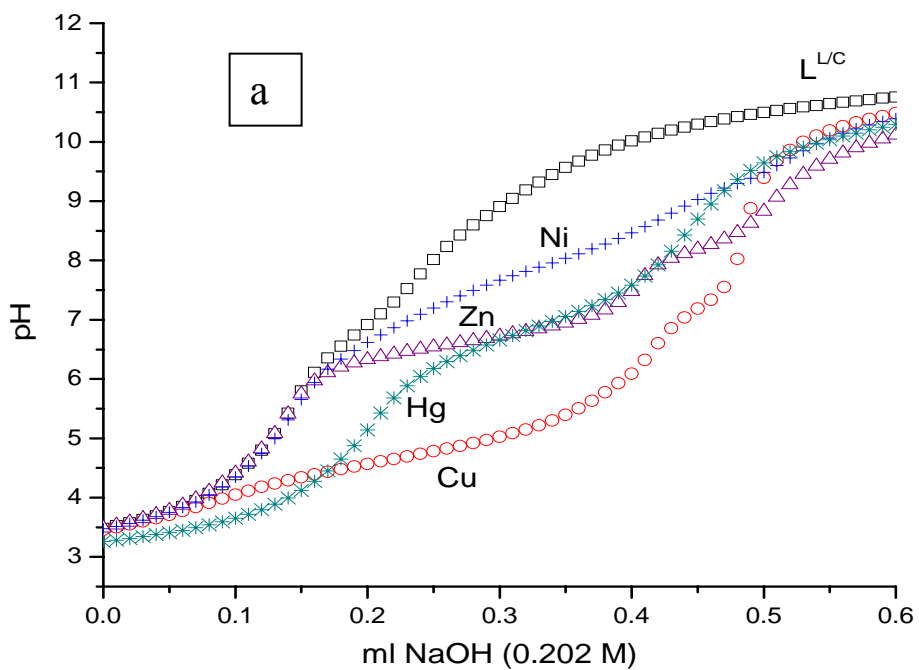


Fig 2. Speciation curves for  $L^{L/C}$ , at 25 °C and  $I = 0.1 \text{ M}$  ( $\text{KNO}_3$ ).



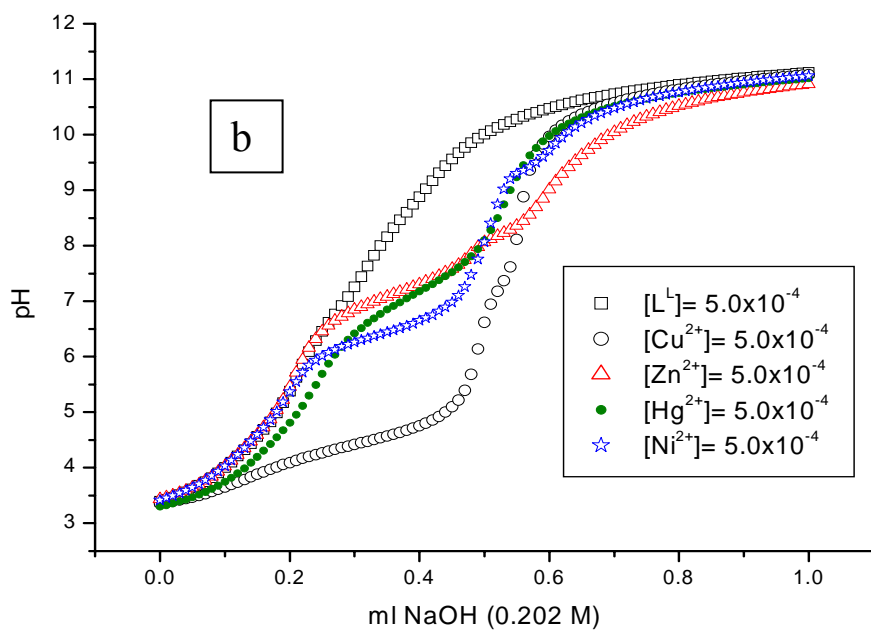


Fig 3. Potentiometric titration curves for  $L^{L/C}$  (a) and  $L^L$  (b) with and without metal ions at 25 °C and  $I = 0.1 \text{ M}$  ( $KNO_3$ ).

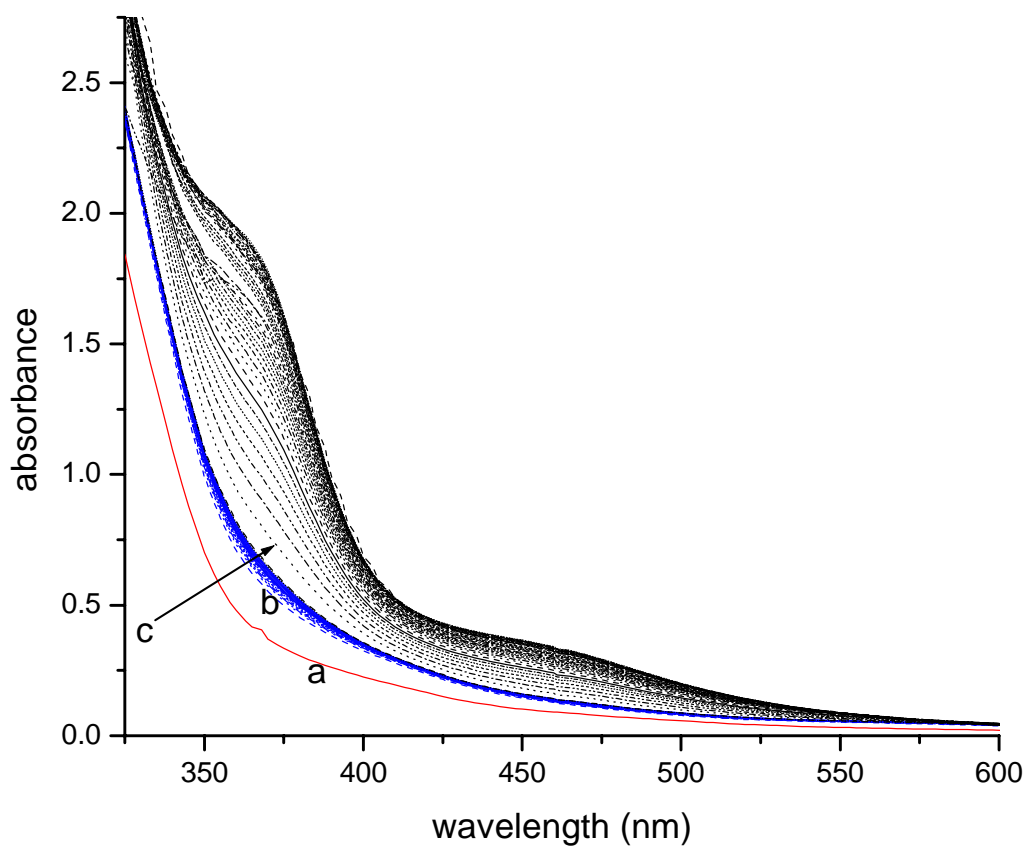


Fig 4. Time dependent spectra recorded for the complexation of  $L^{L/C}$  to nickel(II) in aqueous solution at  $25^\circ$  with  $I= 0.2M$  ( $KNO_3$ ),  $pH = 7.15$ ,  $[L^{L/C}] = 10[Ni^{2+}] = 0.01M$ . a= spectrum of the free ligand. b = spectra of the complex (15 scans; time interval between scans = 2 min). c = spectra of the complex (40 scans; time interval between scans = 1h).

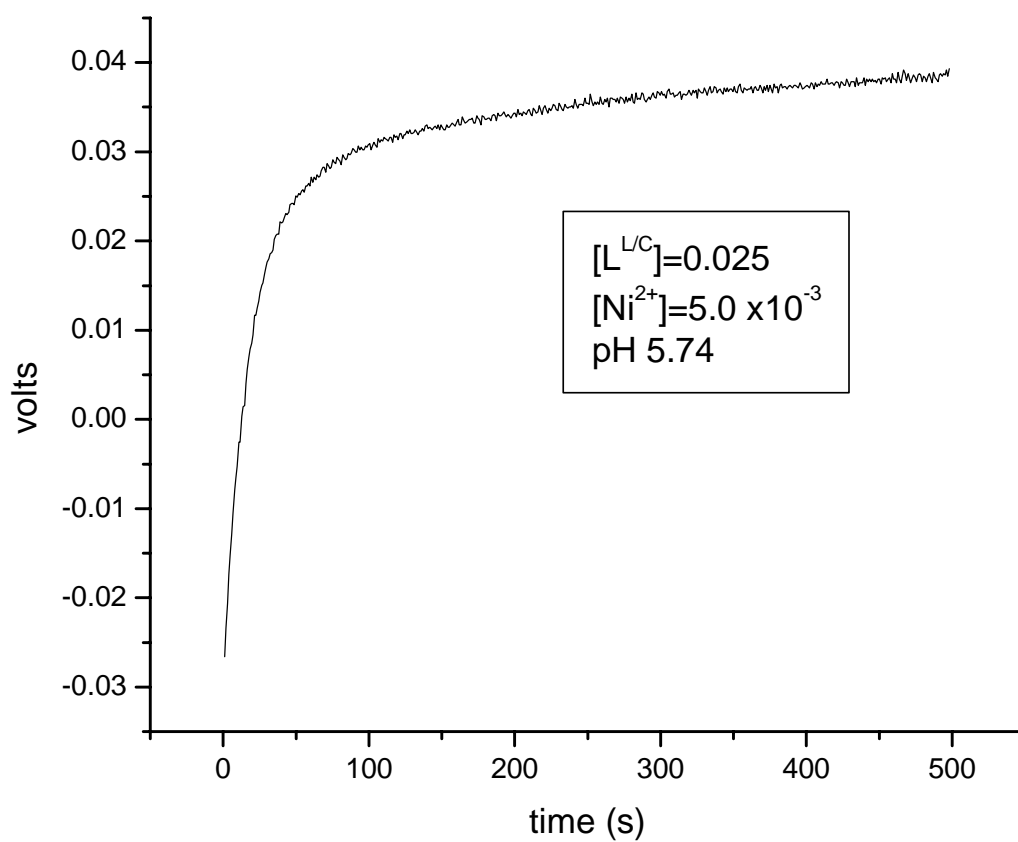


Fig 5. Spectral changes associated with the complexation of  $L^{L/C}$  to Ni(II) at 25°C (fast process,  $\lambda_{max} = 390$  nm).

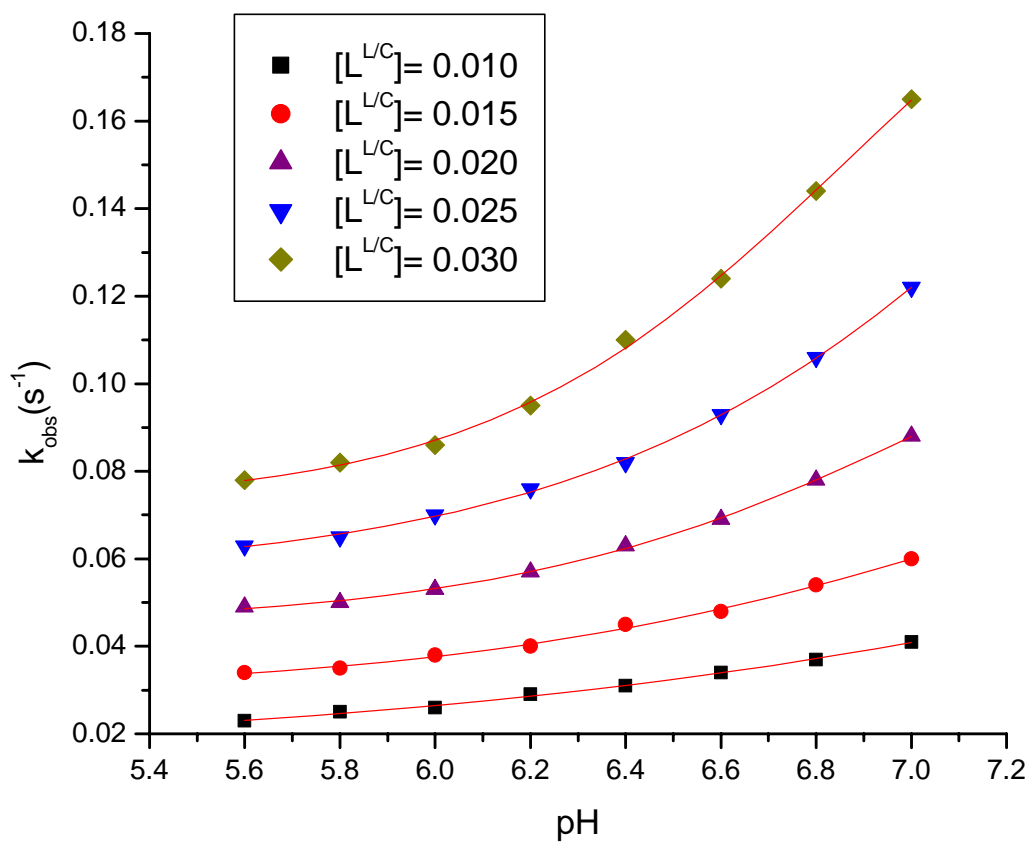


Fig 6. The pH dependence of  $k_{\text{obs}1}$ , at various ligand concentrations, for the initial fast reaction of Ni(II) with  $L^{L/C}$  at 25 °C.

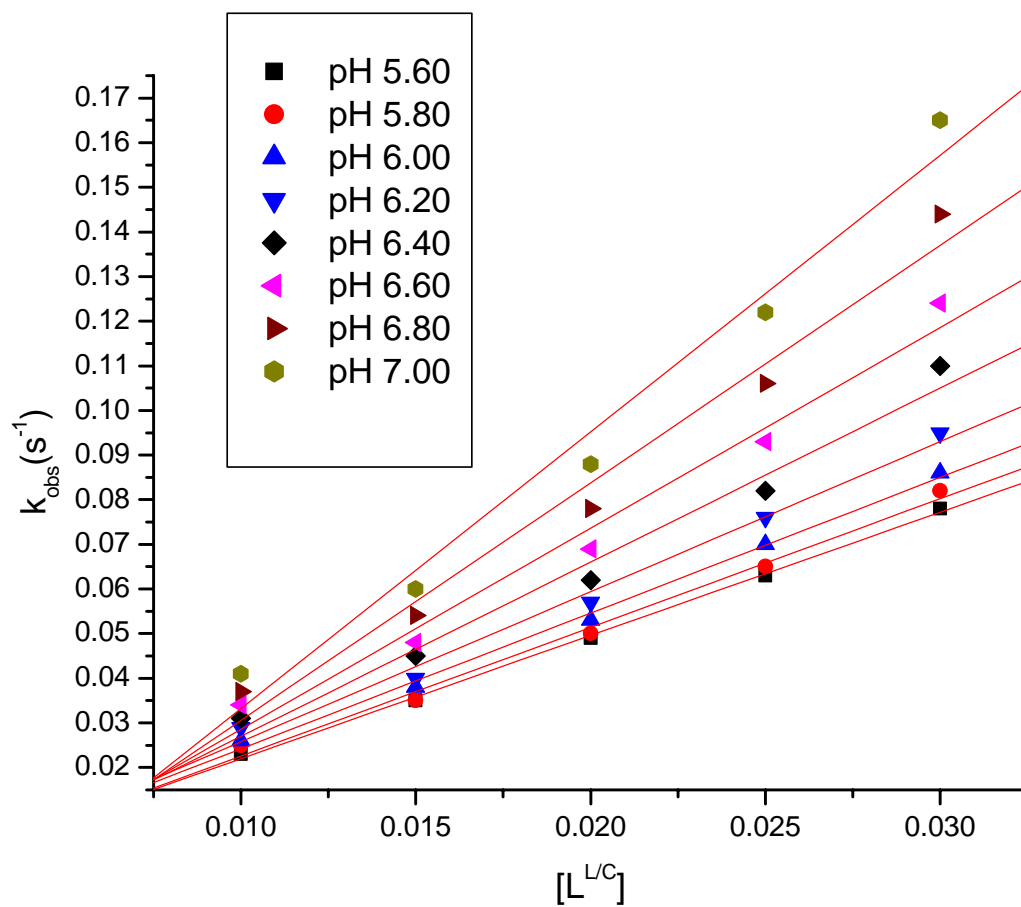


Fig 7. The dependence of  $k_{\text{obs}1}$  as a function of  $T_L$  at various pHs, for the initial fast reaction of Ni(II) with  $L^{L/C}$  at 25 °C.

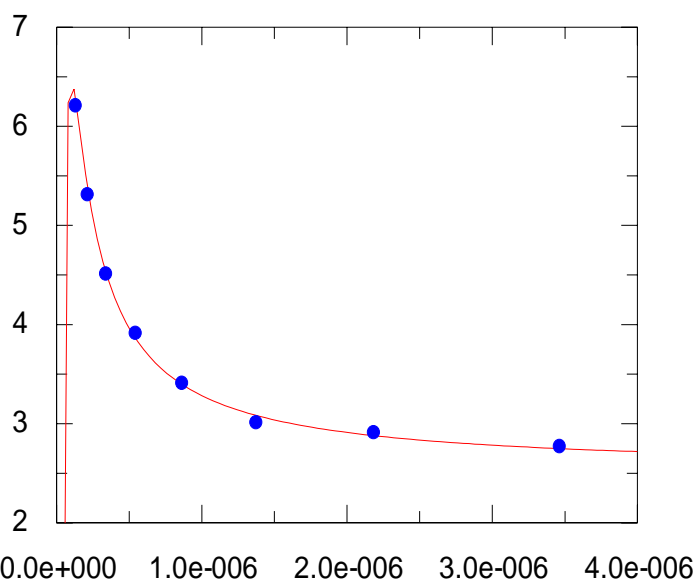
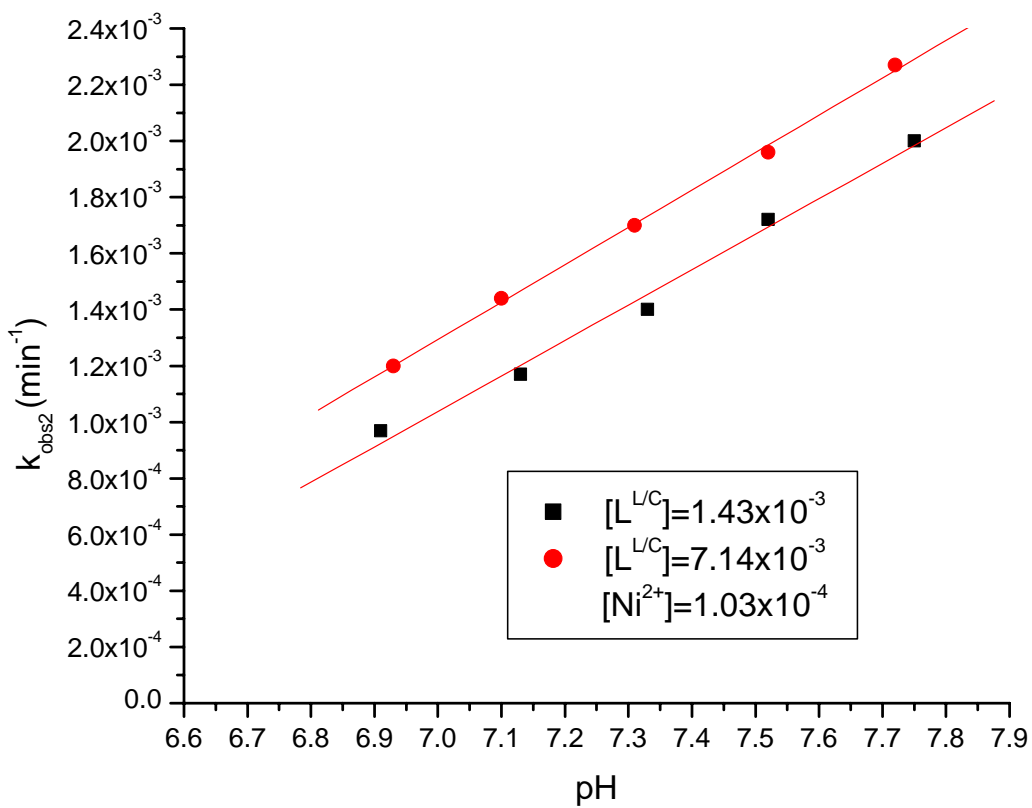


Fig 8. Plot of  $k_f$  vs  $[H^+]$  ( eq 12). The solid line is the calculated curve and the solid points are experimental.



of  $k_{obs2}$  vs pH for the slower reaction of Ni(II) with  $L^{L/C}$  at 25 °C.

Fig 9. Plot

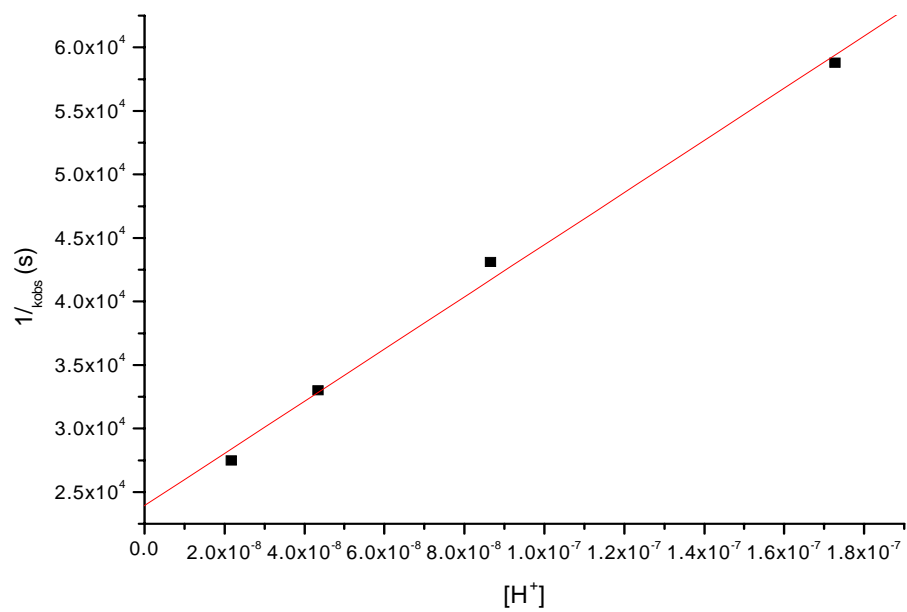


Fig 10. Double reciprocal plot of eq 11

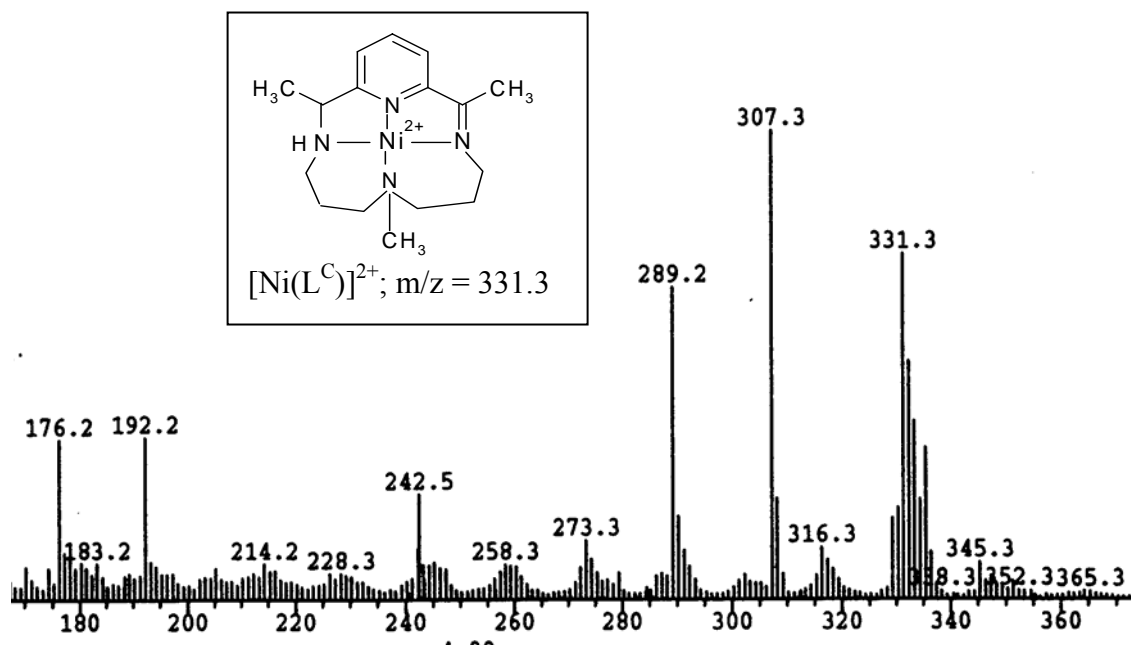


Fig 11. FAB-MS in 3-nitrobenzyl alcohol matrix of the aqueous solution sequestered after UV-vis spectrophotometric studies on the complexation of  $L^{L/C}$  with nickel(II). The spectrum was taken 24 h after the combination of the metal and ligand solutions. The peak at 331.3 (m/z) confirms the in situ formation of  $[Ni(L^C)]^{2+}$  (the peaks 289.2 and 307.3 are matrix lines).

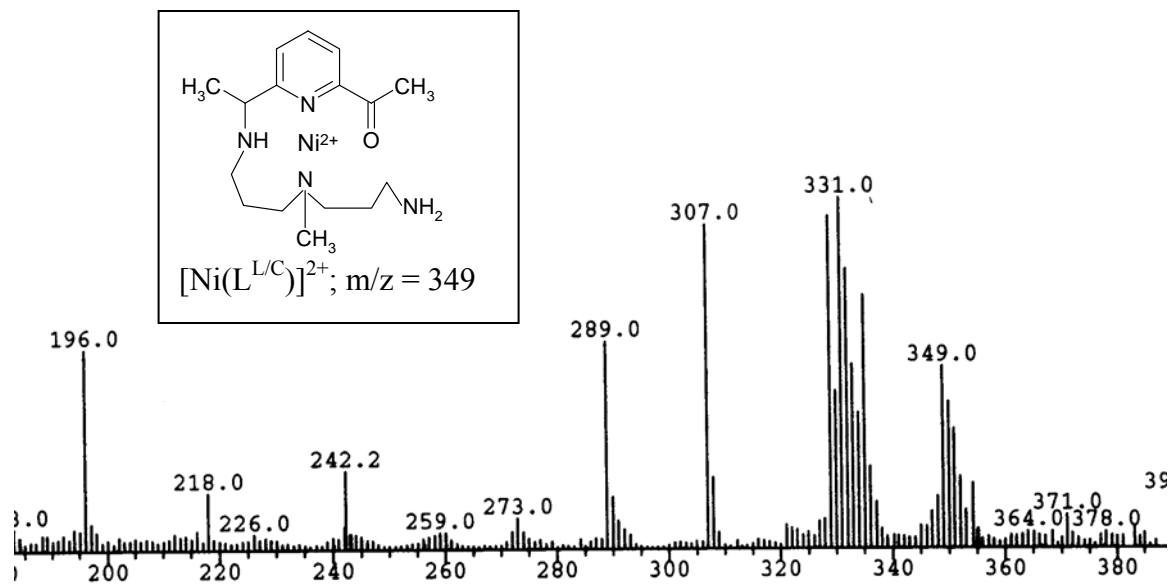


Fig 12. FAB-MS in 3-nitrobenzyl alcohol matrix of the aqueous solution sequestered after UV-vis spectrophotometric studies on the complexation of  $\text{L}^{\text{L/C}}$  with nickel(II). The spectrum was taken 12 h after the combination of the metal and ligand solutions. The peak at 349 (m/z) is for the non cyclic complex  $[\text{Ni}(\text{L}^{\text{L/C}})]^{2+}$  ( the peaks 289.2 and 307.3 are matrix lines).

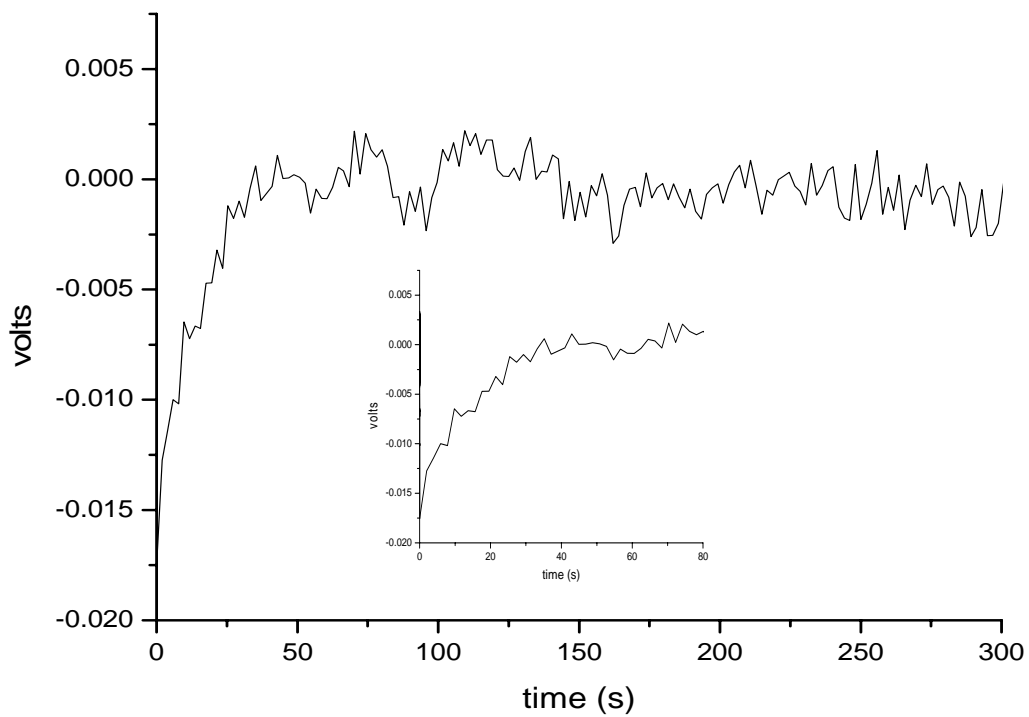


Fig 13.  
Optical change at 360 nm vs time for the complexation of  $L^L$  ( $1.0 \times 10^{-4}$  M) to nickel(II) ( $1.0 \times 10^{-3}$  M) at  $25^\circ\text{C}$  ( the inserted plot is the corresponding optical change in shorter time interval).

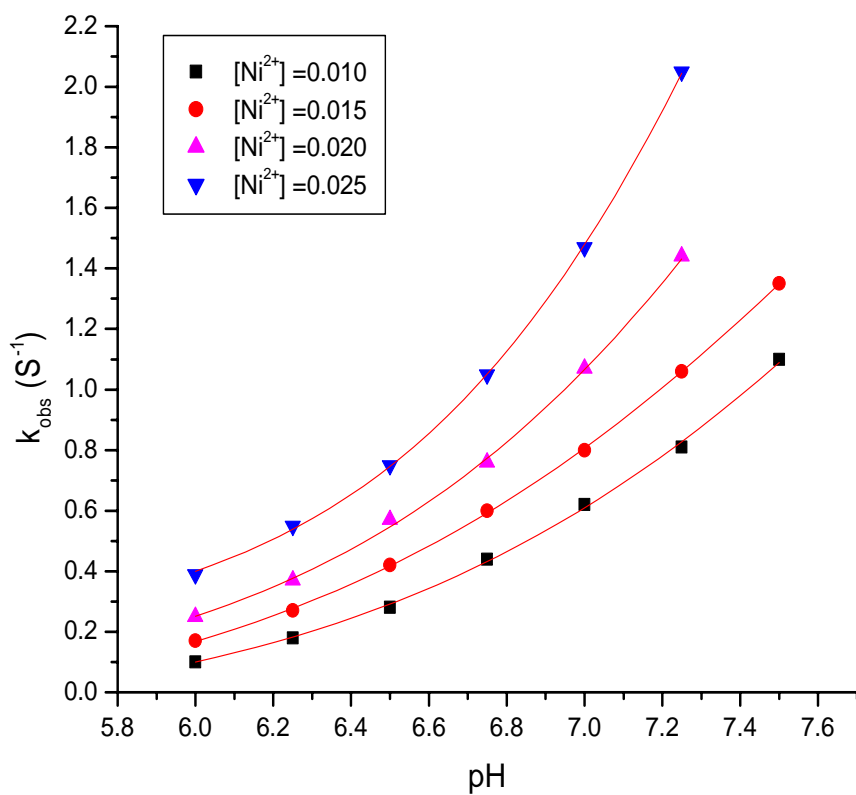


Fig 14. pH dependence of  $k_{\text{obs}}$  for the complexation of  $L^L$  with Ni(II) at 25 °C and  $I = 0.2 \text{ M}$ ,  $[L^L] = 0.001$ .

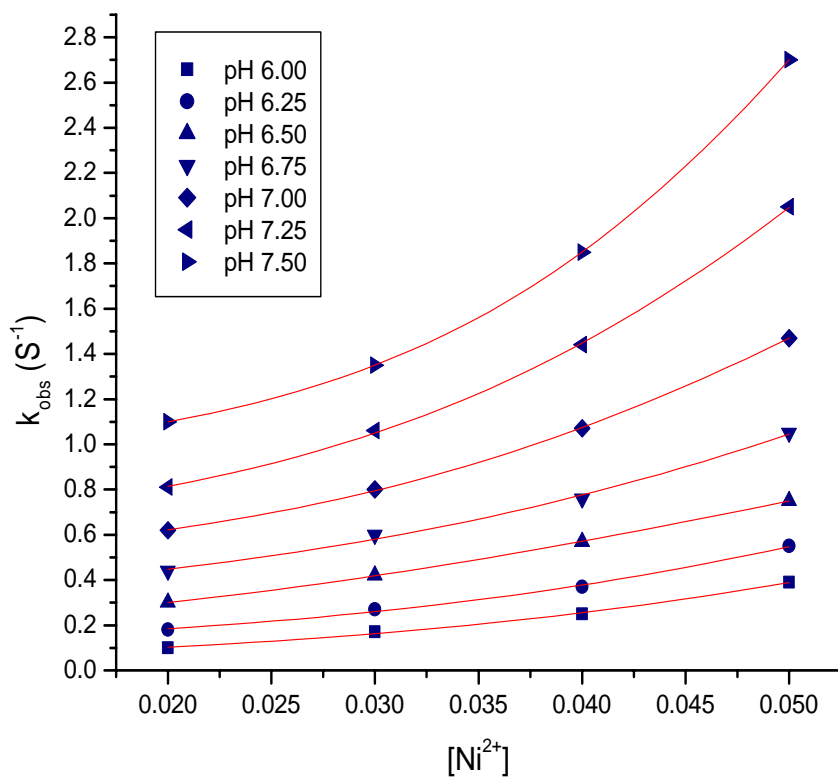


Fig 15. Plots of  $k_{\text{obs}}$  vs. the total concentration of nickel(II) for the reaction with  $L^L$  at  $25^\circ$  and  $I = 0.2$  M,  $[L^L] = 0.001$ .

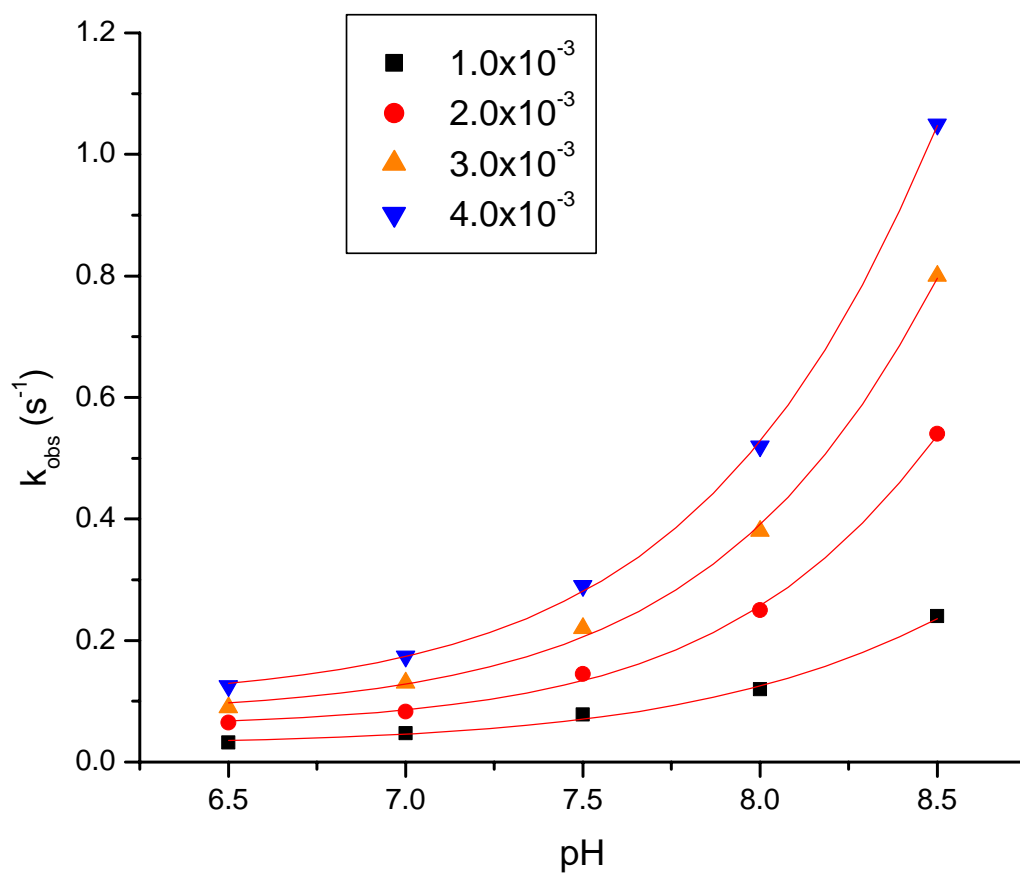


Fig 16. The pH dependence of  $k_{\text{obs}}$ , at various ligand concentrations for the reaction of Ni(II) with  $L^L$  at 25 °C.

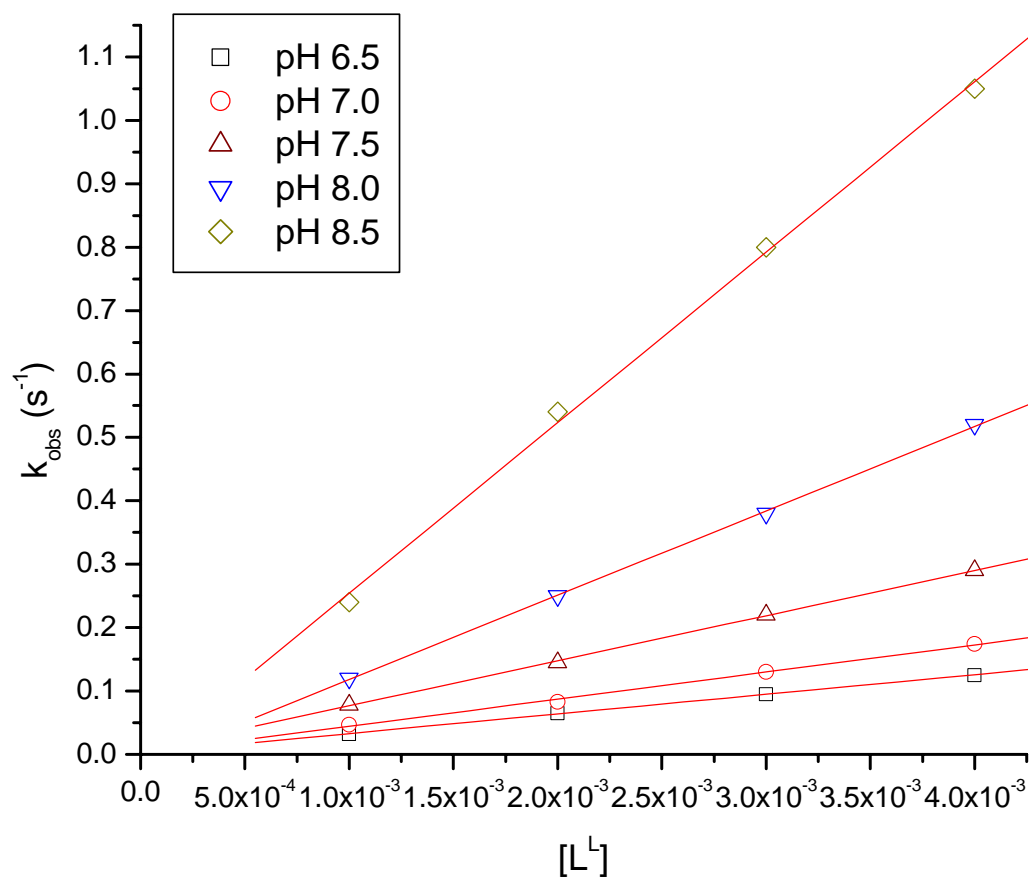


Fig 17.  $k_{\text{obs}}/T_L$  plots at various pHs, for the reaction of Ni(II) with  $L^L$  at 25 °C.

## Figure Captions

Fig 1. pH titration curves for the acid salts of  $L^{L/C}$  and  $L^L$  at 25 °C and  $I = 0.1 \text{ KNO}_3$

Fig 2. Speciation curves for  $L^{L/C}$ , at 25 °C and  $I = 0.1 \text{ M KNO}_3$

Fig 3. Potentiometric titration curves for  $L^{L/C}$  (a) and  $L^L$  (b) with and without metal ions at 25 °C and  $I = 0.1 \text{ M (KNO}_3)$ .

Fig 4. Time dependent spectra recorded for the complexation of  $L^{L/C}$  to nickel(II) in aqueous solution at 25° with  $I = 0.2 \text{ M (KNO}_3)$ ,  $\text{pH} = 7.15$ ,  $[L^{L/C}] = 10[\text{Ni}^{2+}] = 0.01 \text{ M}$ . a = spectrum of the free ligand. b = spectra of the complex (15 scans; time interval between scans = 2 min). c = spectra of the complex (40 scans; time interval between scans = 1h).

Fig 5. Spectral changes associated with the complexation of  $L^{L/C}$  to Ni(II) at 25°C (fast process,  $\lambda_{\text{max}} = 390 \text{ nm}$ ).

Fig 6. The pH dependence of  $k_{\text{obs1}}$ , at various ligand concentrations, for the initial fast reaction of Ni(II) with  $L^{L/C}$  at 25°C.

Fig 7. The dependence of  $k_{\text{obs1}}$  on  $T_L$  at various pH values, for the initial fast reaction of Ni(II) with  $L^{L/C}$  at 25°C.

Fig 8. Plot of  $k_f$  vs  $[\text{H}^+]$  ( eq 12). The solid line is the calculated curve and the solid points are experimental.

Fig 9. Plot of  $k_{\text{obs2}}$  vs pH for the slower reaction of Ni(II) with  $L^{L/C}$  at 25 °C.

Fig 10. Double reciprocal plot of eq 11

Fig 11. FAB-MS of the aqueous solution sequestered in 3-nitrobenzyl alcohol matrix after UV-vis spectrophotometric studies on the complexation of  $L^{L/C}$  with nickel(II). The spectrum was taken 24 h after the combination of the metal and ligand solutions. The peak at 331.3 (m/z) confirms the in situ formation of  $[\text{Ni}(L^C)]^{2+}$  ( the peaks 289.2 and 307.3 are matrix lines).

Fig 12. FAB-MS of the aqueous solution sequestered in 3-nitrobenzyl alcohol matrix after UV-vis spectrophotometric studies on the complexation of  $L^{L/C}$  with nickel(II). The spectrum was taken 12 h after the combination of the metal and ligand solutions. The peak at 349 (m/z) is for the non-cyclic complex  $[\text{Ni}(L^{L/C})]^{2+}$  ( the peaks 289.2 and 307.3 are matrix lines).

Fig 13. Optical change with time at 360 nm for the complexation of  $L^L$  ( $1.0 \times 10^{-4} \text{ M}$ ) with nickel(II) ( $1.0 \times 10^{-3} \text{ M}$ ) at 25°C ( the inserted plot is the corresponding spectral change over a shorter time interval).

Fig 14. pH dependence of  $k_{\text{obs}}$  for the complexation of  $L^L$  with Ni(II) at 25 °C and  $I = 0.2 \text{ M}$ ,  $[L^L] = 0.001 \text{ M}$ .

Fig 15. Plots of  $k_{\text{obs}}$  vs. the total concentration of nickel(II) for the reaction with  $L^L$  at 25° and  $I = 0.2$  M,  $[L^L] = 0.001$  M.

Fig 16. The pH dependence of  $k_{\text{obs}}$ , at various ligand concentrations for the reaction of Ni(II) with  $L^L$  at 25 °C.

Fig 17.  $k_{\text{obs}}$  vs  $T_L$  plots at various pH values, for the reaction of Ni(II) with  $L^L$  at 25°C.

**Table 1. Protonation constants<sup>a</sup> for the ligands  $L^{L/C}$  and  $L^L$  at 25°C and  $I = 0.1$  M ( $KNO_3$ ) and data reported for related ligands.**

	LogK <sub>1</sub>	LogK <sub>2</sub>	LogK <sub>3</sub>	LogK <sub>4</sub>
$L^{L/C}$	10.02 (3)	8.53 (4)	6.61(6)	3.98(8)
$L^L$	10.34(2)	8.61(3)	6.65(8)	4.41(9)
Trien <sup>b</sup>	9.80	9.08	6.55	3.25
Py[14]aneN <sub>4</sub> <sup>c</sup>	9.74	8.67	4.67	< 1

<sup>a</sup>Standard deviations are given in parenthesis.

<sup>b</sup> ref 11

<sup>c</sup> ref 12

**Table 2. Formation Constants for metal complexes for the ligands  $L^{L/C}$  and  $L^L$  with several divalent metal ions at 25.0°C and  $I = 0.1$  M  $KNO_3$ <sup>a</sup>.**

log $\beta_{MLH}$	Cu <sup>2+</sup>	Hg <sup>2+</sup>	Ni <sup>2+</sup>	Zn <sup>2+</sup>
$L^{L/C}$ ligand				
log $\beta_{110}$	14.79(2)	7.72(6)	8.88(1)	8.80(1) <sup>b</sup>
log $\beta_{111}$	19.26(3)	15.57(2)	15.39(2)	14.72(1) <sup>b</sup>
$L^L$ ligand				
log $\beta_{110}$	14.08(2)	7.91(4)	9.53(8)	7.97(1)
log $\beta_{111}$	20.47(4)	15.56	16.01(2)	14.62(8)

---

<sup>a</sup> Standard deviations are given in parenthesis

<sup>b</sup> Iterated independently.

Table 3. Specific rate constants for nickel(II) reacting with various ligand species of L<sup>L/C</sup> and L<sup>L</sup> and other structurally related ligands in aqueous solution at 25 °C.

---

Ligand	specific rate constants ( M <sup>-1</sup> s <sup>-1</sup> )			
	k <sub>LH3</sub>	k <sub>LH2</sub>	k <sub>LH</sub>	k <sub>L</sub>
L <sup>L/C</sup>	...	2.5±0.03	275±9	...
L <sup>L</sup>	...	29±2	556±30	(1.7±1)×10 <sup>3</sup>
trien <sup>a</sup>	...	97	9300	...
cyclam <sup>b</sup>			57	
Py[13]aneN <sub>4</sub> <sup>c</sup>	...	...	73	...

---

<sup>a</sup> Ref 15

<sup>b</sup> Ref 16

<sup>c</sup> Ref 17

## **Toward the *Soil Poulitice* and a New Separations Methodology:**

### **Rebinding of Macrocyclic Metal Complexes to Molecularly Imprinted Polymers Specifically Templated via Non-covalent Interactions**

*Xiaobin Zuo, Donnati Mosha, Stephen J. Archibald, Anne K. McCasland, Abdulhameed M. Hassan, Richard S. Givens, and Daryle H. Busch\**

Department of Chemistry, University of Kansas, Lawrence, KS 66045, USA

#### **Abstract**

The siderophore-based extraction of iron from the soil by bacteria is proposed as a model for a new separation methodology labeled the *soil poulitice*, a molecular device that would selectively retrieve the complex of a targeted metal ion. In this first feasibility study we describe the synthesis and characterization of molecularly imprinted polymers based on non-covalent interactions, and their application in the specific recognition of macrocyclic metal complexes. The imprinting by salts of  $\{N,N',N'',N'''\text{-tetra(2-cyanoethyl)cyclam}\}$  nickel(II) and  $\{N,N',N'',N'''\text{-tetra(2-carbamoylethyl)cyclam}\}$  nickel(II) involve multiple hydrogen bonding interactions when combined during copolymerization with the functional monomer acrylamide or with the crosslinking monomer *N,N'*-ethylenebisacrylamide. Good rebinding capacity for the imprinting metal complex was observed in both acetonitrile and water. Parallel experiments using the vinylsulfonate salt of either nickel(II) complex adds electrostatic interactions, and use of good coordinating groups as functional monomers (e.g. vinyl pyridines) adds a minor ligand component. Imprinted polymers making use of pairs of the interactions (hydrogen bonding plus electrostatic attractions or hydrogen bonding plus minor ligand binding) exhibit greatly increased rebinding abilities, revealing a most promising synergism between pairs of supramolecular modes of attraction. Further, imprinting the polymers with the  $\beta$  isomer of  $\{N,N',N'',N'''\text{-tetra(2-carbamoylethyl)cyclam}\}$  nickel(II) perchlorate led to a marked preference for re-uptake of the  $\beta$  isomer, exemplifying a substantial stereoselectivity. The re-uptake of the  $\beta$  isomer was eight times that of  $\alpha$  isomer. The polymers are resistant to strong acids and oxidizing agents and showed an increase of rebinding capacity during cycles of reuse. The affinities of the same ligands were determined for a number of metal ions, revealing high degrees of selectivity for Hg(II) and Cu(II). The imprinting procedure, combined with the accompanying selective chelation by macrocyclic

ligands, supports the possibility of a new methodology for efficient extraction of metal ions under conditions not necessarily amenable to conventional techniques.

## Introduction

Microbes satisfy their need for iron by secreting extremely powerful ligands called siderophores into their surroundings to extract iron from the iron oxides in the soil, after which the microbe's cell membrane selectively brings the iron-siderophore complex into its interior.<sup>1</sup> We see this natural system as a model for a new way of recovering metal ions from various sources, such as soil deposits and surface contaminations. Such a synthetic system requires a strongly binding, highly selective ligand and that requirement is clearly within the capabilities of modern coordination chemistry.<sup>2</sup> However, the system also requires the equivalent of the cell membrane that selectively adsorbs the targeted metal complex. Here we propose that a molecularly imprinted polymer can serve this latter purpose. For convenience in discussion we will call this synthetic system a "soil poultice", implying that this substance can be contacted with contaminated soil and, like a medicinal poultice, it will cure the ill represented by metal ion contamination.

Because of the great importance of molecular recognition and selective binding to both fundamental science and its many applications, molecularly imprinted polymers (MIPs, first introduced by Wulff in 1972<sup>3</sup>) have received much attention in the fields of chemistry and analytical sciences.<sup>4</sup> In a molecular templating process, an imprint (or template) molecule is reversibly bound to functional monomers and copolymerized in a proper solvent (porogen) with an excess of cross-linking monomer. Removal of the imprint affords tailored binding cavities, which, ideally, are complementary in size, shape and functional group orientation to the imprint molecule. Thus, the resulting polymer can selectively rebind the original imprint in competition with its structural analogues or environmental competitors.

In our soil poultice, it is important that the guest, the metal complex, bind easily and smoothly with the imprinted polymer host. Based on the interactions between an imprint and functional monomers, molecularly imprinted systems can be divided into two groups: covalent and non-covalent. The rebinding capacity of covalent systems is high because of the strong covalent interaction, and often over 80% of the theoretical sites can be reoccupied. In comparison, rebinding capacity of non-covalent systems (e.g. the combination of single-point hydrogen bonding and electrostatic interactions) has not previously exceeded about 20%.<sup>4f,5</sup> However, for many purposes non-covalent MIPs have distinct advantages, including easy and rapid removal of imprint and rapid rebinding. These features make non-covalent MIPs especially attractive for our soil poultice, as indeed it would be for well known separation methodologies, such as chromatography and solvent extraction. Consequently, we are applying the principles<sup>2</sup> of modern coordination chemistry and supramolecular chemistry in studies dedicated to learning how to optimize non-covalent binding by MIPs. For reasons stated above, our focus is on imprinting by and rebinding of complete metal complexes.

Much less attention has been directed at metal-imprinted polymers than those imprinted with organic compounds. About 30 years ago, Nishide *et al.* reported an early study of ionic imprinting in the synthesis of chelating polymers.<sup>6</sup> Recently, Kuchen *et al.*<sup>7</sup> and Lemaire *et al.*<sup>8</sup> developed highly efficient cation imprinted polymers for Cu/Zn and Gd/La separations. Fish *et al.*<sup>9</sup> proposed a sandwich structure for bis{*N*-(4-vinylbenzyl)-1,4,7-triazacyclononane}zinc(II) in a polymer matrix, and Borovik *et al.*<sup>10</sup> have incorporated cobalt(II) dioxygen carriers in imprinted polymers. Typically in most work involving MIPs and metal complexes, the ligand of interest is covalently incorporated in the polymer and any rebinding involves the reaction of the free metal ion with the ligand that is part of the polymer. In our novel metal extraction concept, MIPs rebind the *entire metal complex*, selectively, enhancing any selectivity the ligand may exhibit in binding to the targeted metal ion. This procedure provides two

consecutive recognition events, a combination that, in principle, favours effective selectivity even in the presence of competing metal ions.

In this exploratory study we focus on learning the efficacy attainable through the use of different modes of supramolecular interactions and the synergism that may exist between those different kinds of interactions. Attention is given to binding capacity of the substrate-free imprinted polymers, the selectivity of that re-uptake process, the robustness of the polymers to repeated use, and the relationship of the binding behaviour to the morphology of the polymer samples. The results show that dramatically better results are attainable with noncovalent substrate binding that would be expected on the basis of the literature devoted to the subject.

## Experimental Section

**Materials.** All reagents were obtained commercially and used without further purification. Hydrochloric acid (37%, 99.999% pure) and nitric acid (70%, 99.999% pure) for polymer digestion were purchased from Aldrich. The stock solution of all M(II) nitrates, except mercury(II), were standardized against EDTA (AR, Aldrich) using a copper electrode and calomel reference electrode. The stock solution of Hg(II) nitrate (Reagent Plus, 99.99+%; Aldrich) was prepared by accurate weighing. Carbonate free solutions of sodium hydroxide (0.202 M) were standardized potentiometrically against potassium hydrogen phthalate. 3-Vinyl pyridine was prepared according to a literature procedure.<sup>11</sup>

**Measurements.** NMR spectra were recorded on a Bruker DRX-400 Spectrometer. Fast atom bombardment (FAB) mass spectra were obtained using a VG ZAB MS mass spectrometer equipped with a Xenon gun and 3-nitrobenzyl alcohol (3-NBA) as the matrix material. Nickel analyses were carried out on a JY138 ULTRACE ICP-AES ICP instrument. Surface area and porosity data were collected on a Gemini II 2370 surface area analyzer by the BET gas desorption method.

Potentiometric titrations were performed under N<sub>2</sub> at 25.0°C on a Brinkmann Metrohm 736GB Titrino equipped with an ORION Ross combination electrode (model 81-02). The electrode was standardized by three-buffer calibration using the Titrino's internal standardization method.

Equilibrium measurements were made on 50.0 mL of ligand solution ( $0.5 \times 10^{-3}$  M), first in the absence of metal ions and then in the presence of each metal ion. The [L]:[M] ratios were 1:1, and the ionic strength was maintained constant at 0.1 M (NaNO<sub>3</sub>). The pH data were collected after addition of 0.01 mL increments of standard NaOH solution (with equilibration time of 20-60 s for all the metal ions studied except nickel(II), *vide infra*). The titration data (pH vs mL base) were collected in the Titrino's built-in software. Direct pH meter readings were used for calculation of the protonation and stability constants. The constants determined are mixed constants (also known as Brønsted constants) and they involve the hydrogen ion activity and the concentrations of the other species. The protonation and stability constants were calculated by fitting the potentiometric data with the SUPERQUAD program.<sup>12</sup> Species distribution diagrams were generated with the aid of the HySS2 program.<sup>13</sup>

**Synthesis of the ligands and their nickel(II) complexes.** All the ligands and nickel(II) complexes were synthesized by the methods of Wainwright<sup>14</sup> and Barefield.<sup>15</sup>

***N,N',N'',N'''*-Tetra(2-cyanoethyl)-1,4,8,11-tetraazacyclotetradecane (1).** The ligand (1) was prepared by the reflux of 1,4,8,11-tetraazacyclotetradecane (cyclam) and acrylonitrile.<sup>14</sup> Yield: 76%. <sup>1</sup>H NMR (CDCl<sub>3</sub>): δ 1.6 (quintet, 4H), 2.4 (t, 8H), 2.55 (complex mult., 16H), 2.7 (t, 8H). <sup>13</sup>C NMR: δ 119.3, 51.7, 51.3, 51.2, 24.7, 16.4. Anal. Calcd. for C<sub>22</sub>H<sub>36</sub>N<sub>8</sub>·0.5H<sub>2</sub>O: C, 62.7; H, 8.85; N, 26.6. Found: C, 62.8; H, 8.84; N, 26.4.

***N,N',N'',N'''*-Tetra(2-carbamoyl ethyl)-1,4,8,11-tetraazacyclotetradecane (2).** This compound was prepared by the reflux of 1,4,8,11-tetraazacyclotetradecane and acrylamide in methanol<sup>15</sup> and recrystallized from ethanol/water (5/1). Yield: 50%. <sup>1</sup>H NMR (D<sub>2</sub>O): multiplet centered around δ 2.60

ppm.  $^{13}\text{C}$  NMR:  $\delta$  178.3, 51.1, 49.9, 46.9, 32.9, 20.1. Anal. Calcd. for  $\text{C}_{22}\text{H}_{44}\text{N}_8\text{O}_4$ : C, 54.5; H, 9.15; N, 23.1. Found: C, 54.4; H, 9.16; N, 22.9.

**$\alpha$ -[Ni(1)](ClO<sub>4</sub>)<sub>2</sub>·H<sub>2</sub>O ( $\alpha$ -3).** The  $\alpha$ -isomer of the nickel(II) complex of ligand **1** was prepared as a green solid by the room temperature reaction of **1** and nickel(II) perchlorate in acetonitrile.<sup>15</sup> Yield: 88%. Mass Spec. (FAB/+ve):  $m/z$  569 =  $[\text{NiL}(\text{ClO}_4)]^+$ , 516 =  $[\text{NiL}(\text{ClO}_4)\text{-CH}_2\text{CHCN}]^+$ , 470 =  $[\text{NiL}]^+$ , 413 =  $[\text{L+H}]^+$ . Anal. Calcd. for  $\text{C}_{22}\text{H}_{38}\text{N}_8\text{O}_9\text{Cl}_2\text{Ni}$ : C, 38.4; H, 5.57; N, 16.3. Found: C, 38.7; H, 5.42; N, 16.4.

**$\beta$ -[Ni(1)](ClO<sub>4</sub>)<sub>2</sub>·H<sub>2</sub>O ( $\beta$ -3).** The  $\beta$ -isomer of compound **3** was prepared as a dark green solid by the reflux of  $\alpha$ -[Ni(1)](ClO<sub>4</sub>)<sub>2</sub>·H<sub>2</sub>O in acetonitrile.<sup>15</sup> Yield: 75%. Mass Spec. (FAB/+ve):  $m/z$  569 =  $[\text{NiL}(\text{ClO}_4)]^+$ , 516 =  $[\text{NiL}(\text{ClO}_4)\text{-CH}_2\text{CHCN}]^+$ , 470 =  $[\text{NiL}]^+$ , 413 =  $[\text{L+H}]^+$ . Anal. Calcd. for  $\text{C}_{22}\text{H}_{38}\text{N}_8\text{O}_9\text{Cl}_2\text{Ni}$ : C, 38.4; H, 5.57; N, 16.3. Found: C, 38.2; H, 5.36; N, 16.3.

**$\alpha$ -[Ni(2)](ClO<sub>4</sub>)<sub>2</sub> ( $\alpha$ -4).** This  $\alpha$ -isomer was prepared as a green solid by the room temperature reaction of **2** and nickel(II) perchlorate in water.<sup>15</sup> Yield: 65%. Mass Spec. (FAB/+ve):  $m/z$  641 =  $[\text{NiL}(\text{ClO}_4)]^+$ , 570 =  $[\text{NiL}(\text{ClO}_4)\text{-CH}_2\text{CHCONH}_2]^+$ , 542 =  $[\text{NiL}]^+$ , 485 =  $[\text{LH}]^+$ . Anal. Calcd. for  $\text{C}_{22}\text{H}_{44}\text{N}_8\text{O}_{12}\text{Cl}_2\text{Ni}$ : C, 35.6; H, 5.98; N, 15.1. Found: C, 35.9; H, 6.04; N, 14.7.

**$\beta$ -[Ni(2)](ClO<sub>4</sub>)<sub>2</sub> ( $\beta$ -4).** The  $\beta$ -isomer of  $[\text{Ni}(2)](\text{ClO}_4)_2$  prepared as a light blue solid by the reflux of **2** and nickel(II) perchlorate in water.<sup>15</sup> Yield: 75%. Mass Spec. (FAB/+ve):  $m/z$  641 =  $[\text{NiL}(\text{ClO}_4)]^+$ , 570 =  $[\text{NiL}(\text{ClO}_4)\text{-CH}_2\text{CHCONH}_2]^+$ , 542 =  $[\text{NiL}]^+$ , 485 =  $[\text{LH}]^+$ . Anal. Calcd. for  $\text{C}_{22}\text{H}_{44}\text{N}_8\text{O}_{12}\text{Cl}_2\text{Ni}$ : C, 35.6; H, 5.98; N, 15.1. Found: C, 35.3; H, 5.99; N, 14.6.

**$\beta$ -[Ni(2)](CH<sub>2</sub>=CHSO<sub>3</sub>)<sub>2</sub>·2H<sub>2</sub>O ( $\beta$ -5).** This vinylsulfonate salt was prepared as a pink solid by the reflux of **2** and nickel(II) vinylsulfonate in water. Yield: 27%. Mass Spec. (FAB/+ve):  $m/z$  649 =  $[\text{NiL}(\text{CH}_2\text{CHSO}_3)]^+$ , 578 =  $[\text{NiL}(\text{ClO}_4)\text{-CH}_2\text{CHCONH}_2]^+$ , 542 =  $[\text{NiL}]^+$ , 485 =  $[\text{L+H}]^+$ . Anal. Calcd. for  $\text{C}_{26}\text{H}_{54}\text{N}_8\text{O}_{12}\text{S}_2\text{Ni}$ : C, 39.4; H, 6.85; N, 14.1. Found (2 determinations): C, 39.8, 39.3; H, 6.81, 7.18; N, 13.3, 14.3.

**Polymer Synthesis.** All the polymers were prepared by thermally initiated free radical polymerizations. Typically, a solution of metal complex (imprint, 4 mol%), acrylamide (functional monomer, 16 mol%) and ethylene glycol dimethacrylate (EGDMA, crosslinker, 80 mol%) or *N,N'*-ethylenebisacrylamide (EBA, crosslinker with functional groups; no acrylamide was used in this case, *vide infra*), in a mixture of acetonitrile and methanol, was placed in a polymerization tube and purged with Ar for 5 min, followed by addition of the solid initiator, azobis(isobutyronitrile) (AIBN). The mixture was again purged with Ar for 5 min and the tube was sealed under Ar. The reaction was carried out at 50°C for 24 h. Then the polymers were dried in vacuo, ground and sieved to a 75-125  $\mu\text{m}$  particle size.

**Rebinding Experiments.** The imprint was removed by soxhlet extraction with acetonitrile (24 h). In addition, the polymers incorporating the vinylsulfonate anion were washed repeatedly with a methanolic ammonium chloride solution to exchange any remaining cationic imprinted complex. All the samples were then vacuum dried, and pre-weighed portions were digested in concentrated nitric acid for 12 h. Baseline values for residual nickel(II) in the extracted polymers were obtained from ICP analyses on these samples. To measure the imprint rebinding, a pre-weighed amount of extracted polymer was shaken in a 0.18 M acetonitrile solution of  $\beta$ -4 for 24 h and collected by filtration. The samples were digested in concentrated nitric acid over 12 h and the nickel concentration measured by ICP to determine the amount of nickel(II) complex rebound within the polymer matrix. These values were corrected for residual nickel by subtracting the previous baseline values. Rebinding values were reproducible within 5% and the quantities in Tables 2-7 are reported accordingly.

## Results and Discussion

In its final, fully functional form, the soil poultice will exert selectivity at two levels: first, in the binding of the metal ion by the ligand and, second, in the binding of the metal complex by the molecularly imprinted polymer. In the best case, the selective binding at each of the two stages would be very strong, but the rate at which the binding occurs would be rapid. The present studies have focused on a small number of broad but essential issues. Because covalent interactions tend to involve slow kinetics we restrict attention to those inter-molecular interactions that are non-covalent. The immediate issue then becomes “can non-covalent interactions be strong enough to produce the proposed new methodology?” The literature indicates that imprinting using, for example, hydrogen bonding or electrostatic interaction, instead of covalent binding, supports only 10 to 15%, certainly less than 20%, rebinding capacity. An equally compelling issue relates to the compatibility of the combined goals of selective binding during complex formation and selectivity during the binding of the complex to the polymer. Further, are these porous imprinted polymers likely to be durable enough to actually be used in a separations methodology? In considering these issues the binding capacity has been studied at both the complex formation and the polymer/imprint level for the first system of this kind.

**Selectivity of macrocyclic metal complex formation.** The complexing ability and metal ion selectivity of the macrocyclic ligand 2, (Chart 1) were investigated by equilibrium methods. Protonation constants for 2 and formation constants of 2 with Cu(II), Hg(II), Cd(II), Pb(II), Zn(II) and Ni(II) were determined by glass-electrode titration measurements. Typical titration curves of 2 with NaOH (with and without metal ion present) are shown in Figure 1. It can readily be seen that the ligand presents three protonation constants, two having high values and one, a low value (Table 1). The last constant was not determined because its high acidity prevented a sufficiently accurate determination by potentiometric measurements. The rate of equilibration was rapid for all the metal ion complexes studied in this work, except that of nickel(II), and straightforward glass-electrode measurements yielded the formation constants which are also shown in Table 1. While the nickel(II) complex was slow to equilibrate, it was not so slow as to render conventional glass-electrode measurements impractical. In all cases 1:1 complexes  $ML^{2+}$  were formed under the conditions of the measurements ( $\log\beta_{101}$ ), whereas monoprotonated complexes  $MHL^{3+}$  were also found for the metal ions Cd(II), Pb(II), and Zn(II). It is interesting that Cu(II) and Hg(II), which form complexes having the highest stability constants ( $\log\beta_{101}$ ), also form dimers  $M_2L^{4+}$ . The species distribution diagram for Hg(II) is shown in Figure 2. The large  $\log\beta_{101}$  difference compared to other metal ions ( $>12$ ), is indicative of very strong chelation to Cu(II) and Hg(II).<sup>16</sup> This result for ligand 2 is especially promising for selectively binding these metal ions and possibly removing them from polluted sites. Equilibration of all metal ion complexes showed no precipitate even at high pH values with the exception of Pb(II) which precipitated at pH  $\sim 7$ .

Because of their kinetic inertness, as also shown in our previous study,<sup>17</sup> the nickel(II) complexes with tetradentate tetraazamacrocyclic ligands are less likely to dissociate during the molecular imprinting process. Therefore they have been employed in all of the MIPs studies reported here.

#### Molecularly imprinted polymers

MIPs based on multiple and multi-site hydrogen bonding: EGDMA vs EBA. In the extensively investigated chiral separation of amino acid derivatives, a molar ratio of 1:4:20 (imprint to functional monomer to crosslinker) was found to be an optimized recipe for preparing non-covalent MIPs, using methacrylic acid as the functional monomer (approximately two- to three-fold molar equivalents of the functional monomer relative to each polar group of the template).<sup>18</sup> The maximum rebinding capacity was 10-15%,<sup>4f,5</sup> as mentioned above.

In an effort to build strength into the non-covalent interactions, amide groups were chosen for our MIPs instead of carboxylic acid groups because they form stronger hydrogen bonds than carboxyl groups in polar solvents, such as acetonitrile.<sup>19</sup> Chart 2 (right) shows the interaction mode between the nickel(II) complex **4** (Chart 3) and the functional monomer acrylamide. Pairs of amide groups form two-point hydrogen bonding interactions, creating relatively strong 4-center hydrogen bonded linkages. In addition, the four pendant amide groups on the complex provide ample opportunity for hydrogen bonding with corresponding groups in the polymer. Further, both EGDMA (ethylene glycol dimethacrylate) and EBA (*N,N'*-ethylenebisacrylamide) were investigated as cross-linking agents. Whereas EGDMA can only serve as a proton acceptor in a hydrogen bonding network, EBA adds both proton donors and proton acceptors to the hydrogen bonding inventory.

First, we studied the MIPs imprinted against  $\beta$ -**4**, the thermodynamically stable isomer, because of its ready availability. Table 2 summarizes the synthetic parameters, surface characterization and rebinding capacity of the corresponding MIPs, as well as control polymers prepared with no imprint present. Generally, EGDMA polymers have significantly larger surface area and pore volume than EBA polymers. In both cases there was a decrease in surface area and pore volume with the incorporation of the imprint molecule.

The imprinted polymer **P2**, prepared with a molar ratio of 1:4:20 of  $\beta$ -**4** to acrylamide to EGDMA, showed a re-uptake of 3.5mg Ni/g polymer, or 26% rebinding of the theoretical sites. A noticeable imprinting effect was obtained when comparing this value to that (2.3mg/g) of the control polymer **P1** (Table 3). Because high functional monomer concentration favours the formation of adduct between the imprint and the functional monomer,<sup>20</sup> polymers with a 12:20 ratio of acrylamide to EGDMA were prepared (**P4**). Remarkably, the nickel(II) re-uptake of the resulting imprinted polymer **P4** almost tripled the value previously determined for **P2**. The 12:20 control polymer **P3** also showed an increase in rebinding, however, to a much smaller extent. Thus, the imprinting effect was more pronounced at a lower molar ratio of crosslinker to functional monomer. From these data we have learned that it is possible to produce high binding and rebinding capacities in MIPs by providing an abundance of amide-based hydrogen binding sites. Capacities have been found that far exceed any previously reported.

Polymer recognition of the metal complex can also be realized with different specific positions and orientations of the hydrogen bonding groups in the polymer; e.g., the functional groups can be located on either the functional monomer or the crosslinker. EBA was introduced for two reasons. On one hand, it was known that, under most conditions, not all of the acrylamide enters into the polymerization and the presence of EBA could replace that loss of functional groups (acrylamide). On the other hand, replacing EGDMA with EBA made it possible to learn the effect of increasing the number of amide groups in the polymers (two amide groups in each EBA molecule). Consequently, EBA polymers were prepared in the absence of the usual acrylamide “functional monomer”. The expected hydrogen bonding interaction pattern is the same as that of the EGDMA/acrylamide polymers (Chart 2, right).

As shown in Table 2, EBA polymers exhibited considerably higher nickel(II) re-uptake than EGDMA polymers, which reflects the large excess of amide groups on the crosslinker. For such an imprinted polymer **P6** with 1:18 of  $\beta$ -**4** to EBA, the nickel(II) re-uptake was 38 mg/g, whereas the value for the control polymer was only 22 mg/g. This difference also demonstrates a marked increase in capacity based on the imprinting effect. However, further increases in the relative amount of imprint during the polymerization process resulted in lower rebinding capacity (**P7** and **P8**).

**MIPs based on hydrogen bonding & electrostatic interaction: acetonitrile vs water; Scatchard analysis.** In studies on enantiomeric selectivity by MIPs it has been shown that the combination of

electrostatic binding and hydrogen bonding can be made far more effective than either mode of interaction alone.<sup>4f</sup> We introduced the second mode of interaction, electrostatic attraction, by using the imprint  $\beta$ -5 with a polymerizable counter ion that can also be incorporated into the polymer. As shown in Table 3, the rebinding capacity of the corresponding sample **P9** (1:4:20) amounted to 7.2 mg/g, or 54%, more than three times that of the control polymer **P1** and much higher than those reported in the literature for non-covalently imprinted polymers. The limited overall capacity of the polymer structure was again indicated; the otherwise similar polymer **P10**, with twice amount of imprint, exhibited a lower nickel(II) re-uptake. We note that this is associated with a substantial decrease in surface area and pore volume, suggesting that the impaired binding ability may arise from the altered morphology of the polymer.

Since the relatively weak non-covalent interactions are favored by lower temperature,<sup>21</sup> 2,2'-azobis(2,4-dimethylvaleronitrile) (ABDV), a more reactive initiator than AIBN, was used to foster polymerization at 40°C, in place of the previous 50°C temperature. Unexpectedly, the imprinted polymer **P12**, as well as the control polymer **P11**, exhibited rebinding inferior to those of the AIBN-initiated polymers (Table 3). Nevertheless, the nickel(II) re-uptake by **P12** was still three times that of **P11**, again indicating the selective advantage of two synergistic interactions.

Even larger imprinting effects can be realized by preparing polymers at extremely high crosslinker to functional monomer ratios, e.g. 120:4 for EGDMA:acrylamide. The three polymers, **P13** (control), **P14** (hydrogen bonding alone) and **P15** (hydrogen bonding & electrostatic interaction) have surface areas and pore volumes so close in value reasonable comparisons can be made with little doubt about the close similarities of their important morphologically dependent properties (e.g., availability of accessible sites). As shown in Table 3, the samples whose binding is limited to hydrogen bonding alone, **P13** and **P14**, exhibited very poor rebinding capacity. This result is not surprising because the concentrations of amide groups in the polymers were greatly reduced. On the other hand, the nickel(II) re-uptake by the polymer benefiting from two synergistic modes of interaction (hydrogen bonding and electrostatic attraction) **P15** was enhanced by a factor of 18, compared to that of the control polymer. This is an excellent example of imprint-enhanced rebinding capacity. In the absence of experiments directed at the competition between more than one candidate for complexation at the rebinding site, it is not clear that this improvement in binding should be described as an increase in the selectivity of the imprinted polymer.

All of the results described above come from studies using acetonitrile, both as the porogen (solvent present during polymerization) and as the medium for the rebinding experiments. Corresponding rebinding experiments have also been carried out in water, because water is the appropriate solvent for eventual deployment of the soil poultice. The rebinding behavior of these MIPs in water displayed three distinctive patterns: (1) The nickel(II) re-uptake of control polymers exceeded that in acetonitrile, especially at high crosslinker ratios (**P13**, **P16**); (2) the nickel(II) re-uptake in water of imprinted polymers that bind by hydrogen bonding alone is greater than that in acetonitrile at high crosslinker ratios (**P14**), but less than that in acetonitrile at low crosslinker ratios (**P2**); (3) the nickel(II) re-uptake by the imprinted polymers that benefit from both hydrogen bonding and electrostatic attractions is lower, relative to acetonitrile, at both high and low crosslinker ratios. It is interesting that in all cases in water, these (hydrogen bonding & electrostatic interaction) imprinted polymers bound *ca.* twice as much of the nickel(II) complex  $\beta$ -4 as did the control polymers. Good rebinding in water has also been reported in the molecular imprinting of biologically related compounds.<sup>22</sup> According to the literature,<sup>20,23</sup> water is adverse with respect to hydrogen bonding and electrostatic interactions, while it is conducive to hydrophobic interactions which play an important role in non-covalent binding.

Batch binding tests were also performed to examine the concentration dependence of rebinding to the imprinted polymers. The amount of  $\beta$ -4 bound to samples **P2** (hydrogen bonding alone) and **P9** (hydrogen bonding & electrostatic attractions) was plotted against free  $\beta$ -4 concentration to produce the binding isotherms (Figure 3). It is clear from the binding data that **P9** possesses a substantially larger number of binding sites for  $\beta$ -4. Higher rebinding capacity at low concentrations implies that there are also more strong binding sites in **P9**. The Scatchard plots, derived from the data and shown in Figure 3, reveal quite different binding properties for the two polymers. As shown in Figure 4, the plot for **P9** is nonlinear with two straight lines fitting the Scatchard equation, indicating that there are two populations of binding sites with different affinities for the imprint molecule. The association constants  $K_a$  for the high- and low-affinity binding sites were calculated to be  $(2.3 \pm 0.48) \times 10^3 \text{ M}^{-1}$  and  $52 \pm 4.5 \text{ M}^{-1}$ , respectively. In contrast, the Scatchard plot for **P2** (Figure 5) appears to represent binding sites which are relatively homogeneous and of low binding affinity ( $K_a = 13 \pm 6.1 \text{ M}^{-1}$ ). We rationalize these distinctly different binding sites in terms of the positioning of the co-polymerized counter ions. The strong binding probably arises from sites enjoying both hydrogen bonded linkages and maximum presence of negatively charged sulfonate groups. The weak binding is attributed to sites having one or no counter ions in close proximity to the re-bound cationic metal complex.

**MIPs based on hydrogen bonding & minor ligand bonding.** As functional monomers, vinyl pyridines provide supplementary ligating groups (the pyridine nitrogens) to bind to nickel(II), in addition to those on the primary ligand; e.g., **1** or **2**. Table 4 shows the nickel(II) re-uptake of the polymers based solely on minor ligand interaction with various ratios of imprint,  $\beta$ -4, to vinyl pyridine. As was previously found for the hydrogen bonding (only) polymers, a striking effect of excess functional monomer was observed. As the excess of 4-vinyl pyridine increased from 2:1 to 6:1, the rebinding capacity of the imprinted polymer increased from 2.5 mg/ g to 14 mg/g, and, at the same time, the imprinting effect became more pronounced.

The position of the vinyl substituent on the pyridine has a great influence on the rebinding capacity. Replacing 4-vinyl pyridine with 2-vinyl pyridine, produced an “imprinted” polymer (**P26**) with essentially zero binding ability, and use of 3-vinyl pyridine yielded an intermediate value (compare **P25** with **P26** and **P22**). Thinking of the pyridine as a ligating function projecting out of the surface of a polymer mass, the accessibility of the corresponding nitrogen atom for binding to a metal atom would be expected to follow the order 4-vinyl pyridine > 3-vinyl pyridine > 2-vinyl pyridine, an expectation consistent with the observations.

When 4-vinyl pyridine was added as a second functional monomer (in addition to acrylamide), nickel(II) re-uptake increased by a factor of two. Incrementally increasing the concentration of 4-vinyl pyridine by replacing equivalent molar amount of acrylamide affords continuing improvement of the rebinding capacity (Figure 6). Like the addition of a functional monomer capable of electrostatic attraction, this mode of interaction offers promise of synergistic bimodal binding of the macrocyclic metal complexes to the imprinted polymer.

**Stereoselectivity of MIPs based on hydrogen bonding.** The stereochemistry of macrocyclic metal complexes allows us to study the selective recognition of stereo-isomers by molecular imprinting, which to the best of our knowledge, has not previously been studied.

Earlier work revealed that the nickel complexes **3** and **4** (Chart 3) exist in two isomeric structures (Chart 4): The symbol  $\beta$  (**I**) is assigned to the thermodynamically favored form and  $\alpha$  (**II**), to the kinetically favored form.<sup>15</sup>

Based on Barefield's procedure,<sup>15</sup> four nickel complexes,  $\alpha$ -**3**,  $\alpha$ -**4**,  $\beta$ -**3** and  $\beta$ -**4** were prepared by the reaction of nickel perchlorate with the corresponding macrocyclic ligands at room and reflux temperatures, respectively. Considering the possibility of the transformation of the  $\alpha$  isomer to the  $\beta$

isomer during the thermally initiated polymerizations, we focused on polymers imprinted by the  $\beta$  isomer in this work. The stereoselectivity is expressed as the ratio of  $\beta$  isomer to  $\alpha$  isomer that was found to rebind to the  $\beta$  imprinted polymers.

As shown in Table 5, all the imprinted polymers and control polymers had better rebinding capacities for  $\beta$ -4. It is noteworthy that  $\beta$ -4 binds to the well studied **P2** seven times more strongly than does  $\alpha$ -4. The polymers (**P3** and **P4**) with lower crosslinker ratios (12:20) displayed increased rebinding of both  $\alpha$ -4 and  $\beta$ -4, albeit the stereoselectivity was decreased. Thus, the structure of imprints is crucial to the efficiency of imprinting and rebinding processes. Further, the stereoselectivity of the control polymer **P1** (not imprinted) for  $\beta$ -4 is 5.1. We must conclude that, beyond imprinting, the orientation of the pendant amide groups in  $\beta$ -4 is more favorable for hydrogen bonding. It was not surprising to find that the  $\beta$ -4 imprinted system was superior in binding affinity (0.86 mg/g for  $\beta$ -4) even with the sample **P27** imprinted with  $\beta$ -3, the complex having pendant nitrile groups on its ligand, rather than amide functions.

The rebinding by the two isomers of complex **3**,  $\alpha$ -3 and  $\beta$ -3 (Table 6), having pendant cyano groups rather than amide groups, was inferior. As a result, the aforementioned structure effect was not exhibited in the re-uptake for the complex **3**. The control polymer showed a higher affinity for  $\alpha$ -3 than did either imprinted polymer (**P2** or **P27**), and the rebinding of the isomers of complex **3** was indistinguishable for the polymers imprinted with either complex **3** or complex **4**. The inferior performance of complex **3** is not surprising since cyano groups form weaker hydrogen bonds (single-point, Chart 2, left) than amide groups.

**Reuse of polymers.** Chemical stability is an important property of MIPs. Very recently Nicholls *et al.* studied the chemical stability of theophylline imprinted polymers which were based on the copolymerization of methacrylic acid and ethylene glycol dimethacrylate.<sup>24</sup> The polymers retained their affinity ( $\geq 95\%$ ) for the imprint on exposure (24 h) to 10 M hydrochloric acid. In this work, we studied the durability of the imprinted polymers by treating them with concentrated hydrochloric acid, and, in separate experiments, with concentrated nitric acid, a very strong oxidizing agent.

For each cycle of reuse, a polymer sample was treated with the imprint  $\beta$ -4, then after digestion in acid, it was washed repeatedly with water, methanol and dried in vacuo in order to remove the freshly bound  $\beta$ -4, in preparation for the next re-uptake experiment.

As shown in Table 7, the imprinted polymers **P2** and **P22**, and the control polymer **P1** displayed increases in rebinding during the reuse. The nickel(II) re-uptake was enhanced by a factor of 1.5-2 in the 4<sup>th</sup> or 5<sup>th</sup> rebinding runs when the polymers had been treated with concentrated hydrochloric acid or nitric acid for about 50 h. Clearly, these polymers are quite resistant to strong and oxidizing acids.

The function of acid was indirectly evidenced by a reuse process based on soxhlet extraction. In this process, the imprint was removed after each rebinding run. As shown in Table 7, the nickel re-uptake of **P1** was decreased in the 2<sup>nd</sup> run and the value for the 4<sup>th</sup> run was even lower than that for the 1<sup>st</sup> run.

The mechanism by which acid treatment increases rebinding capacity remains unknown. Solid-state <sup>13</sup>C NMR analyses showed nearly identical spectra (Figure 7) for the samples before and after nitric acid digestion,<sup>25</sup> although the ester groups in EGDMA units are subject to hydrolysis under such harsh conditions.<sup>4f</sup> Elemental analyses showed an increase in nitrogen content after nitric acid treatment.<sup>26</sup> Further, the color of the polymers was changed from pure white to light yellow, supporting the possibility of introduction of nitro groups, whose presence could bring about additional hydrogen bonding in the polymers.

Imprint removal with hydrochloric acid followed by soxhlet extraction had no obvious influence on the polymer morphology. To the contrary, nitric acid treatment led to a marked decrease of surface area and pore volume (Table 7).

## Conclusions

These feasibility studies provide strong indications that the *soil poultice* concept may someday be realized. Success will depend on maximizing the rebinding capability and selectivity of MIPs designed specifically for the soil poultice. The requirements are very strong binding with great lability and our strategy to impart these properties on a molecularly imprinted polymer has been focused on optimising combinations of the known supramolecular interactions; e.g., hydrogen bonding, electrostatic attraction, and additional monodentate ligand binding. Using macrocyclic nickel complexes having pendant functional groups, we have developed molecularly imprinted polymer systems having non-covalent rebinding capabilities that are much greater than has previously been observed. This clearly shows that the potential of labile, non-covalent binding MIPs has not been fully developed. In view of the limited attention that has been given to systems of this kind, these results are viewed as very promising.

A general principle of the soil poultice is the presence of dual selective processes that are built into the system: (1) chelate selectivity associated with metal ion binding to the ligands of choice and (2) MIPs selectivity associated with selective adduct formation between the complex and the imprinted polymer. For the MIPs studies themselves, low spin square planar, substitution-inert nickel(II) complexes were used in these studies to avoid any possibility of complications, during polymerisation, due to rapid dissociation of the imprinting complex.

The chelate selectivity of ligands employed in the MIPs studies was explored by determining the binding constants for a selection of metal ions. The protonation constants for the ligand **2** and the stability constants for the complexes of **2** with the labile metal ions Cu(II), Hg(II), Cd(II), Pb(II) and Zn(II) were determined, leading to important results. **2** is highly selective toward Cu(II) and Hg(II) compared to the other metal ions. This suggests the possibility of using a MIPs system based on **2** for recovering Cu(II) and/or Hg(II) from spills. These matters are the subjects of on-going investigations.

According to the literature, hydrogen bonded MIPs are weak in performance with their rebinding capacities being limited to 10 to 15% of the available polymer sites. In our design, the first and simplest polymers depending on hydrogen bonding alone exceeded these limits substantially (~26%). We showed by careful choice and balance of the components of the polymer very large binding capacities can be achieved through hydrogen bonding alone—but that does not necessarily assure high selectivity.

Proceeding on the basis of leads provided by earlier studies on chiral substrates, we showed that synergism between pairs of supermolecular modes of binding can lead to very strong and selective substrate binding. With the combination of hydrogen bonding and electrostatic attraction rebinding in excess of 50% is readily available. However, in many cases, the addition of imprints results in deleterious modifications in the polymer morphology. Under proper conditions the morphology can be maintained constant and the impact of binding group changes has been clearly demonstrated. Under such conditions, hydrogen bonding alone gives marginal results, as reported in the literature; however, the synergism between hydrogen bonding and electrostatic attraction produces ~20 times better rebinding. Careful control of composition and functional parameters can move these polymer materials from behaviours properly described as not especially interesting to those recognized to be quite useful. The combination of a monodentate ligand delivered as a functional monomer in the polymer and a hydrogen bonding functional monomer gives results parallel to those found for the hydrogen bonding plus electrostatic attraction duo.

All of the initial studies were carried out with acetonitrile as porogen. The ideal medium for a soil poultice is water. Remarkably, water is, at least in some cases, about 90% as good as acetonitrile when it comes to rebinding of substrates to the imprinted polymers benefiting from two supramolecular modes of interaction. This is surprising in view of the expectation that water would be a poor solvent for hydrogen bonding and electrostatic interactions.

Some more detailed studies on systems having both electrostatic and hydrogen bonding groups revealed two distinctive kinds of binding sites with affinities for substrates differing by a factor of 40-50x. It is proposed that the strongly binding sites have a maximum positioning of vinyl sulfonate moieties in their near vicinities, as compared to the weaker sites. Further, even the weaker site is some 4x stronger than the binding sites in polymers linking to substrates by hydrogen bonding alone.

Stereoselectivity is evident and reflects the uniqueness of the macrocyclic complex imprinted systems. We have also shown that the rebinding capacity improves with reuse and that the MIPs are robust in the presence of oxidizing agents and strong acids.

### Acknowledgment

The work was supported by the Department of Energy (Grant no. DE-FG07-96ER14708). We thank Dr. Al-Ammr Assad Saleam for ICP analyses and Drs. Christopher J. Lyon and Vidya Sagar Reddy-Sarsani for surface characterization. We are also grateful to Prof. Eric J. Munson and Dr. Joseph W. Lubach for their kind help in solid state  $^{13}\text{C}$  NMR analyses.

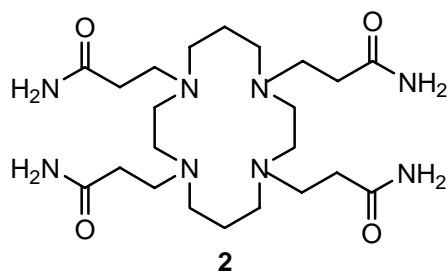


Chart 1

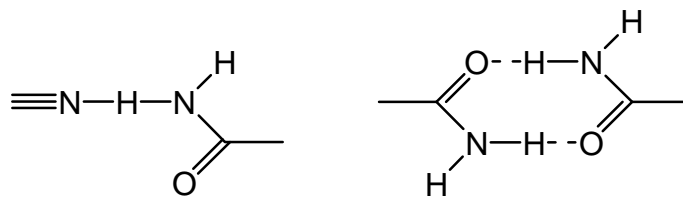


Chart 2

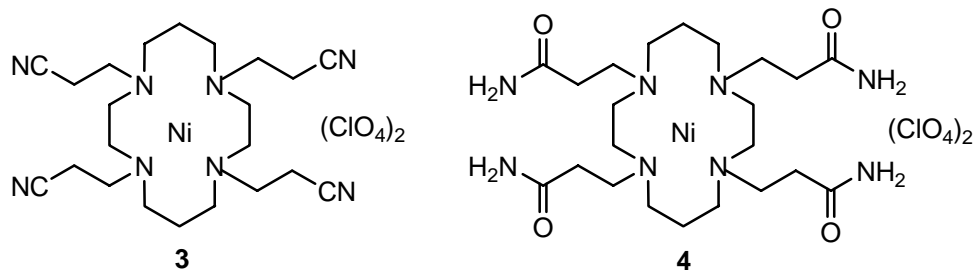


Chart 3

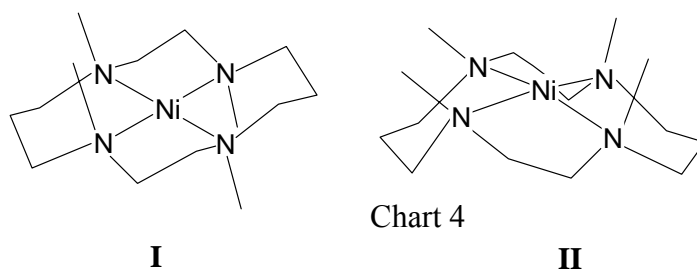


Chart 4

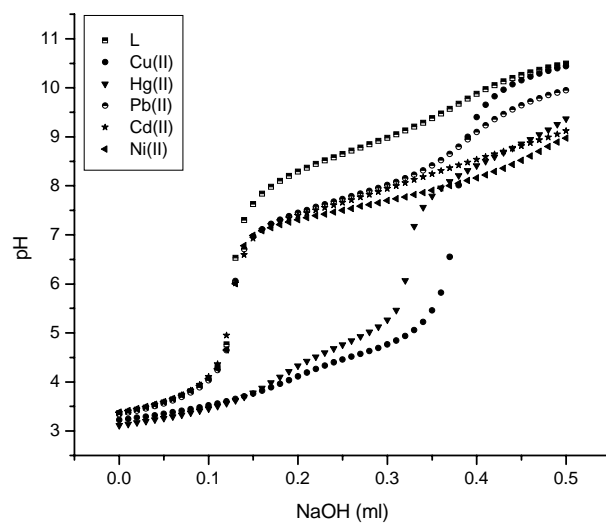


Figure 1 Potentiometric titration curves for **2** with and without M(II) at 25°C and I= 0.1M NaNO<sub>3</sub>.

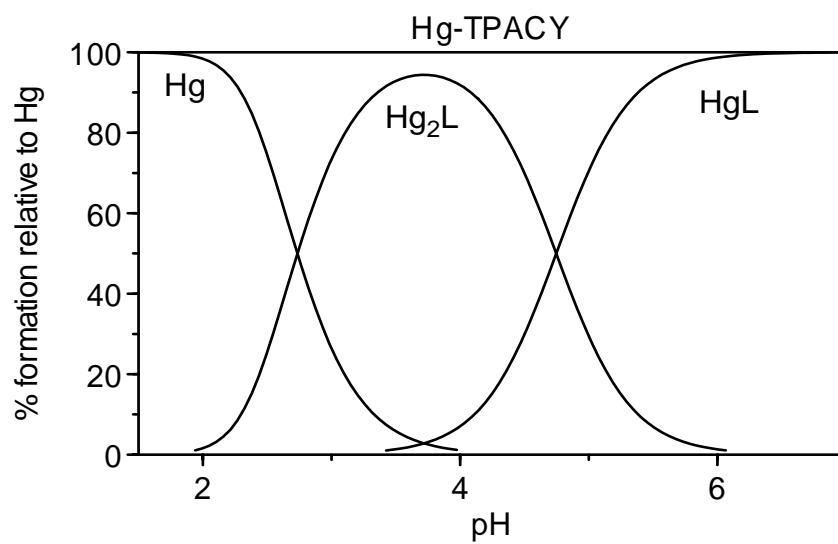


Figure 2 Species distribution diagram for solutions containing  $1.0 \times 10^{-3}$  M **2** and  $1.0 \times 10^{-3}$  M Hg(II) calculated with the HySS2 program.

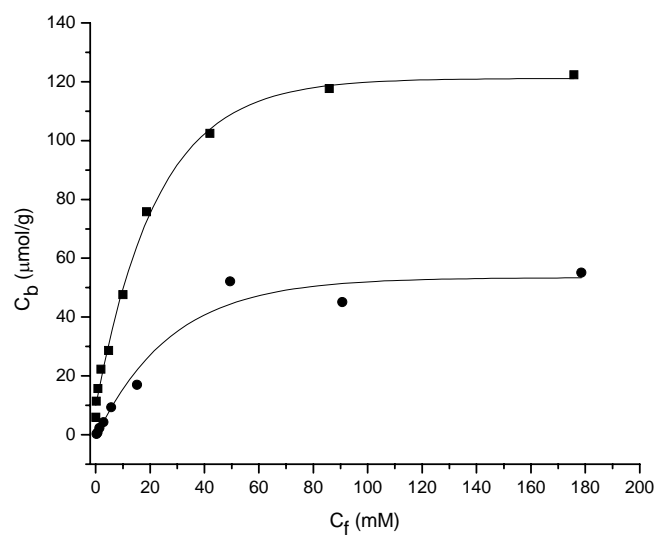


Figure 3 Binding isotherms of **P2** (●) and **P9** (■) in acetonitrile.

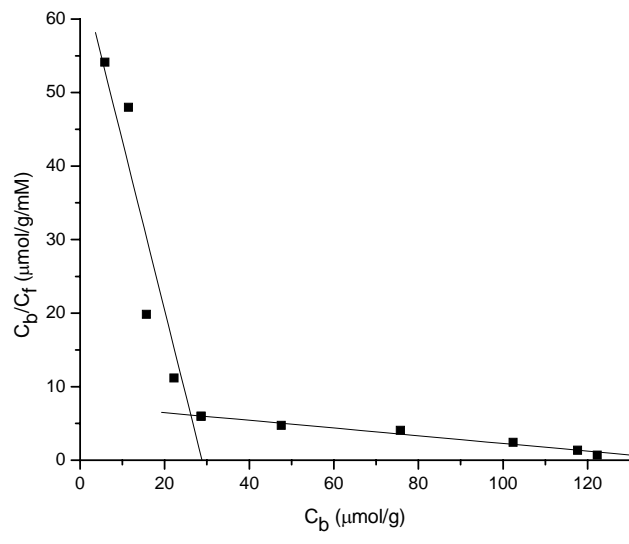


Figure 4 Scatchard plot of **P9** in acetonitrile.

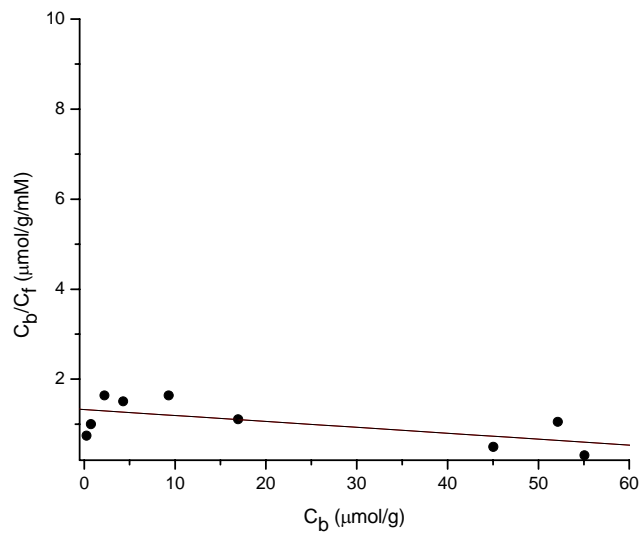


Figure 5 Scatchard plot of **P2** in acetonitrile.

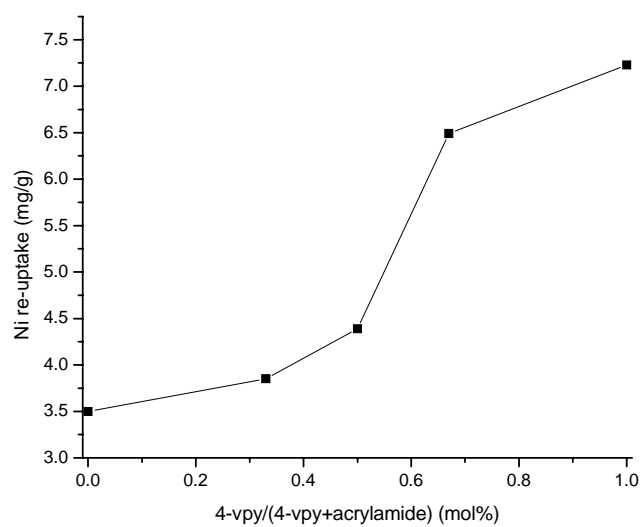


Figure 6 Rebinding capacity of the MIPs (AIBN, 50°C;  $\beta$ -4/ 4-vinyl pyridine+acrylamide/EGDMA=1/4/20).

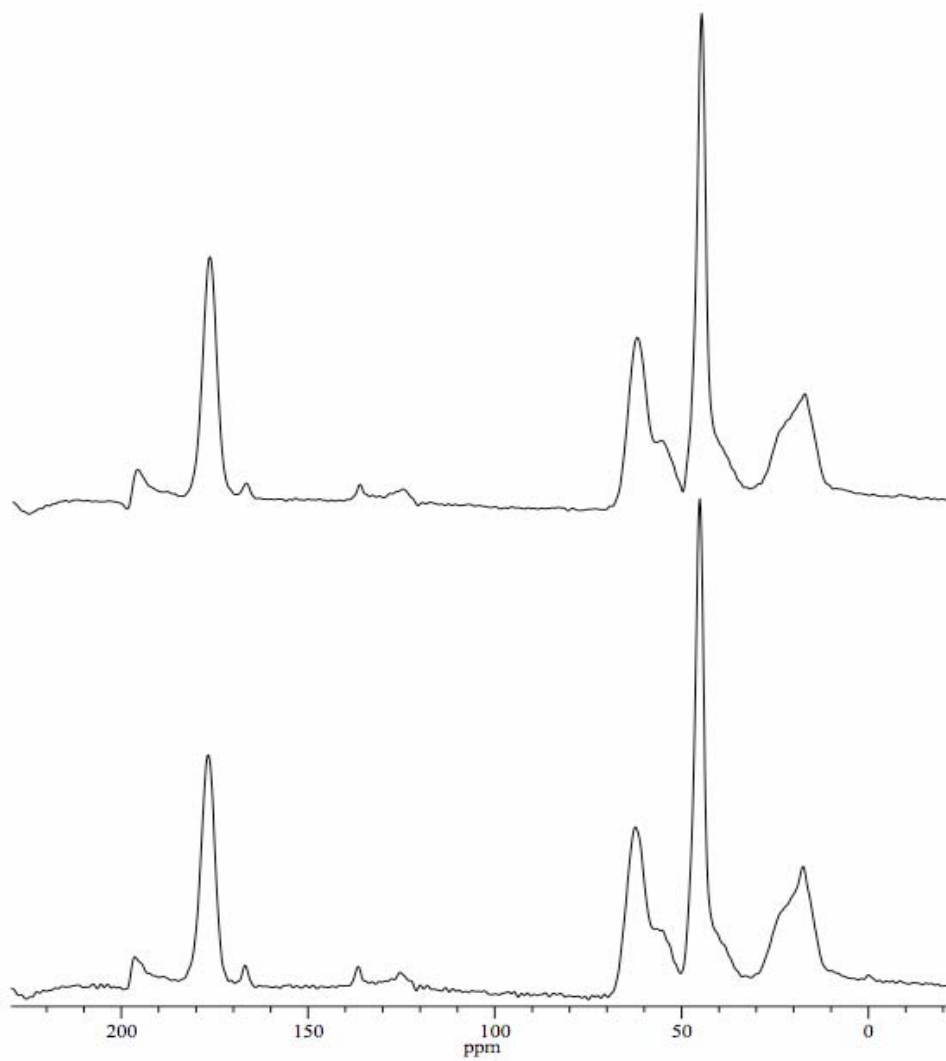


Figure 7 Solid state  $^{13}\text{C}$  NMR of **P1** before (bottom) and after (top) concentrated acid nitric acid treatment.

Table 1 Overall Equilibrium Constants for the Ligand **2** and Its Metal Complexes at 25.0°C and I=0.1 NaNO<sub>3</sub><sup>a</sup>

logβ <sub>MHL</sub>	H(I)	Hg(II)	Cu(II)	Ni(II)	Pb(II)	Cd(II)	Zn(II)
logβ <sub>011</sub>	9.289(4)						
logβ <sub>021</sub>	17.985(2)						
logβ <sub>031</sub>	26.297(8)						
logβ <sub>101</sub>		18.44(2)	18.48(2)	6.42(5)	6.13(5)	6.29(1)	6.48(1)
logβ <sub>111</sub>		-----	-----	-----	13.35(4)	14.43(1)	15.64(1)
logβ <sub>201</sub>		24.22(4)	23.74(3)	10.60(8)	-----	-----	-----

<sup>a</sup>The numbers in parentheses represent the standard deviation in the last significant figure.

Table 2 Synthesis, Characterization and Nickel Rebinding Capacities of Polymers<sup>a</sup>

Polymer	Crosslinker	I/F/C <sup>b</sup>	BET <sup>c</sup> (BJH <sup>d</sup> )	Ni re-uptake (mg/g polymer)
<b>P1</b> (control)	EGDMA	0/4/20	365 (0.51)	2.3
<b>P2</b>	EGDMA	0/4/20	332 (0.44)	3.5

<b>P3</b> (control)	EGDMA	0/12/20	197 (0.42)	2.6
<b>P4</b>	EGDMA	1/12/20	179 (0.37)	10
<b>P5</b> (control)	EBA	0/0/18	200 (0.56)	22
<b>P6</b>	EBA	1/0/18	121 (0.28)	38
<b>P7</b>	EBA	2/0/18	69 (0.24)	29
<b>P8<sup>e</sup></b>	EBA	9/0/18	89 (0.25)	25

<sup>a</sup> Initiated by AIBN at 50°C, acetonitrile/methanol=1/1 for **P1-P4, P8**, 2/1 for **P5-P7**; <sup>b</sup> Molar ratio of imprint ( $\beta$ -4) to functional monomer (acrylamide) to crosslinker; <sup>c</sup> BET surface area (m<sup>2</sup>/g); <sup>d</sup> BJH cumulative pore volume for pores between 1.7 and 300 nm in diameter (mL/g); <sup>e</sup> Treated with concentrated nitric acid to further remove the residual nickel(II) after soxhlet extraction.

Table 3 Synthesis, Characterization and Nickel Rebinding Capacities of Polymers<sup>a</sup>

Polymer	Imprint	I/F/C <sup>b</sup>	BET <sup>c</sup> (BJH <sup>d</sup> )	Ni re-uptake in MeCN <sup>e</sup>	Ni re-uptake in H <sub>2</sub> O <sup>e</sup>
<b>P1</b> (control)	None	0/4/20	365 (0.51)	2.3	2.6
<b>P2</b>	$\beta$ -4	1/4/20	332 (0.44)	3.5	2.1
<b>P9</b>	$\beta$ -5	1/4/20	143 (0.14)	7.2	5.4
<b>P10</b>	$\beta$ -5	2/4/20	41 (0.02)	3.0	-----
<b>P11</b> (control)	None	0/4/20	397 (0.59)	1.9	-----
<b>P12</b>	$\beta$ -5	1/4/20	108 (0.25)	5.7	-----

<b>P13</b> (control)	None	0/4/120	389 (0.47)	0.25	2.0
<b>P14</b>	$\beta$ -4	1/4/120	381 (0.61)	0.33	2.4
<b>P15</b>	$\beta$ -5	1/4/120	370 (0.41)	4.5	4.0
<b>P16</b> (control)	None	0/4/70	-----	0.68	1.8
<b>P17</b>	$\beta$ -5	1/4/70	-----	4.8	4.3

<sup>a</sup> Initiated by AIBN at 50°C except **P11** and **P12** (ABDV at 40°C), acetonitrile/methanol=1/1; <sup>b</sup> Molar ratio of imprint to functional monomer (acrylamide) to crosslinker (EGDMA) <sup>c</sup> BET surface area (m<sup>2</sup>/g); <sup>d</sup> BJH cumulative pore volume for pores between 1.7 and 300 nm in diameter (mL/g); <sup>e</sup> Unit: mg/g polymer.

Table 4 Synthesis, Characterization and Nickel Rebinding Capacity of Polymers<sup>a</sup>

Polymer	Functional monomer	I/F/C <sup>b</sup>	BET <sup>c</sup> (BJH <sup>d</sup> )	Ni re-uptake (mg/g polymer)
<b>P18</b>	4-vinyl pyridine	1/1/20	-----	1.1
<b>P19</b> (control)	4-vinyl pyridine	0/2/20	420 (0.86)	2.2
<b>P20</b>	4-vinyl pyridine	1/2/20	393 (0.94)	2.5
<b>P21</b>	4-vinyl pyridine	1/3/20	-----	5.3
<b>P22</b>	4-vinyl pyridine	1/4/20	332 (0.57)	7.2
<b>P23</b> (control)	4-vinyl pyridine	1/6/20	315 (0.52)	4.6
<b>P24</b>	4-vinyl pyridine	1/6/20	296 (0.58)	14
<b>P25</b>	3-vinyl pyridine	1/4/20	363 (0.61)	3.2
<b>P26</b>	2-vinyl pyridine	1/4/20	313 (0.59)	0.17

<sup>a</sup> Initiated by AIBN at 50°C, acetonitrile/methanol=1/1; <sup>b</sup> Molar ratio of imprint ( $\beta$ -4) to functional monomer (vinyl pyridine) to crosslinker (EGDMA); <sup>c</sup> BET surface area (m<sup>2</sup>/g); <sup>d</sup> BJH cumulative pore volume for pores between 1.7 and 300 nm in diameter (mL/g).

Table 5 Rebinding Capacity & Stereoselectivity of Polymers<sup>a</sup>

Polymer	Imprint	Re-uptake of $\alpha$ -4 (mg Ni/g polymer)	Re-uptake of $\beta$ -4 (mg Ni/g polymer)	Selectivity ( $\beta/\alpha$ )
<b>P1</b> (control)	None	0.45	2.3	5.1
<b>P2</b>	$\beta$ -4	0.45	3.5	7.8
<b>P3</b> (blank)	None	1.9	2.6	1.4
<b>P4</b>	$\beta$ -4	2.2	10	4.5
<b>P27</b>	$\beta$ -3	0.20	0.86	4.3

<sup>a</sup> Initiated by AIBN at 50°C, acetonitrile/methanol=1/1 except **P27** (neat acetonitrile); functional monomer (acrylamide)/ crosslinker (EGDMA)=4/20 for **P1**, **P2**, and **P27**, 12/20 for **P3** and **P4**.

Table 6 Rebinding Capacity & Stereoselectivity of Polymers<sup>a</sup>

Polymer	Imprint	Re-uptake of $\alpha$ - <b>3</b> (mg Ni/g polymer)	Re-uptake of $\beta$ - <b>3</b> (mg Ni/g polymer)	Selectivity ( $\beta/\alpha$ )
<b>P1</b> (control)	None	0.64	0.50	0.78
<b>P2</b>	$\beta$ - <b>4</b>	0.31	0.49	1.6
<b>P27</b>	$\beta$ - <b>3</b>	0.32	0.49	1.5

<sup>a</sup> Initiated by AIBN at 50°C, acetonitrile/methanol=1/1 for **P1** and **P2**, neat acetonitrile for **P27**; functional monomer (acrylamide)/ crosslinker (EGDMA)=4/20.

Table 7 Reuse of Polymers

Polymer	Treatment	Ni re-uptake (mg/g polymer)					BET <sup>b</sup> (BJH <sup>c</sup> )	BET <sup>b</sup> (BJH <sup>c</sup> )
		#1	#2	#3	#4	#5	before #1	after #4 ( #5)
<b>P1</b> (blank)	SE <sup>a</sup>	2.3	2.8	2.6	2.1	-----	365 (0.51)	373 (0.63)
<b>P1</b> (blank)	37% HCl	2.2	3.1	3.4	3.8	4.2	365 (0.51)	365 (0.48)
<b>P2</b>	37% HCl	2.9	4.5	4.4	4.3	5.1	332 (0.44)	331 (0.68)
<b>P2</b>	70% HNO <sub>3</sub>	3.5	3.8	4.2	4.4	5.1	332 (0.44)	258 (0.36)
<b>P22</b>	70% HNO <sub>3</sub>	7.2	8.2	9.8	11	-----	332 (0.57)	163 (0.36)

<sup>a</sup> Soxhlet extraction; <sup>b</sup> BET surface area (m<sup>2</sup>/g); <sup>c</sup> BJH cumulative pore volume for pores between 1.7 and 300 nm in diameter (mL/g).

### References and notes

- 1) (a) Telford, J. R.; Raymond, K. N. In *Supramolecular Chemistry*; Gokel, G. ed.; Permagon: Oxford, **1996**; pp 245. (b) Telford, J. R.; Raymond, K. N. In *Bioinorganic Chemistry, An Inorganic Perspective of Life*; Kluwer: Dordrecht, **1995**; pp 25.
- 2) (a) Busch, D. H. "The Compleat Coordination Chemistry--What a Difference A Century Makes", Werner Centennial Volume, ACS Symposium Series 565, **1994**; pp. 148-164. (b) Busch, D. H. "Ligand Design for Enhanced Molecular Organization--Selectivity and Specific Sequencing in Multiple Receptor Ligands, and Orderly Molecular Entanglements", in *Transition Metal Ions in Supramolecular Chemistry*; Fabbrizzi, L. ed.; Kluwer: Dordrecht, **1994**; pp 55-79.
- 3) (a) Wulff, G; Sarhan, A. *Angew. Chem. Int. Ed. Engl.* **1972**, *11*, 341. (b) Wulff, G; Sarhan, A; Zabrocki, K. *Tetrahedron Lett.* **1973**, *14*, 4329-4332.
- 4) For reviews see: (a) Wulff, G. *Chem. Rev.* **2002**, *102*, 1-28. (b) Mosbach, K. *Anal. Chim. Acta* **2001**, *435*, 3-8. (c) Sellergren, B. *Angew. Chem. Int. Ed. Engl.* **2000**, *39*, 1031-1037. (d) Whitcombe, M. J.; Alexander C.; Vulfson, E. N. *Synlett.* **2000**, 911-923. (e) Andersson, L. I. *J. Chromatogr. B* **2000**, *745*, 3-13. (f) Wulff, G. *Angew. Chem. Int. Ed. Engl.* **1995**, *34*, 1812-1834.
- 5) (a) Sellergren, B. *Makromol. Chem.* **1989**, *190*, 2703-2711. (b) Kempe M.; Mosbach, K. *Anal. Lett.* **1991**, *24*, 1137-1145. (c) Sellergren B.; Shea, K. J. *J. Chromatogr.* **1993**, *635*, 31-49.
- 6) Nishide, N.; Tsuchida, E. *Makromol. Chem.* **1976**, *177*, 2295-2310.
- 7) Kuchen, W.; Schram, J. *Angew. Chem. Int. Ed. Engl.* **1988**, *27*, 1695-1697.
- 8) Garcia, R.; Pinel, C.; Madic C.; Lemaire, M. *Tetrahedron Lett.* **1998**, *39*, 8651-8654.

- 9) Chen, H.; Olmstead, M. M.; Albright, R. L.; Devenyi, J.; Fish, R. H. *Angew. Chem. Int. Ed. Engl.* **1997**, *36*, 642-645.
- 10) Sharma, A. C.; Joshi, V.; Borovik, A. S. *J. Polym. Sci. A: Polym. Chem.* **2001**, *39*, 888-897.
- 11) Alumni, S.; Laureti, V.; Ottavi, L.; Ruzziconi, R. *J. Org. Chem.* **2003**, *68*, 718-725.
- 12) Gans, P.; Sabatini, A.; Vaca, A. *J. Com. Soc., Dalton Trans.* **1985**, 1195-1200.
- 13) Alderighi, L.; Gans, P.; Ienco, A.; Peters, D.; Sabatani, A.; Vacca, A. *Coord. Chem. Rev.* **1999**, *184*, 311-318.
- 14) Wainwright K. P. *J. Chem. Soc., Dalton Trans.* **1980**, 2117-2120.
- 15) Freeman, G. M.; Barefield, E. K.; Van Derveer, D. G. *Inorg. Chem.* **1984**, *23*, 3092-3103.
- 16) The DOTAM (a cyclen-based ligand with four pendant groups  $-\text{CH}_2\text{CONH}_2$ ) complexes of  $\text{Cd}^{2+}$  were described as six-coordinate with secondary coordination of the other two oxygen donors. Maumela, H.; Hancock, R. D.; Carlton, L.; Reibenspies, J. H.; Wainwright, K. P. *J. Am. Chem. Soc.* **1995**, *117*, 6698-6707.
- 17) (a) Warner, L. G.; Busch, D. H. *J. Am. Chem. Soc.* **1969**, *91*, 4092-4101. (b) Warner, L. G.; Rose, N. J.; Busch, D. H. *J. Am. Chem. Soc.* **1967**, *89*, 703-704.
- 18) O'Shannessy, D. J.; Anderson, L. I.; Mosbach, K. *J. Mol. Recognit.* **1989**, *2*, 1-5.
- 19) Yu, C.; Mosbach, K. *J. Org. Chem.* **1997**, *62*, 4057-4064.
- 20) Nicholls, I. A.; Adbo, K.; Anderson, H. S.; Anderson, P. O.; Ankarloo, J.; Hedin-Dahlström, J.; Jokela, P.; Karlsson, J. G.; Olofsson, L.; Rosengren, J.; Shoravi, S.; Svenson, J.; Wikman, S. *Anal. Chim. Acta* **2001**, *435*, 9-18.
- 21) O'Shannessy, D. J.; Ekberg, B.; Mosbach, K. *Anal. Biochem.* **1989**, *177*, 144-151.
- 22) Anderson, L. I.; Müller, R.; Vlatakis, G.; Mosbach, K. *Proc. Natl. Acad. Sci. USA* **1995**, *92*, 4788-4792.
- 23) Adbo, K.; Anderson, H. S.; Ankarloo, J.; Karlsson, J. G.; Norell, M. C.; Olofsson, L.; Rosengren, J.; Svenson, J.; Örtengren, U.; Nicholls, I. A. *Bioorg. Chem.* **1999**, *27*, 363-371.
- 24) Svenson, J.; Nicholls, I. A. *Anal. Chim. Acta* **2001**, *435*, 19-24.
- 25) The control polymer was selected to avoid the complication caused by the nitrogen-containing residue imprint (ca. 3% of the starting material) in the imprinted polymer.
- 26) The nitrogen content of **P1** is 1.59%. After the treatment with concentrated hydrochloric acid and concentrated nitric acid, the values are 1.40% and 2.08% respectively.

## **QUANTITIES/PACKAGING**

This subject is not applicable to the project described herein.